Enhancing and optimising the reaction rate of thin film photocatalysts in a photocatalytic spinning disc reactor

Wan Mansor, Wan Salida

Award date:
2017

Awarding institution:
University of Bath

ENHANCING AND OPTIMISING THE REACTION RATE OF THIN FILM PHOTOCATALYSTS IN A PHOTOCATALYTIC SPINNING DISC REACTOR

Wan Salida Wan Mansor

A thesis submitted for the degree of Doctor of Philosophy
University of Bath
Department of Chemical Engineering
NOVEMBER 2017

DECLARATION OF AUTHORSHIP

This is all my own work except where I have indicated via references or other forms of acknowledgement.

Signature:

Date:

Dedicated to the memory of

Dr. Darrell Alec Patterson

I am forever indebted to my PhD supervisor, for his enthusiasm, guidance, and unrelenting support throughout this process.
He has routinely gone beyond his duties to fire fight my worries, concerns, and anxieties, and have worked to instil great confidence in both myself and my work.
I would like to thank him for his unremitting encouragement.
Put simply, I have never met anyone who believes in me more.
Thank you for making me more than I am.
It was an honour to have known such a great person and I will truly miss him.
He was a wonderful man and was cherished by everyone who knew him.
For the person can only be physically gone but never the life lived and the memories shared.
He will always be remembered, as he will be carved in the deepest chambers of my hearts.

ACKNOWLEDGEMENT

In the name of God, most Gracious and Merciful. I wish to express my sincere appreciation to those who have contributed to this thesis and supported me in one way or the other during this amazing journey. Undertaking this PhD has been a truly life-changing experience for me and it would not have been possible to do without the support and guidance that I received from many people.

Firstly, I would like to express my sincere gratitude to my late supervisor Dr. Darrell Alec Patterson for the non-stop support on my PhD study and related research, for his patience, support, motivation, and valuable knowledge. He helped me in all the time of research and writing of this thesis. I could not have imagined having a better supervisor and mentor for my PhD study.

I am also very grateful to Dr. Emma Anna Carolina Emmanuelsson as my co-supervisor for her scientific advice and knowledge and many insightful discussions and suggestions.

Besides my supervisors, I would like to thank the rest of my examiners: Prof. Dr. Davide Mattia and Prof. Dr. Joe Wood, for their encouragement and insightful comments.

It is a pleasure to thank my friends in Patterson's group who are extremely knowledgeable in just about everything, helpful, and friendly especially: Kemi Lawal, Emily Hayward, Harriet Manning, Lili Xu, Chris Davey, Nick Low and Kim Wu. Best wishes to all of them.

I also thank people who were not part of the Patterson's group but helped me out, including Lucecita Medina, Hendrick DuToit, Nur Rinah Ghafar, Harina Amer, Fraeya Whiffin, Anyela Ramirez Canon, Michael Gobs, and Antonio Jose Exposito Serrano.

I would like to extend my gratitude to Fernando Ramon Acosta, Robert Brain, Daniel Lou-Hing, Alexander Ciupa, Suzanne Barkley, Brigite Nunes Simoes Rodrigues and John Bishop, the technical team (for all their help these past three years with bringing our needed chemicals and supplies and their help with the technical in general), Paul Frith and Guy Brace (who has helped to design and build the reactor part), Philip Jones (the glass blower), Gabriele Kociok-Köhn (the crystallographer – pXRD) and Anneke

Lubbin (Mass Spectrometry Facility Manager). I also thank the administrative staffs for all the administrative help. I also thank the wonderful staff in the Chemical Engineering Department as well as in other departments for continually being so helpful and friendly. People here are really nice and want to help you out and I'm happy to have interacted with many of them. If I have forgotten anyone, I apologise.

I also thank to all my friends in UK and Malaysia (too many to list here but you know who you are!) for providing support and friendship that I needed.

Last but not least, I would like to thank to my mom, dad, and brothers for their patience, prayers, support and understanding during writing this thesis and my life in general. I love them so much, and without them I would not have made it this far. I know I always have them to count on when times are rough.

In conclusion, I recognise that this research would not have been possible without the financial assistance of Universiti Malaysia Terengganu, Ministry of Education Malaysia and the Marie Curie Career Integration Grants (CIG) for supporting this work with grant (FP7- 333952), and express my gratitude to those agencies.

ABSTRACT

Process intensification can be described as any chemical engineering development that leads to a substantially smaller, cleaner and more energy efficient technology. The principle of spinning disc reactor (SDR) technology is based upon the formation of a thin liquid film (20–300 μm) on a rotating disc induced by centrifugal and shear forces. This creates a high surface-to-volume-ratio. For instance, the suitability of the spinning disc reactor for polymerization reactions, organic synthesis, photocatalysis, or precipitation reactions was investigated.

The photocatalytic spinning disc reactor (pSDR) overcomes many of the aforementioned problems with chemical catalysts. The catalyst is immobilised, so does not need to be recycled and/or separated. Different flow can form across the surface of the disc depending on the flow rate, rotational speed, and liquid properties. To address these limitations, this research continues the development and optimisation of the pSDR by introducing textured discs (meshes and grooves as a macrostructure) to both increase the potential photocatalyst surface area on the disc as well as improve mixing. More photocatalyst can be coated on the increased disc area also.

In doing this, this work therefore significantly extends the previous work on the pSDR through investigating the use of a range of different photocatalyst textured macrostructures (meshes and grooves in the photocatalyst disc) in order to increase the micromixing and photocatalyst surface area, to increase the overall degradation rate in the pSDR The effect of rotating speed, disc surface structure (meshes/grooves/smooth), oxidant input amount (oxygen added or not) and volumetric flowrate were investigated and related to four key reaction/reactor parameters: reaction rate (using photocatalytic degradation of water soluble organics - methylene blue and ibuprofen), thin film hydrodynamics (by high speed photography of the liquid thin films), residence time distribution (measured by tracer analysis) and micro-mixing (measured by the Villermaux-Dushman reaction). A titanium dioxide (TiO_2) sol gel coated glass disc with coated additional macrostructures were used as the photocatalyst.

Results demonstrated that reaction rate can be optimised through identification of the optimal rotating speed, disc surface structure (meshes/grooves/smooth), oxidant input and volumetric flowrate. Higher disc spinning speeds make the residence time

distributions more plug flow in behaviour and increase micro-mixing, which is known to increase reaction rate. For methylene blue degradation, an intermediate disc speed of 300 rpm and 20 mL/s inlet flow for a mesh/textured disc with a square grooved pattern was found to give the highest reaction rate (4.546×10^{-7} mol/L.s) without added oxygen (the oxidant for the photocatalytic degradation). For ibuprofen degradation an intermediate disc speed of 300 rpm and 10 mL/s inlet flow for smooth disc was found to give the highest reaction rate (1.580×10^{-5} mol/L.s) also without added oxygen (the oxidant for the photocatalytic degradation). This indicates that the self-aeration of oxygen by the pSDR spinning liquid film contacting air produces sufficient and more optimal oxidant input for both compounds.

Analysis shows that using a patterned/mesh disc is optimal since it smooth out the surface flow across the disc, which both increases local UV penetration (less scattering) and provides more uniform volumetric utilisation of the catalyst. This effect appears to dominate the other positive effects of higher spinning speeds.

Overall this work shows that reactor and photocatalyst surface macrostructure and design plays an important role in increasing photocatalytic treatment efficiency. Moreover, the process intensification (higher reaction rates and photonic efficiency) and self-aeration demonstrated here, further demonstrates the significant advantages of the pSDR over other photocatalytic reactors.

TABLE OF CONTENTS

TITLE **i**

DECLARATION OF AUTORSHIP **ii**

ACKNOWLEDGEMENT **iv**

ABSTRACT **vi**

TABLE OF CONTENTS **viii**

LIST OF TABLES **xii**

LIST OF FIGURES **xiii**

LIST OF ABBREVIATIONS **xvii**

LIST OF NOMENCLATURE **xviii**

1 INTRODUCTION 1

2 LITERATURE REVIEW 3

2.1 Advanced Oxidation Processes 3

2.1.1 Photolysis 3

2.1.2 Fenton and Fenton-Like Process 4

2.1.3 Ozone (O_3) and UV-Assisted Ozone Water Reaction 5

2.1.4 Photocatalysis 5

2.2 Semiconductor Heterogeneous Photocatalysis 5

2.2.1 Modifications of Titanium Dioxide 8

2.2.2 Reactions of Titanium Dioxide by UV Light 10

2.2.3 Reaction Kinetics 11

2.3 Photocatalytic Reactors 12

2.3.1 Slurry Photocatalyst 16

2.3.2 Immobilised TiO_2 18

2.4 Spinning Disc Reactor 22

2.4.1 Spinning Disc Reactor Characteristics 23

2.4.2 Flow Regime on Spinning Disc Reactor Flow Regime and Residence Time Distribution on Spinning Disc Reactor 24

2.4.3 Spinning Disc Reactor Application 26

2.5 Pharmaceutical Wastewater 28

2.5.1 Ibuprofen 28

3 PROJECT OBJECTIVES 31

4 MATERIALS AND METHODS 32
4.1 Materials 32
4.2 Spinning Disc Reactor 32
4.3 Catalyst Immobilisation 34
4.4 Experimental Overview 35
4.5 Residence Time Distribution Studies 36
4.5.1 Residence Time Distribution Analysis 38
4.5.2 Determination of the Residence Time 39
4.5.3 Residence Time Behaviour of Reactor 40
4.6 Micromixing Study 40
4.6.1 Determination of Micro-Mixing Using the Villermaux-Dushman Reaction 41
4.7 Analytical Techniques 43
4.7.1 Scanning Electron Microscopy 43
4.7.2 X-ray Diffraction 43
4.7.3 High Performance Liquid Chromatography 43
4.7.4 UV-Vis 44
4.7.5 Liquid Chromatography–Mass Spectrometry 45
4.7.6 Total Organic Carbon 45
4.7.7 Dissolved Oxygen and pH Monitoring 46
5 SPINNING DISC REACTOR CHARACTERISATION - HYDRODYNAMICS OF THE FLUID FILM, RESIDENCE TIME DISTRIBUTION AND MICROMIXING 47
5.1 Introduction 47
5.2 Hydrodynamics of the Fluid Film 48
5.3 Residence Time Distribution Studies 56
5.3.1 Effect of Flowrate and Rotational Speed 58
5.3.2 Effect of Disc Surface 61
5.4 Micromixing Studies 67
5.4.1 Micromixing Analysis Using the Iodide-Iodate Reaction – Examining the Effect of Rotational Speed and Volumetric Flowrate 67
5.4.2 Micromixing Analysis Using the Iodide-Iodate Reaction – 70

Examining the Effect of Structure of the Disc
5.5 Conclusion 71
6 ENHANCING AND OPTIMISING THE REACTION RATE OF THE TIO_2 THIN FILM PHOTOCATALYST IN THE PHOTOCATALYTIC SPINNING DISC REACTOR (SDR) FOR METHYLENE BLUE AND IBUPROFEN 73
6.1 Introduction 73
6.2 Characterisation of the Titanium Dioxide Film 73
6.2.1 Scanning Electron Microscopy Analysis of Glass Disc Coatings 74
6.2.2 X-Ray Diffraction analysis 75
6.3 Photon flux and photonic efficiency 76
6.4 Adsorption and Photolysis Experiments in the Spinning Disc Reactor for Methylene Blue 77
6.5 Characterisation of the Photocatalytic Spinning Disc Reactor for Methylene Blue 78
6.5.1 Effect of Initial Reactant Concentration: Primary Degradation of Methylene Blue 79
6.5.2 Effect of Oxygen Feed, Rotational Speed and Feed Flowrates on Primary Degradation (Methylene Blue) 81
6.5.3 Examination of the Reaction Pathway – Reaction Intermediates Analysis 90
6.5.4 Reusability of the Thin Films 91
6.6 Adsorption and Photolysis Experiments in the Spinning Disc Reactor for Ibuprofen 93
6.7 Characterisation of the Photocatalytic Spinning Disc Reactor for Ibuprofen 94
6.8 Conclusions 101
7 PROCESS INTENSIFICATION IN THE PHOTOCATALYTIC SPINNING GROOVE DISC REACTOR 103
7.1 Characterisation of the Photocatalytic Spinning Mesh Disc Reactor for Methylene Blue 103
7.2 Characterisation of the Photocatalytic Spinning Groove Disc 106

Reactor for Methylene Blue
7.2.1 Effect of Disc Surface 106
7.2.2 Effect of Inlet Flowrate 108
7.2.3 Effect of Spinning Speed 110
7.2.4 Overall Comparison: SD, MGD and SGD 110
7.2.5 Intermediate Analysis 111
7.2.6 Smooth disc reaction intermediates 112
7.3 Characterisation of the Photocatalytic Spinning Groove Disc Reactor for Ibuprofen 118
7.3.1 Effect of Spinning Speed 118
7.3.2 Effect of Inlet Flowrate 119
7.3.4 Effect of Disc Surface 120
7.3.5 Effect of Added Oxygen 121
7.3.6 Overall Comparison of Reaction Rates 121
7.3.7 Intermediate Analysis 124
7.4 Conclusion 129
8 Conclusions and Recommendations for Future Work 131
8.1 Conclusions 131
8.2 Recommendations for Future Work 134
References 136
Appendices
Appendix A 150
Appendix B 156
Appendix C 157

LIST OF TABLES

Table No.		Page
2.1	Catalyst configuration advantages and disadvantages	15
4.1	Reagent concentrations used in this study	42
5.1	Dispersion parameters for water on smooth disc at different flowrates and rotational speeds.	61
6.1	Reaction rate constants for MB reactions at 10mL/s	85
6.2	Reaction rate constants for MB reactions at 300rpm speed	87
6.3	Effect of oxygen presence, spinning speed and feed flowrate on reaction rate and rate constant.	87

LIST OF FIGURES

Figure No.		Page
2.1	Schematic representation of the excitation of semiconductors by light irradiation	7
2.2	Position of the VB and CB as well as their band gaps for various metal oxides compared to the normal hydrogen electrode	8
2.3	Detail of the crystal lattice of rutile	9
2.4	Section of the crystal lattice of anatase	9
2.5	Kinetics of the photocatalytic reaction	12
2.6	Apparatus equal in accordance with heat and mass transfer capabilities	14
2.7	Examples of improved slurry reactors	17
2.8	Examples of monolithic catalysts	19
2.9	Selected microreactors	20
2.10	Spinning Disc Reactor	22
2.11	Chemical structure of ibuprofen	28
2.12	Formation of side chain products, their deep oxidation products and open ring intermediates of ibuprofen during photocatalytic degradation	29
4.1	SDR experimental set up	33
4.2	Dip coater	34
4.3	Disc surface	36
4.4	Set-up of probe and sampling shoe in reactor housing	37
5.1	Photographs of the liquid film on the rotating smooth disc, taken at different spinning speeds and inlet flowrates	50
5.2	Photographs of the liquid film close-up on the rotating smooth disc, taken at different numbers of revolutions.	51
5.3	Photographs of the liquid film on the rotating mesh disc, taken at different numbers of revolutions	53
5.4	Photographs of the liquid film on the rotating grooved disc, taken at different numbers of revolutions	55
5.5	Reproducibility of experiments on different disc surface	57
5.6	Influence of rotational speed on RTD on smooth disc	59
5.7	Effect of flowrate on RTD on smooth disc	60

5.8	Influence of grooved disc on RTD curves	63
5.9	The mean residence time at different spinning speeds and flow rates	64
5.10	The number of tanks-in-series (N) at different spinning speeds and flow rates	65
5.11	Number of tanks-in-series for smooth disc vs. grooved disc at different disc rotational speed.	66
5.12	Segregation index dependent on the disc speed and the volume flow at a dosing distance of r = 10 mm.	68
5.13	Calculated film thickness versus the rotational speed	69
5.14	Influence of the disc texture on the mixing quality (Q_{tot} = 9 mL/s).	70
6.1	Surface morphologies of the TiO_2 thin films before and after photocatalysis	74
6.2	Cross-sectional view of the surface morphologies of the TiO_2 thin films before and after photocatalysis.	75
6.3	XRD pattern of the TiO_2 coated onto glass disc calcined at 550°C	76
6.4	UV light intensity distribution near the surface of the disc in the photocatalytic spinning disc reactor.	77
6.5	Methylene Blue control experiments - adsorption and photolysis inside SDR	78
6.6	Effect of initial concentration of the photocatalytic degradation of MB in pSDR (UV-Vis).	80
6.7	Kinetics of MB degradation in pSDR with different concentration	81
6.8	Effect of spinning speed and oxygen feed (with and without) at 10mL/s flowrate (UV-Vis).	83
6.9	Reaction rate versus concentration for the results in Figure 6.8 showing that an apparent first order kinetic fit is appropriate now.	84
6.10	Effect of added oxygen and inlet flow rate on the primary degradation of MB at 300rpm spinning speed	85
6.11	Plot on the reaction rate at 300rpm speed	86
6.12	(a) Effect of flow rate and rotational speed on the surface rate constants of the degradation of methylene blue, (b) without added O_2 average initial reaction rate surface plot and (c) with added O_2 average initial reaction rate surface plot.	88
6.13	Reaction profile comparison of the reaction intermediates from methylene blue photocatalysed (15mL/s)	91
6.14	Relative Concentration of MB reduction with UV and with	92

	photocatalyst (15mL/s).	
6.15	Plot on the reaction rate	92
6.16	Ibuprofen adsorption and photolysis inside SDR	93
6.17	(a) Ibuprofen and (b) TOC degradation of 25 mg/L Ibuprofen at 10mL/s.	96
6.18	Reaction rate versus concentration for the results in Figure 6.18a showing that an apparent first order kinetic fit.	97
6.19	(a) Ibuprofen and (b) TOC degradation of 25 mg/L Ibuprofen at 15mL/s	98
6.20	Plot on the reaction rate of 25 mg/L Ibuprofen at 15mL/s.	99
6.21	Effect of flow rate and rotational speed on the rate of reaction of ibuprofen	100
7.1	Relative concentration of MB degradation	103
7.2	Relative concentration MB degradation at C_i=25mg/L.	104
7.3	Reaction rate for methylene blue degradation	105
7.4	Relative concentration of methylene blue degradation for SGD, C_i = 15mg/L.	107
7.5	Relative concentration of methylene blue degradation for MGD, C_i = 15mg/L.	108
7.6	Relative concentration of methylene blue degradation at 300rpm, Ci = 15mg/L.	109
7.7	Relative concentration of methylene blue degradation at 200rpm, Ci = 15mg/L.	109
7.8	Volumetric reaction rates comparing effect of rotational speed and inlet flowrate for the square grooved discs, mesh grooved discs and smooth disc.	111
7.9	Reaction profile comparison of the reaction intermediates for methylene blue photocatalysed on the smooth disc – SD	113
7.10	Reaction profile comparison of the reaction intermediates for methylene blue photocatalysed on the square grooved disc – SGD	114
7.11	Reaction profile comparison of the reaction intermediates for methylene blue photocatalysed on the mesh grooved disc – MGD	115
7.12	Possible degradation pathway of dyes MB	116
7.13	Reaction profile comparison of the highest and lowest reaction rate intermediates for methylene blue photocatalysed.	117
7.14	Relative concentration of ibuprofen degradation at different	119

flowrates, rotational speed and disc surface configuration.

7.15 Reaction rate of ibuprofen degradation at different flowrates, rotational speed and disc surface configuration. 120

7.16 Reaction rate of ibuprofen mineralisation in the spinning grooved disc reactor. 122

7.17 Relative concentration of TOC mineralisation degradation in the spinning grooved disc reactor. 123

7.18 Reaction rate constant of TOC mineralisation in the spinning grooved disc reactor. 124

7.19 Intermediates observed at the end of photocatalytic treatment of IBU. 125

7.20 Reaction profile comparison of the reaction intermediates for ibuprofen photocatalysed (smooth disc – SD) 126

7.21 Reaction profile comparison of the reaction intermediates for ibuprofen photocatalysed (square grooved – SGD) 127

7.22 Reaction profile comparison of the highest and lowest reaction rate intermediates for ibuprofen photocatalysed. 128

LIST OF ABBREVIATIONS

SDR	spinning disc reactor
pSDR	photocatalytic spinning disc reactor
pSGDR	photocatalytic spinning groove disc reactor
SGD	square groove disc
MGD	mesh groove disc
AOP	advanced oxidation processes
TiO_2	Titanium dioxide
VB	valence band
CB	conduction band
NHE	normal hydrogen electrode
MB	methylene blue
AA	Azure A
AB	Azure B
AC	Azure C
IBU	ibuprofen
TFA	trifluoroacetic acid
UV	ultraviolet
HPLC	high performance liquid chromatography
UV-Vis	ultra violet visible spectrophotometer
XRD	x-ray diffraction
SEM	scanning electron microscopy
LC-MS	liquid chromatography-mass spectrometry
TOC	total organic carbon
DO	dissolved oxygen
RTD	residence time distribution study

LIST OF NOMENCLATURES

S	Exposed Surface Area [m^2]
t	Time [min or s]
V	Liquid Volume [m^3 or L]
E(t)	Age distribution function [min^{-1}]
E(θ)	Age distribution function [min^{-1}]
V_R	Volume of reaction in operating condition [ms^{-1}]
k	Rate constant [s^{-1}]
θ	Dimensionless time parameter [-]
F(t)	Residence time function [min^{-1} or s^{-1}]
X_S	Segregation index [-]
Y	Actual amount of iodine produced [-]
Y_{TS}	Amount of iodine at maximum yield [-]
τ	Mean residence time [min or s]
$\dot{V}$	Volumetric flow rate [L/min or m^3/s]
N	Number of tanks-in-series

CHAPTER 1 INTRODUCTION

Over the past 10 years, increasing numbers of studies have identified numerous different water sources containing pharmaceutical. After use of the pharmaceuticals by humans, the constituents are excreted unchanged or as metabolites through urine and faeces and are subsequently incorporated into the influent of wastewater treatment plants. They then pass through the treatment plants into effluent streams practically unaffected and are discharged into surface waters (Kümmerer, 2001).

The common pharmaceutical compounds found in wastewater and the environment include antibiotics, prescription analgesic drugs, anti-epileptic drugs, and non-prescription drugs (Kümmerer, 2001; Kolpin *et al.*, 2002). Environmental effects consist of the development of antibiotic resistant bacteria in water treatment processes and in the aquatic environment; retardation of nitrite oxidation and methanogenesis and the potential increased toxicity of chemical combinations and metabolites (Kümmerer, 2001). However, the possible effects on human beings and aquatic ecosystems are not clearly understood.

Pharmaceuticals are present in surface waters and wastewaters around the world. Some pharmaceuticals are thought to be recalcitrant, inhibitory or toxic to biological treatment in both wastewater treatment works and in the environment. A number of studies have illustrated that advanced oxidation technologies (such as photocatalysis) can be used to improve the biodegradability of many of these compounds or even mineralise them. Thus, advanced oxidation may be the ideal technology to pre-treat these compounds for further biological treatment (such as in a municipal wastewater treatment works). The degradation by advanced oxidation of a number of important pharmaceuticals has yet to be studied and the breakdown mechanisms, identification of intermediates and oxidation products, their toxicity and biodegradability have yet to be quantified, indicating further work is required in this area.

This project will focus on optimising the key parameters controlling the reaction kinetics and mechanisms of the advanced oxidation by photocatalysis in an enhanced spinning disc reactor to obtain the optimal degree of pre-treatment of biologically recalcitrant compounds in pharmaceutical containing wastewaters to break them down into more biologically amenable compounds. Building on previous research by the Patterson research group, a new grooved surface catalyst for the UV spinning disc

reactor was developed and characterised. The grooved is intended to enhance mixing on the thin film: for conventional spinning disc reactors flow is typically laminar and not well mixed, leading to mass transfer limitations in heterogeneous catalytic reactions in such reactors. The grooved surface configuration will overcome these issues, producing a new technology, the photocatalytic spinning grooved disc reactor (pSGDR).

CHAPTER 2 LITERATURE REVIEW

2.1 Advanced Oxidation Processes

The use of alternative technologies that aim to transform the refractory molecules into other compounds that could be further biodegradable have become attention for many researchers. Advanced oxidation process (AOP) have been used for the treatment of wastewater containing volatile organic compounds such as pesticides, surfactants, and colouring. AOPs have been successfully used as a pre-treatment method for reducing the concentration of toxic organic compounds that inhibit the biological wastewater treatment process (Stasinakis, 2008).

The main mechanism function of AOPs is the generation of highly reactive free radicals. The hydroxyl radical (HO) are effective in destroying the organic chemical as it reacts quickly and non-selective with almost all the electron rich organic compounds. These radicals are capable of mineralising the portion of the substrate by reducing it to CO_2 and H_2O (Hernández *et al.*, 2009). This technique is used by many of researchers to degrade pollutants in wastewater, including synthetic dyes (Hernández *et al.*, 2009; Özcan *et al.*, 2009; Vatanpour, Daneshvar and Rasoulifard, 2009), and landfill leachate (Atmaca, 2009).

2.1.1 Photolysis

The formation of OH radicals by photolytic cleavage of water (see Equations. 2.1 and 2.2) occurs at wavelengths below 190 nm (VUV range) (Gonzalez and Braun, 1995; Lopez *et al.*, 2000; Oppenländer, 2003; Gonzalez *et al.*, 2004).

$$H_2O \xrightarrow{hv(185\ nm)} {}^{\cdot}OH + H^{\cdot} \qquad \varphi(+{}^{\bullet}OH) = 0.33 \qquad (2.1)$$

$$H_2O \xrightarrow{hv(185\ nm)} {}^{\cdot}OH + H^{+} + e^{-}_{aq} \qquad \varphi(+e_{aq}^{-}) = 0.045 \qquad (2.2)$$

The OH radicals formed are capable of forming hydrogen peroxide by recombination. In addition to OH radicals, hydrogen atoms and solvated electrons, which are strong oxidizing or reducing agents, are formed in this process. The photolysis process is an extended oxidation process that requires no further use of chemicals (Legrini, Oliveros

and Braun, 1993). The absorption coefficient of water at 185 nm is $\alpha = 1.8\ cm^{-1}$ (25°C). Based on this, it was calculated that 90% of the radiation intensity is absorbed within 5 mm of the layer thickness of the water (Han *et al.*, 2004). Lopez *et al.* (2000), a layer of only 300 μm is indicated, in which the radiation is to be completely absorbed. As a result, the photo-induced formation of OH radicals can only take place in this thin layer around the dip tube (Oppenländer, 2003). As a result of this film formation, the radicals formed are subject to a relatively uneven distribution, which can strongly influence the performance of the system. In addition, the average irradiation strength can only be ensured in the entire reactor chamber by thorough mixing (turbulent conditions).

2.1.2 Fenton and Fenton-Like Process

One of the most important AOPs is the Fenton system, consisting of the reaction H_2O_2 and Fe^{2+} to form $^{\bullet}OH$. Hydrogen peroxide is a compound that is environmentally friendly only leaving O_2 and water as by-products. These compounds are used as disinfectants in the medical and industrial as well as an oxidant in the synthesis of product and wastewater treatment. The direct use of hydrogen peroxide for wastewater treatment was limited due to the low oxidation (Hernández *et al.*, 2009).

The Fenton reaction involves several stages in which the hydroxyl free radical ($^{\bullet}OH$) and hydroperoxyl ($HO_2^{\bullet}$) result. The mechanism for free radical formation is as follows (Vatanpour, Daneshvar and Rasoulifard, 2009):

$$Fe^{2+} + H_2O_2 \rightarrow Fe^{3+} + {}^{\bullet}OH + OH^- \quad (2.3)$$

$$^{\bullet}OH + H_2O_2 \rightarrow H_2O + HO_2^{\bullet} \quad (2.4)$$

$$Fe^{3+} + HO_2^{\bullet} \rightarrow Fe^{2+} + H^+ + O_2 \quad (2.5)$$

$$Fe^{2+} + HO_2^{\bullet} \rightarrow Fe^{3+} + HO_2^- \quad (2.6)$$

$$Fe^{2+} + {}^{\bullet}OH \rightarrow Fe^{3+} + OH^- \quad (2.7)$$

2.1.3 UV/Peroxide Process (UV/H_2O_2)

Under UV irradiation with wavelengths below 280 nm, dissociation of hydrogen peroxide leads to the formation of OH radicals (Equation 2.8). The formation of OH by means of UV/$_2O_2$ is strongly pH-dependent (Legrini, Oliveros and Braun, 1993).

$$\cdot OH + \cdot OH \xleftrightarrow{hv < 280\ nm} H_2O_2 \leftrightarrow H^+ + HO_2^- \quad (2.8)$$

An advantage is that hydrogen peroxide is commercially available, stable and readily soluble in water. Operation is simple and low cost. However, hydrogen peroxide itself can act as a free-radical scavenger and has only a small absorption at the wavelength used (254 nm) (Sarathy and Mohseni, 2006). Since the OH radicals formed can recombine within the solvent, the quantum yield for the dissociation of hydrogen peroxide in aqueous solutions is only 0.5. Furthermore, residual concentration of hydrogen peroxide need to be removed from the water after the treatment.

2.1.4 Photocatalysis

The precise definition of the term "photocatalysis" is still controversially discussed in the literature. Decisive for the large number of definitions is the role played by photons in the catalytic process. Serpone *et al.* (1993) try to use a common glossary of different common terms, e.g. photoinduced catalytic reaction, catalysed photoreaction, photoassisted catalysis, and more to clarify and to standardise the terms (Serpone and Emeline, 2002). The same authors give a simple definition for photocatalysis: “Photocatalysis is the acceleration of a photoreaction by the action of a catalyst”.

2.2 Semiconductor Heterogeneous Photocatalysis

Semiconductors as photocatalysts have been intensively researched since the end of the 1960s. Work began by Fujishima and Honda, 1972, which described the photochemical decomposition of water on titanium dioxide electrodes. The first successful materials are from Frank and Bard, 1977, work on the decomposition of organic which successfully decomposed cyanides in aqueous solution. Since these pioneering work of the 1970s, the interest in the photoactive semiconductors has grown steadily. Many studies have been published dealing with the decomposition of

organic pollutants and also greenhouse gases by semiconductor under irradiation with UV light. In the case where the semiconductors are usually inexpensive and chemically stable materials, these are predestined to provide environmental friendly methods e.g. for drinking and wastewater purification. The semiconductors used are usually TiO_2, ZnO or CdS, with TiO_2 being the most widely used semiconductor for these applications since it is also not toxic.

The use of the term "photocatalysis" in the use of semiconductors for the decomposition of pollutants is very controversial. However, the light "reacts" with the semiconductor to bring it into an excited state, so the designation of a photo-induced or photoactivated reaction is actually the correct one. Since it has been found in the literature to state as semiconductor photocatalysis, this term is also used here. Semiconductor photocatalysis in principle, is heterogeneous catalysis. There are basically two possibilities. First, the irradiated light can be used to excite a molecule adsorbed on the catalyst surface, which then reacts in the excited state with the catalyst in the basic state. This is also referred to as a catalysed photoreaction. The second one, the catalyst itself can be excited, which then interacts with the adsorbed molecule in the basic state in the excited state. This case is also referred to as a sensitized photoreaction. Both cases are generally summarized under the term "heterogeneous photocatalysis" (Hoffmann *et al.*, 1995; Mills and Le Hunte, 1997).

The semiconductor is activated by absorbing a photon with an energy sufficient to transfer an electron from the valence band (VB) into the conduction band (CB). This is given when the energy of the incident light which is inversely proportional to the wavelength (typically UV light) is greater than the band gap of the titanium dioxide. The band gap is defined as the energy necessary to transfer an electron from the VB to the CB. This results in an electron gap (h^+) in the VB and an electron excess (e^-) in the CB. These electron hole pairs can now recombine either inside or on the surface of the semiconductor (Figure 2.1a, b) or with surface adsorbed electron acceptors (e.g. O_2) (Figure 2.1c) or donors (e.g. OH^-) 2.1d). This is shown schematically in Figure 2.1 (Wilhelm and Stephan, 2007).

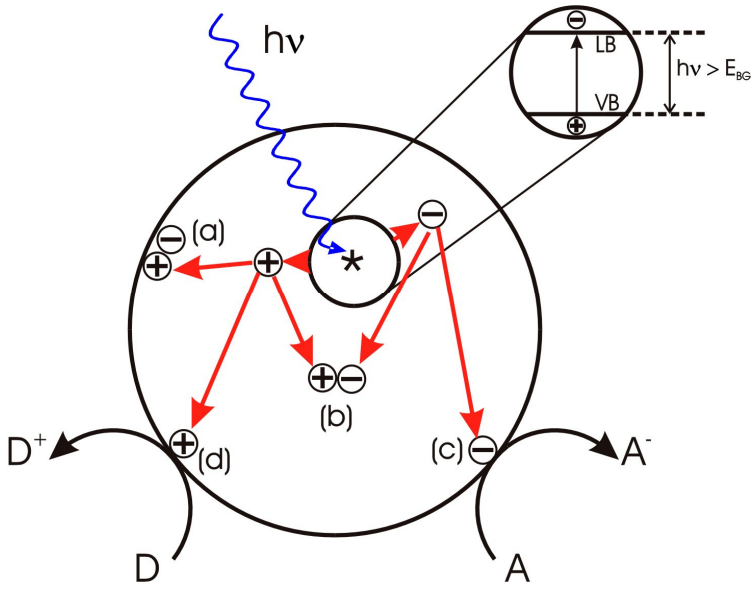

Figure 2.1: Schematic representation of the excitation of semiconductors by light irradiation (Wilhelm and Stephan, 2007).

In order for a semiconductor to photoreduce a species, the conduction band of the semiconductor must have more negative potential than the reduction potential of the species. For photooxidation, the valence band must have more positive potential than the oxidation potential of the species to be oxidized. An overview of the position of the VB and CB as well as the band gaps of semiconductors compared to the normal hydrogen electrode (NHE) is shown in Figure 2.2.

As clearly can be seen from the figure, the decomposition of water with the use of a rutile anode had to be subjected to additional voltage because the potential of rutile is not sufficient to reduce protons to hydrogen (Fujishima and Honda, 1972). When anatase is used, which has a slightly larger band gap, this is possible without further energy supply.

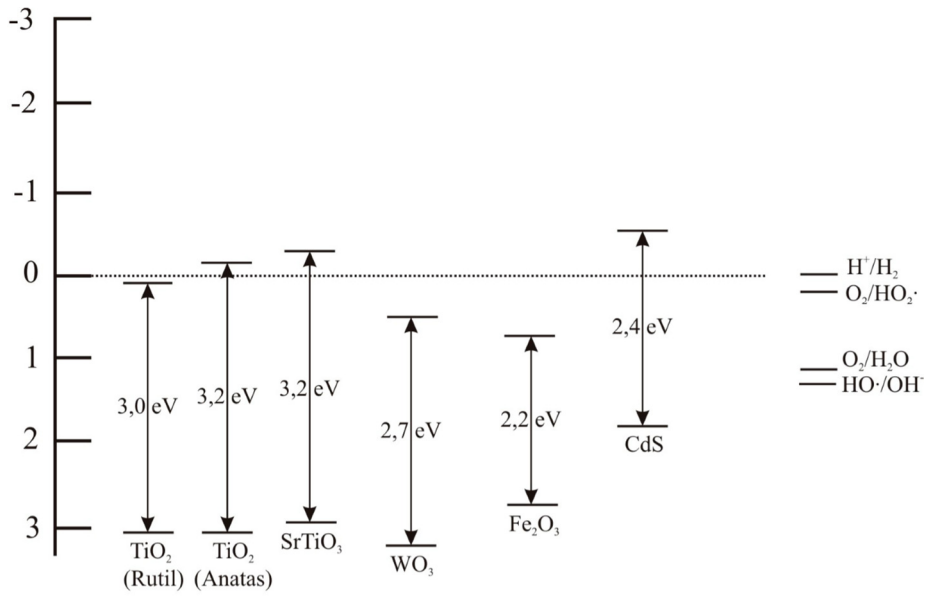

Figure 2.2: Position of the VB and CB as well as their band gaps for various metal oxides compared to the normal hydrogen electrode (Mills and Le Hunte, 1997).

2.2.1 Modifications of Titanium Dioxide

The semiconductor titanium dioxide occurs in three modifications with different crystal structures, which have different physical properties. These are anatase, rutile and brookite. Rutile represents the thermodynamically stable modification, which is why the two other modifications are rearranged at temperatures of 750°C (brookite) and 915°C (anatase) to rutile. However, only the modifications of rutile and anatase are of technical importance; therefore the representation of the crystal structure and physical properties of brookite is omitted in this work.

In all modifications, the titanates are distorted octahedrically by oxygen atoms. In the case of rutile, a hexagonal densest spherical packing of the oxygen atoms occurs, with half of the octahedron gaps occupied by titanate atoms. In the modification of anatase, a cubic-dense spherical packing of the oxygen atoms occurs, in which half of the tetrahedron gaps are occupied by titanate atoms. Figure 2.3 shows a section of the crystal structure of rutile. From the crystal structure, octahedral chains occur in the rutile, which are bridged over two common edges. The octahedron chains, in turn, are linked to each other by another octahedron. In the case of anatase (Figure 2.4), the octahedral in a layer are connected to each other by four corners. Upwards and

downwards, each octahedron is linked to the neighbouring octahedral via two edges each (Winkler, 2013).

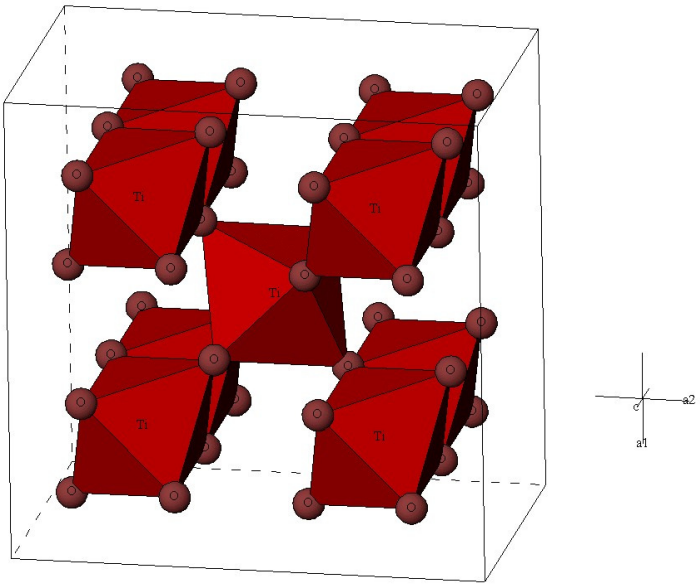

Figure 2.3: Detail of the crystal lattice of rutile

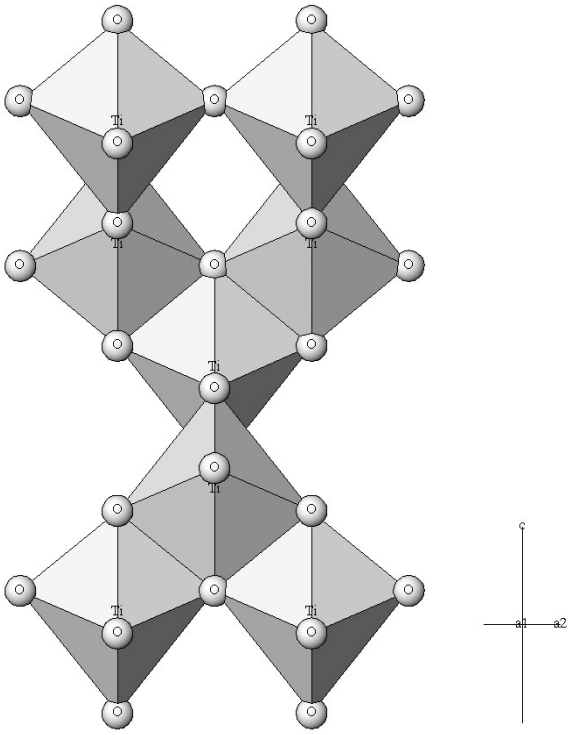

Figure 2.4: Section of the crystal lattice of anatase

Both modifications have a high refractive index (anatase: 2.55, rutile: 2.7), which is the basis for the use as white pigment (high covering force). Since anatase has a lower Mohs hardness than rutile, anatase is mainly used as white pigment, where the lower abrasiveness offers a technical advantage (e.g., paper and textile industry). As described in Section 2.2.1, rutile is mainly used in white colouring pigments because it has a lower photocatalytic activity compared to anatase. The lower photocatalytic activity of the rutile is due to the absorption edge shifted into the visible region of the light ($\lambda \approx 397$ nm). Anatase has an absorption edge ($\lambda \approx 350$ nm) shifted into the UV range and is therefore the photocatalytically more active modification. The difference absorption behaviour results in the different band gaps of the two semiconductor modifications. Rutile has a band gap of about 3.0 eV, while anatase is about 3.2 eV, which in turn explains the higher activity of the anatase. Since both titanium dioxide modifications are chemically very stable and non-toxic, they are also used as fillers and pigments in tablets, toothpaste and foodstuffs (Winkler, 2013).

2.2.2 Reactions of Titanium Dioxide by UV Light

As already mentioned in Section 2.2, the semiconductor titanium dioxide is excited by irradiation with light of sufficient energy, and the processes presented in Figure 2.1 can occur. For the rutile modification with a bandgap E_g = 3.0 eV this corresponds to light with a wavelength of approx. 410 nm and in the case of anatase with E_g = 3.2 eV approx. 380 nm (Carp, Huisman and Reller, 2004). This means that UV light is necessary to excite both modifications. Anatase is the more reactive of the two modifications because it has a higher bandgap. The electron hole pairs can now react with adsorbed electron acceptors or donors on the surface. In the case of O_2 as the acceptor, superoxide ions O_2^- and OH· are formed as donor hydroxyl radicals. Both species are very reactive and are known to decompose organic material (Carp, Huisman and Reller, 2004; Tennakone and Wijayantha, 2005). Equations 2.9 – 2.13 shows an overview of the reactions occurring.

$$TiO_2 \rightarrow TiO_2 + h^+ + e^- \tag{2.9}$$

$$O_2(g) + e^- \rightarrow O_2^-(ads) \tag{2.10}$$

$$H_2O \rightleftharpoons H^+ + OH^- \tag{2.11}$$

$$O_2^-(ads) + H^+ \rightleftharpoons HO_2 \cdot (ads) \quad (2.12)$$

$$h^+ + OH^- \rightarrow \cdot OH(ads) \quad (2.13)$$

The presence of moisture and oxygen is necessary to form the reactive radical species. In addition to the formation of hydroxyl radicals and superoxide ions, the material to be decomposed can also interact directly with the titanium dioxide in its basic state or excited state, as a result of which its decomposition is also induced.

2.2.3 Reaction Kinetics

When the photocatalyst, TiO_2, is excited with UV radiation (λ = 320 nm - 400 nm), the reactive OH radicals are generated on its surface of adsorbed water molecules (see Section 2.1). These radicals can cause the oxidation of organic water contaminants. The process can be described as follows:

a. Excitation of the catalyst and generation of OH radicals.

b. Transport of organic substances and O_2 to the surface of the catalyst.

c. Adsorption of organic substances and O_2 on TiO_2.

d. Reaction of water impurities (and oxidation intermediates) with OH radicals and reaction of O_2 and e^- on the surface. Recombination of charge carriers, h^+ and e^-

e. Desorption of the oxidation products.

f. Transport the products back into the solution.

Steps **a** to **f** are shown in Fig. 2.5. Since the processes take place successively, the slowest step determines the degradation rate when it is much slower than the other steps. Bahnemann et al., 1984 reported a very rapid excitation of the catalyst and generation of $OH^{\bullet}$, therefore step **a** can be neglected. In order to minimize the influence of the oxidation intermediates, the initial degradation rate is taken into account when formulating kinetic approaches. Thus, processes **e** and **f** can be neglected. The kinetics are determined by the steps **b**, **c** and **d**, namely, mass transport, adsorption and reaction.

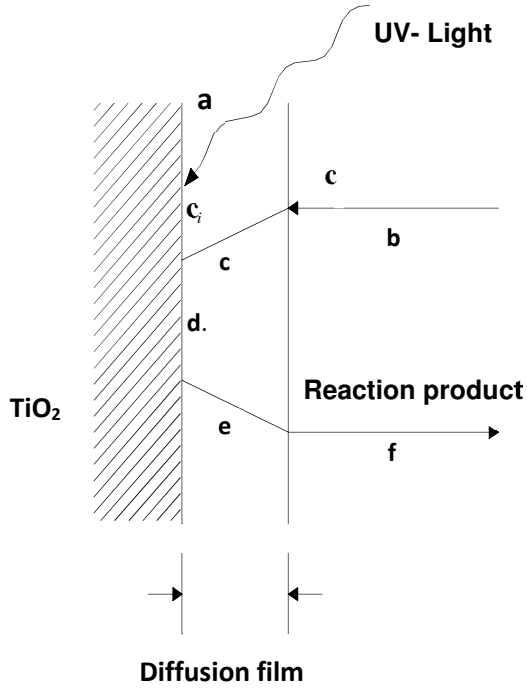

Figure 2.5: Kinetics of the photocatalytic reaction: **a**. Excitation of the catalyst; **b**. Transport of substances; **c**. Adsorption; **d**. Reaction; **e**. Desorption; **f.** Transport of the products.

2.3 Photocatalytic Reactors

One of the most important factors for photocatalytic reactors design is the kinetics of the process. It is mainly influenced by the following parameters: light intensity, type of catalyst and its concentration, concentration of pollutant, adsorption of the pollutant to the catalyst, nature of the water (pH, concentration of dissolved substances such as HCO_3^-, Cl^-, PO_4^{3-}, SO_4^{2-}, humic acid, etc.). In the case of the immobilised catalyst, the flow ratio plays an important role; in the case of TiO_2 in suspension, the separation of the catalyst is the greatest obstacle, and in the case of reactors with circulation, care must be taken that the dead volume in the circulation tank does not adversely affect the performance of the reactor.

In the case of TiO_2 in suspension, a plateau of the velocity is usually reached at concentrations of catalyst above 1 g/L. The use of higher concentrations does not contribute much to the acceleration of the process, but could make the separation of the catalyst considerably more difficult. For TiO_2, a plateau is formed on glass plates with TiO_2 layer thicknesses between 2 and 10 μm (Chang, Wu and Zhu, 2000). This corresponds to TiO_2 concentrations between 6.4 and 32 g/m^2. However, the catalyst

layer becomes brittle on glass plates from concentrations above 20 g/m^2 and is therefore not suitable.

In the case of high pollutant concentrations, the reactor must be supplied with an external supply of air or oxygen, so that no limitation by oxygen input occurs. This is the case with most sewers. However, the addition of pure oxygen or electron acceptors (H_2O_2, Ag^+, etc.) is not useful at low light intensities, as is the case with solar reactors.

In principle, the effect of different influencing variables on adsorption can be determined from the relevant literature or by experimental investigations. However, it can generally be assumed that the Langmuir isotherm gives a good representation of the adsorption. Strongly hydrophilic substances are not adsorbed as well as substances which have hydrophobic groups in their structure. Substances which are negatively charged in an acidic environment (e.g., organic acids) are adsorbed more strongly at low pH values, and substances which are neutrally charged are adsorbed more strongly in the neutral environment. Normally the oxidation is promoted by higher loading, but an inhibition of the reaction could occur if the loading is above 110 µmol/g.

A high concentration of inorganic ions such as Cl^-, PO_4^{3-}, SO_4^{2-}, etc. can impair the oxidation by adsorbing these substances preferentially to TiO_2, and thus only small amounts of substrate can be achieved. A high concentration of HCO_3 or humic acids can make oxidation more difficult, since these substances can act as $OH^\bullet$ scavengers, thereby impairing the oxidative effect of the catalyst.

Ajona and Vidal (2000) reported the interpretation, construction and preliminary results of a solar reactor. In this reactor, TiO_2 was used in suspension at a concentration of 0.5 g/L to convert the herbicide EPTC (S-ethyl-N, N-dipropyl thiocarbamate) from an initial concentration of 20-500 µg/L to one concentration lower than 0.1 µg/L. It was a Pyrex glass tube reactor, and in the rear part, reflectors were installed in a special configuration to make the best use of sunlight. The design of the reflectors and the position of the reactor with respect to the light irradiation were optimized by modelling. In the degradation experiments, the reaction was operated discontinuously and a_{ill} was about 30 m^{-1}. The herbicide is rapidly degraded and a pseudo-first-order kinetics coefficient between 0.15 - 0.17 min^{-1} was determined. The pollutant concentration decreases below 0.1 µg/L within 30 to 50 min.

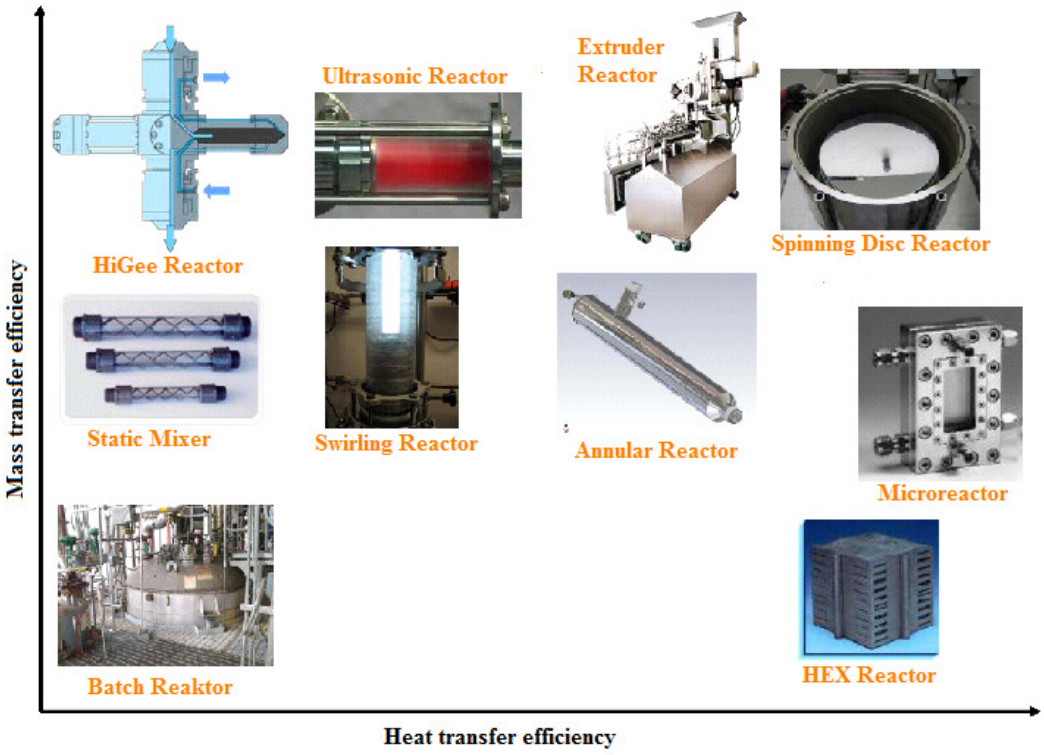

Figure 2.6: Apparatus equal in accordance with heat and mass transfer capabilities.

The ability of a reactor with effective heat and mass transfer determines the advantage of using high reaction temperatures in application. In Figure 2.6, different reactor are presented according to their efficiency for heat and mass transfer (Stankiewicz and Moulijn, 2000, 2004; Van Gerven *et al.*, 2007; Górak and Stankiewicz, 2011). On the one hand, three conventional apparatuses (batch reactor, plate heat exchanger, static mixer) are selected as the basis for this comparison. On the other hand, reactors under process intensification, such as the reactive extruder, ultrasonic reactor HiGee reactor, microreactor and SDR as process intensifying reactors are taken into consideration. A comparison of all reactors is applied in Figure 2.6.

As shown in Figure 2.6, the static mixer reactor, the microreactor, the extruder reactor and the SDR are considered as reactors which at the same time have good heat transfer and good mass transfer and can also be operated at high temperatures.

There are two main categories of catalyst configurations: slurry and immobilised. Slurry catalysts are usually insoluble powders mixed with the reactants and fed into the reactor together. Immobilised catalyst usually involves fixing the catalyst onto

support substrates which will be kept inside the reactor for certain periods of reaction cycles. Both types of catalyst configuration have their advantages and disadvantages (Table 2.1).

Table 2.1: Catalyst configuration advantages and disadvantages

Catalyst Configuration	Advantages	Disadvantages	Reference
Powdered (slurry)	• Huge total surface area can be achieved by reducing powder size • High mass transfer • Pre-adsorption of reactants onto the catalyst prior to entering reactor • Degussa P25 powder very photoactive	• May agglomerate to form into larger particles, reducing surface area • Continuous stirring required to prevent powders from precipitating • The smaller the powder size, the harder it is to recover the catalyst • Shadowing effect reduces the penetration of photons deeper into the solution	Sclafani, Palmisano and Schiavello, 1990; Kumazawa, Inoue and Kasuya, 2003; Jiang *et al.*, 2010; Kim, Choo and Park, 2010; McCullagh *et al.*, 2010; Ehrampoosh, 2011; Cheng *et al.*, 2012
Coated reactor wall	• Catalyst recovery is simple • Can be very transparent for better photon penetration	• Surface area always limited • Lower mass transfer • Catalyst only at the walls of the reactor • Requires larger coating equipment compared to plate and beads	Akyol and Bayramoglu, 2010; Jović *et al.*, 2012
Coated plate	• Catalyst recovery is simple • Easy to fabricate for laboratory experiments • Easy to analyse coating properties • Does not require large coating equipment	• Small surface area • Lower mass transfer • Coating onto stainless still will fully block photon penetration	Černigoj, Štangar and Trebše, 2007; Donaldson and Zhang, 2011; Stephan, Ludovic and Dominique, 2011
Coated beads	• Higher surface area than coated wall and plate • Can be packed together to disrupt laminar flow	• Both coating and beads needs to be very transparent for good photon penetration • Unless only 1 layer of beads is used, it	Geng and Cui, 2010; Pozzo *et al.*, 2010; Yurdakal *et al.*, 2010; Rao, Chaturvedi and Li Puma, 2012

	resulting in higher mass transfer • Easy to recover catalyst • Does not require large coating equipment	can take a lot of beads to pack up a reactor • Quartz beads may be required in multi-layered beads packing	
Coated mesh/foam	• Higher surface area • Depending on arrangement, can disrupt laminar flow thus increasing mass transfer • Easy to recover catalyst • Can either be structural or in plate-like dimensions for flexibility of implementation	• May require larger coating equipment than plates and beads • The common substrate – stainless steel will block photon penetration	Zhu *et al.*, 2012
Monolith/capillary	• Large available surface area for catalyst immobilisation • Channelled flow of fluids	• A higher pressure drop compared to annular reactors • Construction and coating of the monolith/capillary structure can be complicated, especially for photocatalysis • Difficult to clean	Zhang *et al.*, 2012

2.3.1 Slurry Photocatalyst

When designing reactors with TiO_2 in suspension, it is first necessary to consider whether the catalyst is excited by sunlight or by lamps. Since, at high light intensities, the recombination of charge carriers can become the rate-limiting step, the use of lamps with high intensities allows the reaction to be accelerated by the addition of electron scavengers such as hydrogen peroxide or pure oxygen. In order to be able to exploit the best light intensity, doped (often with Pt) catalysts could be used. If the catalyst is irradiated with sunlight or with low light intensities, the addition of electron scavengers or the use of doped catalysts often only results in a moderate improvement in the process, since the reaction mainly depends on the adsorption phenomena.

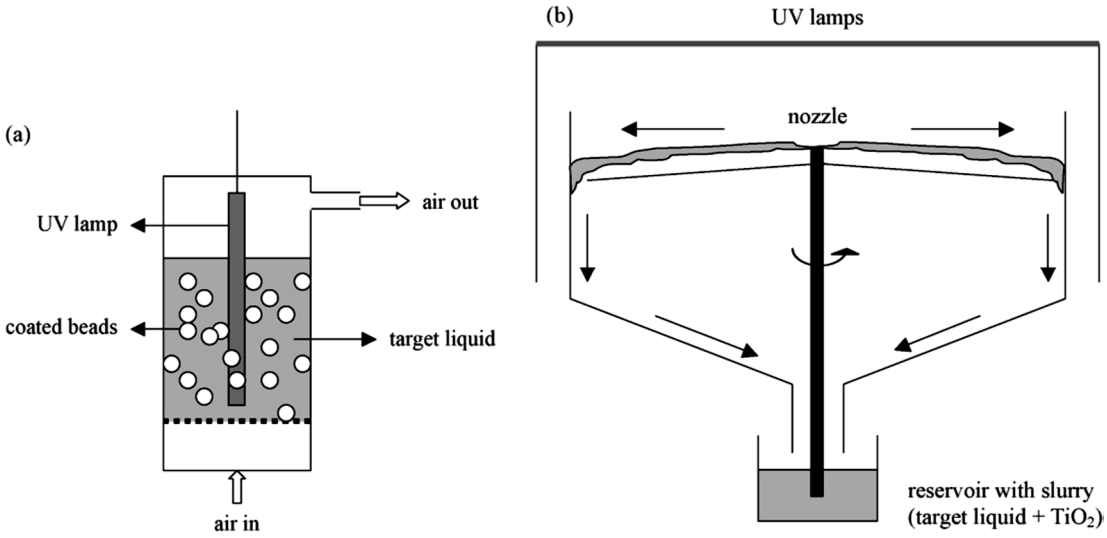

Figure 2.7: Examples of improved slurry reactors: (a) fluidised bed reactor and (b) fountain reactor (Li Puma and Yue, 2001; Lim and Kim, 2004)

Li Puma and Yue (2001) (Figure 2.7) developed a special reactor configuration in order to best utilize the light intensity of a UV lamp. The activity in the reactor was based on the irradiation of a falling film of a TiO_2 suspension. A UV lamp (black light 36W) was installed in a stainless steel tube. The reactor flow was from its upper side with the TiO_2 suspension. A thin film of the suspension flowed down the inner wall of the tube. According to the authors, this reactor is best to exploit the UV light, since the radiation reflected by the TiO_2 particles remains within the reactor and ultimately leads to a reaction.

The use of sunlight as a source of light can be an advantageous option for wastewater purification in areas where solar radiation is strong. For example, various pesticides were treated under sunlight in TiO_2 suspensions (P-25; 0.2 g/L) in the technical plant "Solar Platform" in Almería-Spain (4380 solar hours per year) (Malato *et al.*, 1999). The most important investigated substances were: imidachloroprid, pyrimethanyl and oxymyl. The initial concentration of the solutions was approximately 100 mg/L TOC. The reaction volume was 0.247 m^3 and the exposed surface area was 8.9 m^2. This corresponds to a specific irradiated surface of about 36 m^{-1}. The UV irradiation intensity of a sunny day in Almería is on average about 18.6 W/m^2.

Wang (2000) investigated the photocatalytic oxidation of eight different dyes. Solutions with 20 mg/L of dye and 1 g/L of TiO_2 (Beijing Chemical Industrial Company, Anatase, $\alpha_{BET} = 9\ m^2/g$) were irradiated with sunlight for 4 hours (average light intensity of 21.3 W/m^2). It has been found that all solutions are decolorized between 80% and 100% within this period. The content of dissolved organic carbon (DOC) is only eliminated by approx. 20%. Chloride and sulfate were determined as degradation products.

2.3.2 Immobilised Titanium Dioxide

Although the reaction in the suspended catalyst is two to three times faster than with immobilised titanium dioxide (TiO_2), the separation of the catalyst is an obstacle to the use of this technology. Immobilising TiO_2 on carrier materials proves to be an interesting alternative solar reactor configurations.

Feitz, Boyden and Waite (2000) compared two solar reactors with immobilised TiO_2 for the oxidation of phenol. In the first reactor (dimensions: 6.5 m; length: 0.5 m width), TiO_2 was immobilized on glass fibers at a concentration of catalyst of 5 g/m^2. 200 L of phenol solution (2.3 mg/L) with a flowrate of 5 L/min were fed into the reactor from a storage container. This results in a residence time in the reactor of 30 s and a ratio of specific irradiated surface area to total volume was 16 m^{-1}. The second reactor was a fixed-bed reactor filled with TiO_2-coated Raschig rings. The reactor of stainless steel had the following dimensions: 2 m in length; 1 m width; 6.5 cm deep. The reactor was flow with 100 L of phenol solution (2.3 mg/L), which was circulated at a flowrate of 3 L/min. The residence time in the reactor is approximately 30 minutes and approximately sunlight irradiation was 20 m^{-1}. Air was fed to the reactor by a compressor.

It was found that the elimination of phenol at comparable light intensities is much faster in the fixed-bed reactor with the Raschig rings than in the reactor with the coated glass fibers. The coefficients of a kinetics of pseudo-first order are 0.021 min^{-1} in the first case and 0.0024 min^{-1} in the second case. The greatly reduced speed in the reactor with the glass fibers, on the one hand, can be attributed to a large dead volume in the storage container. On the other hand, it must be considered that a much higher concentration of TiO_2 is present in the fixed bed reactor. With the assumption of a

specific surface area of the Raschig rings about 600 m^{-1} and a coating of about 5 g/m^2, a TiO_2 content is obtained with a reactor volume of 130 L (hollow volume 70%) and a volume of the solution of 100 L about 4 g/L (based on the volume of the solution). In the reactor with the glass fibers, a total amount of TiO_2 in the reactor of 16.25 g (5 $g/m^2 \times 3.25\ m^2$) and a concentration of less than 0.1 g/L (based on the volume of the solution is obtained by 200 L).

The fixed-bed reactor proves to be a good reactor configuration, since an acceptable speed can be achieved despite an excessively high space requirement with $\alpha_{ill} \sim 20\ m^{-1}$. The main disadvantage of this reactor is the detachment of the TiO_2 layer by friction between the Raschig rings, which could occur during the supply of water or air.

On the other hand, reactors under process intensification also being applied in immobilisation catalyst reactor, such as the monolith, microreactor and SDR as process intensifying reactors are taken into consideration.

2.3.2.1 Monolith Catalyst

The so-called "open-cross-flow structure catalyst" has been developed for reactions which are catalyzed by solids and at the same time require good mixing. Structured packs are often used in the range of distillation processes.

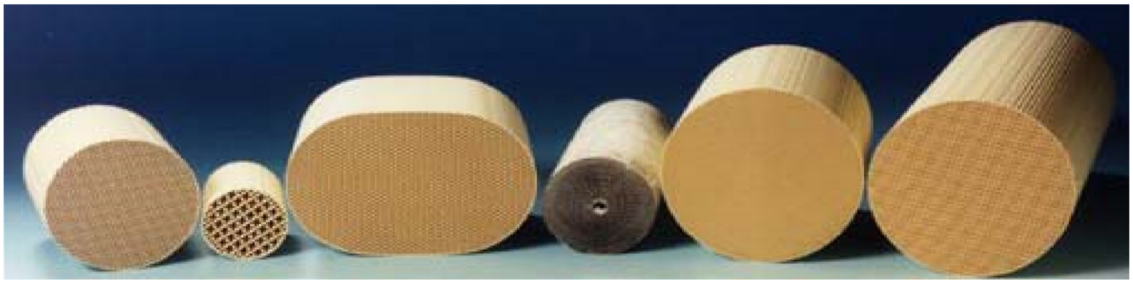

Figure 2.8: Examples of monolithic catalysts (Kapteijn *et al.*, 1999)

Heterogeneous catalytic processes can normally be intensified by the use of monolithic catalysts (Kapteijn *et al.*, 1999). Monolithic catalysts consist of metallic or ceramic

materials and have many straight and narrow channels with a certain uniform cross-sectional shape, the so-called honeycomb structure (Figure 2.8).

To provide sufficient porosity and increase the catalytically active surface, monolithic catalysts are normally coated with a "washcoat". The washcoat consists of a powder suspension (often a mixture of aluminum oxide, silicon oxide and other metal oxides). This (usually aqueous) powder suspension is applied to the honeycomb, dried, then impregnated with an active metal component (e.g. platinum, rhodium or palladium) and subsequently activated by calcination. Monolithic catalysts have very low pressure losses (10 to 100 times lower than conventional fixed bed packs), high geometric surfaces per reactor volume (one to four times higher than particle catalyst reactors) and high catalytic performance (almost one hundred percent) due to the very short diffusion path in the washcoats (Stankiewicz, 2001).

2.3.2.2 Microreactor

Microreactors are small scale chemical reactors and usually have a sandwich structure (Figure 2.9).

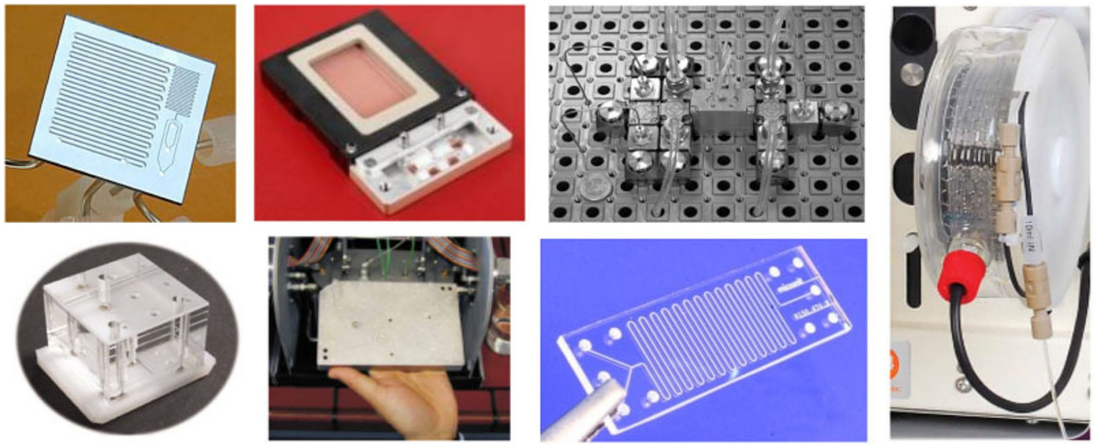

Figure 2.9: Selected microreactors (Geyer and Seeberger, 2009)

In such a structure, there are several layers with microchannels. The diameter of the microchannels is normally in the range of 10 to several 100 µm (Fig. 2.9). This layered structure of the microreactors can perform various functions, such as mixing, catalytic

reactions, heat exchange, and material separation. The combination of different functions in one operating unit is an important advantage of the microreactors. The very high heat transfer capacity of the microreactors allows isothermal processes for strongly exothermic reactions. Because of the very low volume-to-surface ratio, microreactors are a potential alternative for reactions with toxic or explosive precursors.

2.3.2.3 The Spinning Disc Reactor

The Spinning Disc Reactor (SDR) was developed by Ramshaw's group at the University of Newcastle (Ramshaw, 1985). As an alternative to the HiGee reactor, a rotating disc (spinning disc) is used for the SDR. The objective of this development is to produce a regular thin liquid film on the disc when a liquid is supplied into the disc center or its vicinity. This liquid is first accelerated tangentially by the shear stress which is formed at the boundary surface between the disc and the liquid. This acceleration leads to the approach of the liquid speed to the angular velocity of the disc. Thereafter, the liquid normally moves outward through the predominantly centrifugal acceleration in the form of a diluting and spreading film. A representation of the SDR is shown in Figure 2.10.

Liquid or solutions can be flow to the rotating disc by using of nozzle. Liquid which are applied to the disc are accelerated and carried outwards. After leaving the disc, the liquid are thrown against the inside of a peripheral internal wall, run down on it and are finally collected at an outlet. Both the disc and the wall can be controlled separately. The SDR has a cover in which there are several openings for, inlet feed, pressure control, and vacuum operation.

The SDR brings with it features such as continuous operation, short residence time, and good heat and mass transfer, and thus, as a potentially alternative apparatus for process intensification, gains more and more interests and observations in the chemical industries (Ramshaw, 1985).

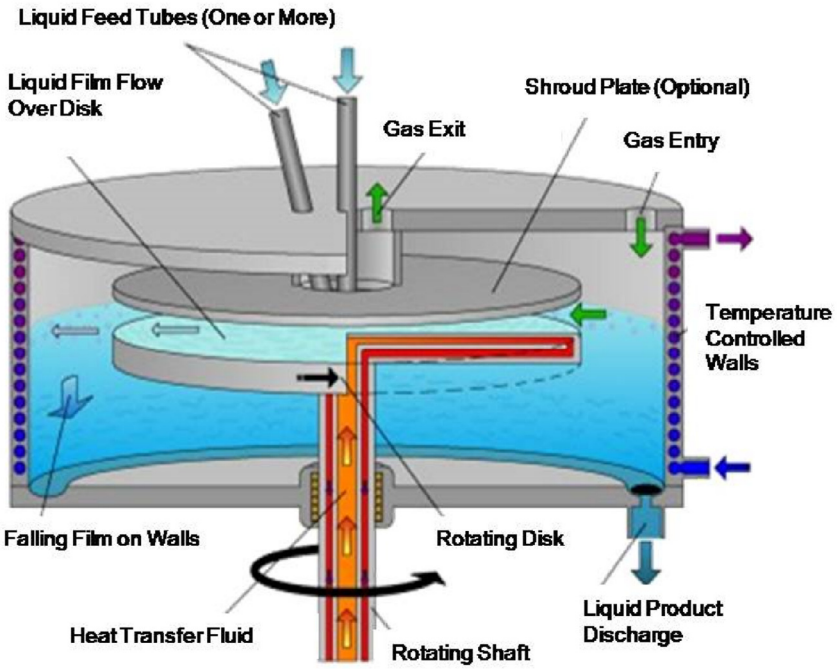

Figure 2.10: Spinning disc reactor (Ramshaw, 1985).

2.4 Spinning Disc Reactor

The pursuit of the chemical industry for increasingly efficient and smaller reactors for providing sustainable and safe production processes is currently being driven not only by economic interests, but also by legal regulations and the growing environmental awareness among the public. Under the slogan of process intensification efforts to drastic improvement of existing or newly developing processes are summarized.

The drastic improvement of existing chemical processes by introducing new and innovative equipment and procedures is a major goal of process intensification (Stankiewicz and Moulijn, 2000). The focus targets such as more efficient and cost-effective production, a higher environmental impact, increased reliability and improved product properties in the foreground. Based on the HIGEE Technology, the use of high acceleration forces in rotating packed beds in early 1980s by Colin Ramshaw, a promising reactor concept for this purpose which is the spinning disc reactor (SDR) has been developed (Ramshaw, 1985). The principle of the SDR based on the formation of a thin liquid film in the order of magnitude between 20 and 300 µm on a rotating surface. This liquid film is formed due to high tangential and radial acceleration, which are caused by the shear and centrifugal forces on the disc. This

provides a very good and high micromixing due to the high surface to volume ratio mass and heat transfer coefficients arise.

These properties are useful in a variety of reactions, such as homogeneous or heterogeneous-catalysed reactions, as well as precipitation processes is of great importance, since the rapid dissipation of heat and the high degree of micromixing leads to an improved product quality. The micromixing is of particular importance; if the time of the reaction in the same order as the mixing time, the reaction time is shorter than the mixing time, the reaction is carried out under inhomogeneous conditions, which may result in lower yields or production of undesirable side reactions or in precipitation reactions, larger particles with a broad distribution will be produced.

In micromixing, the homogenization takes place by diffusion at a molecular level. Therefore, the size of individual, non-mixed fluid elements is a crucial parameter for the micromixing. In microreactors different versions of a high degree of micromixing is generated by high turbulence in very narrow channels. However, these are very prone to clogging or fouling. The spinning disc reactor, combines the advantages of high micromixing in thin fluid film with an unsusceptible to clogging construction. These properties of the SDR has great potential for the continued operation of precipitation reactions.

2.4.1 Spinning Disc Reactor Characteristics

SDRs have different characteristics that may affect their purpose or performance. Overall the main design characteristics are:

1. Rotational speed – The most common rotational speed range used is within 200–1500 rpm (Aoune and Ramshaw, 1999; Yatmaz, Wallis and Howarth, 2001; Burns, Ramshaw and Jachuk, 2003; Burns and Jachuck, 2005; Vicevic, Boodhoo and Scott, 2007; Vicevic *et al.*, 2008), however slow rotational speeds down to 40 rpm (Boodhoo and Jachuk, 2000; Tsibranska *et al.*, 2009) also employed.
2. Feed flowrate – The flowrate is used is generally less than 50 mL/s, tending to be in the 10 mL/s and lower range.

3. Spinning disc size – The majority used around 30 cm in diameter, the larger discs having diameters up to 50 cm. The size of the disc may be governed by application factors (heating/cooling within the disc, probes, catchment area).
4. Spinning disc surface texture and material – Material is varied based on purpose and machinability. For example, Perspex is light and easily machinable, but not suitable for applications that require high heat transfer rates and high concentrated chemical.
5. Feed inlet design - Several feed inlet designs have been used, with the most common and most simple being the liquid being fed centrally through a thin pipe onto the top of the centre of the disc. However, less common arrangements also exist, with a bottom fed design (Yatmaz, Wallis and Howarth, 2001; Boiarkina, 2012), and a design where the liquid is introduced at some distance, *r*, from the centre of the disc (Meeuwse, Schaaf and Schouten, 2010).

2.4.2 Flow Regime and Residence Time Distribution on Spinning Disc Reactor

The flow regime on a rotating disc is a function of the rotational disc speed and flow rate (Charwat, Kelly and Gazley, 1972). It has been reported with change of the rotational speeds, and flow rates several flow regimes can form on the spinning disc such as smooth waves, concentric waves, spiral waves, irregular waves and film break up (Espig and Hoyle, 1965; Charwat, Kelly and Gazley, 1972).

Boiarkina et. al. (2011; 2013) observed the boundaries of different water waves with a high speed camera using dye streak method. They found a significant dragging took place at higher flow rates and rotational speeds with increased formation of waves. Whereby the dye was dragged by the disc in the direction of rotation, and spread in the opposite direction via the action of the waves. This made it difficult to discern whether turbulence or micromixing was present at higher flow rates or rotational speeds. However, streaklines in the dye indicate that at least some segregation is taking place, otherwise micromixing would ensure that the dye was dispersed. Feng (2014) found the tailing of the residence time distribution which explained the dragging effect that took place at higher flow rates and rotational speeds.

The residence time behaviour of a large number of reactors can be described as a combination of ideal reactors (Levenspiel, 1999). In principle, a relatively good

replication can often be achieved, since elements without (ideal plug flow tube) or with complete mixing (ideal stirred tank) can possibly be combined with each other almost as desired, using various interconnection variants.

A prerequisite for an ideal plug flow is that the flow velocity is constant in the radial direction *r*, a complete mixing takes place in the transverse direction (radial) and no mixing occurs in the flow direction *z* (axial). This results in a plug flow. Since all particles remain in the reactor for the same length, the output function corresponds to the input function delayed by time *t*.

Investigated by Mohammadi and Boodhoo (2012), and also Feng *et al.* (2014), residence time distribution (RTD) analysis for SDR showed that the flow pattern on the spinning disc became close to plug flow with the increase of rotational speed and flowrate. Generally, a very narrow and symmetrical RTD curve means that the flow pattern is close to ideal plug flow, and in contrast, a very broad and asymmetrical RTD curve represents a large deviation from plug flow, where dispersion becomes more prominent (Levenspiel, 1999). With the increases in the disc rotational speed and the liquid flowrates, the RTD of the thin film flowing on the rotating disc becomes narrower. At higher disc speeds, the greater centrifugal force pulling the liquid film to the edge of the disc surface, which prevent of any possibility for dispersion into the radial direction. Also, it is suggested that greater transverse mixing induced by more numerous surface waves formed at higher disc rotational speed contributes to equalising the velocity profile and induced greater transverse mixing. Mohammadi and Boodhoo (2012) observed where they explained that a uniform velocity profile in the direction perpendicular to the flow direction and negligible dispersion in the direction of flow can be achieved at higher spinning speeds and flow rates, thus resulting in a near plug flow behaviour. Previous studies have reported that the waves on the spinning disc changed from smooth to spiral and unstructured with an increase of the rotational speed (Charwat, Kelly and Gazley, 1972; Boiarkina, Pedron and Patterson, 2011), so an unstructured wave might be a reason for the more asymmetric RTD curve. At higher disc spinning speeds, these resistances are overcome enabling the fluid to bypass these pathways and take a more direct route (narrowing the residence time distribution and removing the observed tails in the distribution). In addition, long tails have been found to be an indication of laminar flow or stagnation areas (Bošković *et al.*, 2011; Dubois *et al.*, 2011; Gutierrez, Dias and Gut, 2011). However, with an

increase of the rotational speed and the flow rate the RTD curve became more symmetric and the tail decreased. Overall, this investigation provides important understanding the operating conditions of the SDR which generating flow profiles approaching plug flow behaviour. The results will help in choosing the operating parameters for reactions conducted by the SDR in order to maximise the yield and selectivity and also can control product properties.

2.4.3 Spinning Disc Reactor Application

The SDR has been investigated for a variety of other areas. A selection of these includes:

- Organic synthesis - Very encouraging results were achieved to prepare a drug intermediate and the recrystallization of an active pharmaceutical ingredient by Oxley *et al.* (2000)
- Polymerisation reactions – Boodhoo and Jachuk (2000) investigated the free radical initiated polymerisation of styrene and found significantly improved reaction rates and improved molecular weight distribution. Vicevic *et al.* (2008) investigated the kinetics of styrene polymerisation across a SDR.
- Photocatalytic reactions - Yatmaz, Wallis and Howarth (2001) used SDR to degrade aqueous solution of 4-chlorophenol and salicylic acid.
- Mass transfer – SDRs have been investigated for increasing the mass transfer across the spinning disc (Aoune and Ramshaw, 1999; Burns and Jachuck, 2005; Meeuwse *et al.*, 2007, 2010, 2011; Tsibranska *et al.*, 2009; Meeuwse, Schaaf and Schouten, 2010; Visscher *et al.*, 2012; Haseidl, Pottbacker and Hinrichsen, 2016).
- Application to reaction synthesis – Brechtelsbauer *et al.* (2001) investigated the application of the SDR for chemical synthesis. Vicevic, Boodhoo and Scott (2007) investigated the application of the SDR for the catalytic formation of campholenic aldehyde and found that the SDR increased selectivity.

All these studies demonstrate the wide range of SDR, with about choosing the operating parameters directly influence the responses and the product characteristics can be taken.

In Patterson research group (Boiarkina, Pedron and Patterson, 2011; Boiarkina, Norris and Patterson, 2013a, 2013b; Expósito *et al.*, 2016) the SDR has been investigated for application as a thin film photocatalytic system. Different flow regimes can form across the surface of the disc depending on the rotational speed, flow rate, and liquid properties. Boiarkina, Pedron and Patterson (2011) found that the photocatalytic surface rate of reaction was independent of these flow regimes. However, the SDR thin film photocatalytic system has disadvantages if a thin film catalyst is coated directly onto the SDR disc (Boiarkina, Pedron and Patterson, 2011), then the catalysts amount and surface area is largely limited to the surface area of the disc. And also, nanostructured catalysts cannot be readily used when coated directly on the SDR disc, since they are readily deactivated (through high shear forces) at the spinning speeds and flowrates needed to produce process intensification.

Therefore, a new process intensification technology is proposed: the spinning grooved disc reactor (SGDR). The SGDR is a relative of the more common spinning disc reactor (SDR) (Pask, Nuyken and Cai, 2012) and the rotating packed bed reactor (RPBR) (Burns, Jamil and Ramshaw, 2000) . Consequently, the SGDR is a superior way of applying a catalyst effectively in a SDR type reactor. Furthermore, the SGDR overcomes many of the aforementioned problems with chemical catalysts. The catalyst is immobilised on the disc surface, so does not need to be recycled and/or separated. Like the SDR, the SGDR should overcome the mass transfer limitations of these catalysts, but can also protect them from mechanical and hydraulic forces related to deactivation. Indeed, the mesh material, size, and thickness, as well as spinning speed and flow rate can all be optimised to minimize deactivation and maximise reaction rate (Boiarkina, Pedron and Patterson, 2011). For photocatalytic reactions, the problem of poor UV penetration through the coloured liquid films is overcome by the intrinsic production of a thin fluid film in the reaction zone. One potential disadvantage is that the SGDR is complex - in terms of its mechanics due to the need for bulk rotation - compared to conventional chemical reactors (such as batch, continuous stirred tank and plug flow). This work will therefore need to establish the operating conditions under which this can be offset by the advantages provided by the process intensification.

2.5 Pharmaceutical Wastewater

Reaction processes of pharmaceutical drugs, such as direct or indirect photolysis, are often very complex reactions involving a wide range of competing reactions. These can lead to various reaction products which:

- Are potentially toxicologically more relevant than the starting material
- may still have the pharmacological properties of the parent compound (e.g. antibiotic activity, proven on photolysis products of the tetracycline)
- but can also have lost all pharmaceutical activity and toxicity (Petrovic and Barceló, 2007)

In principle, these hypotheses can also be applied to photooxidative reactions or AOPs, such as photocatalysis. For this reason, it is of great importance to consider the resulting transformation products of residues-contaminated waters when applying new oxidative treatment techniques.

2.5.1 Ibuprofen

2-[3-(2-methylpropyl) phenyl] propionic acid, commercially available as ibuprofen (IBU) (Fig. 2.11). It is a white crystalline powder with a molecular weight of 206.29 g/mole. Practically it is insoluble in water however very soluble in most organic solvents and slightly soluble in ethyl acetate. It is extensively used as an anti-inflammatory and antipyretic drug especially prescribed for the treatment of arthritis, fever, migraine, muscle aches, and tooth aches. Due to its extensive applications, several kilotons of ibuprofen has been synthesised worldwide (Buser, Poiger and Muller, 1999). Industrial and domestic routes were identified as the major contamination pathways for IBU in aquatic environments (Richardson and Bowron, 1985). Industrial pollution occurs because the pharmaceutical companies release of untreated or fully treated effluents. While the domestic pollution occurs due to the use of IBU as a medicinal drug by human beings and livestock. Therefore, IBU and its metabolised products enter the surface water by sewage treatment plants. Sometimes, the metabolites formed are more hazardous than the parent organic compounds (Idaka, Ogawa and Horitsu, 1987; Sweeney, Chipman and Forsythe, 1994; Wong and Yuen, 1996). So, the treatment for removal of these compounds is important before

discharging the treated water into the ecosystem. There are several advanced oxidation processes available in the literature for the degradation of wastewater namely TiO_2 photocatalysis, Fenton and photo-Fenton oxidation, electrolysis, sonolysis, ozonolysis, and many others (Esplugas *et al.*, 2007; Selli *et al.*, 2008).

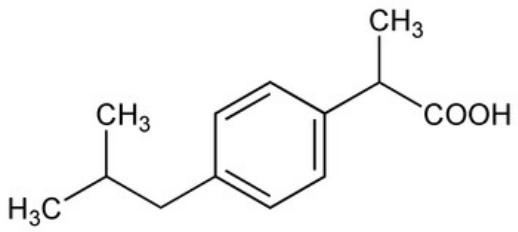

Figure 2.11: Chemical structure of ibuprofen

The photocatalytic treatment of ibuprofen has been studied. Figure 2.12 shows the by-products from the photocatalytic treatment and possible transformation pathways followed by ibuprofen. The initial solution of IBU-Na exhibits two main absorption bands located at 222 nm and 190 nm, which are related to the benzene ring (Fig. 2.11). After irradiation, the intensity of these bands decreases markedly due to fast photocatalytic oxidation of IBU-Na, finally resulting in oxidative ring opening (Fig. 2.12). It looks that the side group oxidation and oxidative ring opening of the benzene ring of ibuprofen happen simultaneously. Generally, the concentration of temporary reaction products was too small to be detected by GC/MS analysis. According to Choina *et al.* (2013), with catalyst concentration of 10 mg/L ca. 85% of removal is achieved after 180 min. With increase of the catalyst amount to 20 and 40 mg/L complete removal is achieved after 180 and 120 min, respectively. Obviously, the activity of the photocatalyst is basically determined by the most active site, the electron holes under these conditions.

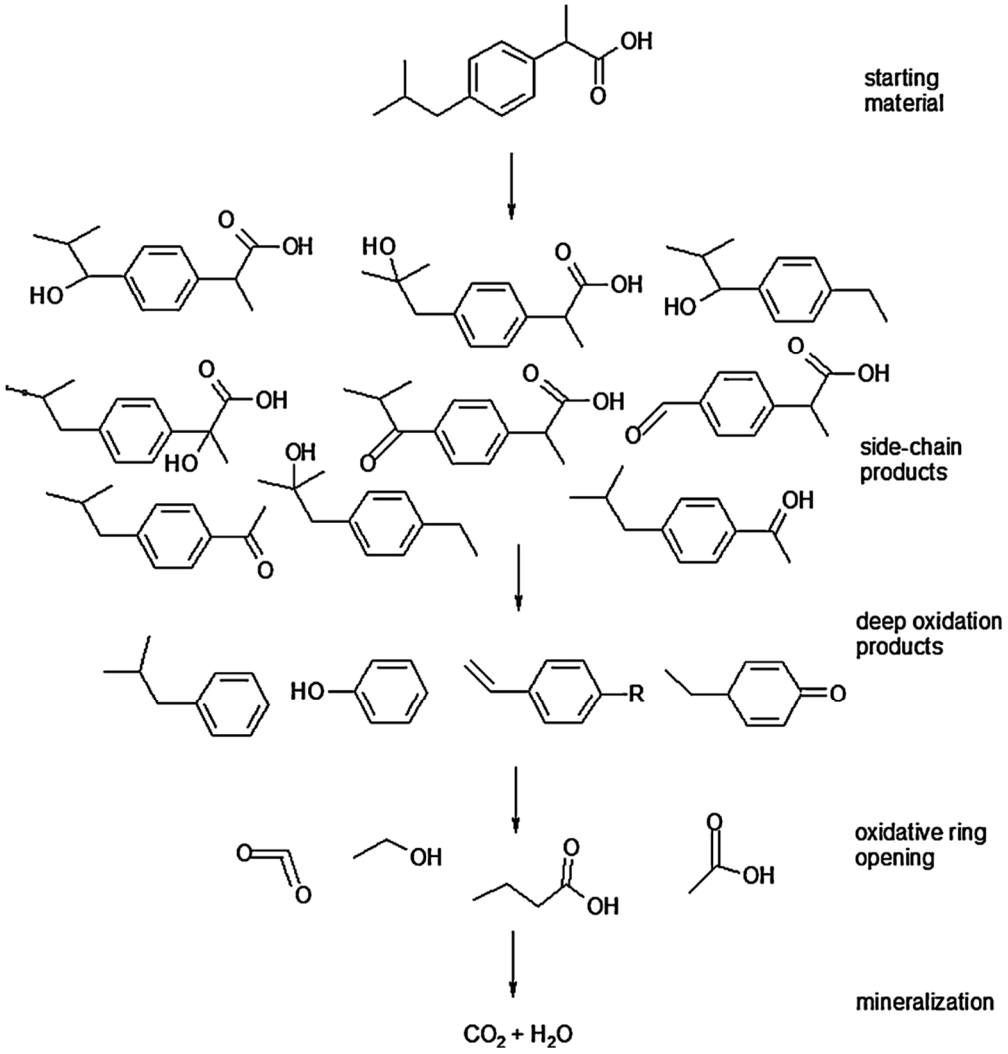

Figure 2.12: Formation of side chain products, their deep oxidation products and open ring intermediates of ibuprofen during photocatalytic degradation (Choina *et al.*, 2013).

CHAPTER 3 PROJECT OBJECTIVES

The overall aim of this project is to optimise the performance of mesh supported photocatalysts for the partial oxidation and mineralisation of wastewaters containing pharmaceutical compound in a spinning disc photoreactor. The model compounds to be used are methylene blue (a model azo dye waste compound and the universally used benchmark compound for photocatalysis, enabling comparison to a wide range of other studies) and the omnipresent pharmaceutical ibuprofen.

A systematic, multi-disciplinary (chemical engineering, chemistry and materials science) and holistic approach were used, correlating the microstructural and mechanical properties of the immobilised catalysts before and after reaction to computational and experimental evaluation of the reactions and reactors. Therefore the specific objectives are:

(A) To determine durable and high activity coating/immobilization techniques for the catalysts for use in the spinning disc reactors. The initial focus was on optimising glass discs and stainless steel meshes with a thin film of nanostructured anatase titanium dioxide.

(B) To determine under what conditions both stable reactor operation and process intensification is achieved. To do this the durability, long term catalytic activity, mass transfer effects (determining mass transfer coefficients), reaction mechanisms and reaction kinetics of these immobilized catalysts were quantified and understood. This involved setting up, troubleshooting and comprehensively characterising the reactions and operation of the pSMDR.

(C) To reconcile the mechanisms underpinning the above results. This achieved through combining experimental reactor characterisations and computational analysis, involving systematic kinetic analysis (including quantifying mass transfer), residence time distribution (RTD) quantification, and high speed camera analysis of the flows in the meshes when under flow in the pSMDR.

CHAPTER 4 MATERIALS AND METHODS

4.1 Materials

Pure azure A, B and C were obtained from Acros Organics and the methylene blue was obtained from Sigma-Aldrich (≥95%). 99.5% pure oxygen from BOC gases was used for saturation of the reactant solution. IBU was obtained from Sigma-Aldrich, ≥98%. The reagents used for TiO_2 sol gel preparation were glacial acetic acid (Sigma-Aldrich, 99.7%), acetylacetone (Sigma-Aldrich, 99%), isopropanol (Sigma-Aldrich, 99.5%), titanium isopropoxide (Sigma-Aldrich, 97%) and deionised water. The chemicals used for analysis were acetonitrile (Sigma-Aldrich, 99.8% for methylene blue and LC-MS then for IBU analysis), and TFA (Sigma- Aldrich, 99%). All deionised water was obtained from an ELGA Maxima Ultra purifier system and all reagents were used as received.

4.2 Spinning Disc Reactor

The SDR was custom designed and built at the University of Auckland (Boiarkina, 2012).

A process flow diagram and photograph of the SDR rig used can be found in Figure 4.1(a) and 4.1(b) respectively. The experiments were run with complete recycle. The liquid was pumped from a stirred reservoir, a 500 mL Pyrex beaker, to the reactor using a Masterflex L/S Easy-Load II peristaltic pump. The liquid passed through a tightly sealed Erlenmeyer glass flask and a Liebig cooler before entering the reactor. The glass flask acted as buffer tank and as pulsation dampener. The Liebig cooler was used to maintain the temperature of the reactant mixture at 20–24°C. All transparent parts of the system were wrapped with aluminium foil to prevent photolysis of the model compounds. The liquid flow through the centre of the supporting disc rotating shaft before being redirected by and flowing out of the nozzle through an annular gap with an outlet radius of 21 mm, shown schematically in Figure 4.1(c). This to ensure the UV light was not obstructed by the inlet pipe coming from the top. A 20 W low pressure mercury lamp (monochromatic, peak wavelength at λ = 254 nm UV,

Steriflow, supplied by Davey Water Products NZ, part nr. GPH369N/S) was fitted in a quartz sleeve in the reactor lid with the lamp being situated at the focus of a parabolic mirror, to improve the homogeneity of the irradiation. The liquid returned back to the reactant reservoir via gravity. The reservoir was continuously sparged with oxygen to ensure that the solution was saturated. The total volume of liquid used was 750 mL, of which 150 mL was initially poured into the buffer tank. The setup was run for 30 min in the dark before the lamp was switched on and the reaction started to allow for the adsorption of methylene blue to reach equilibrium.

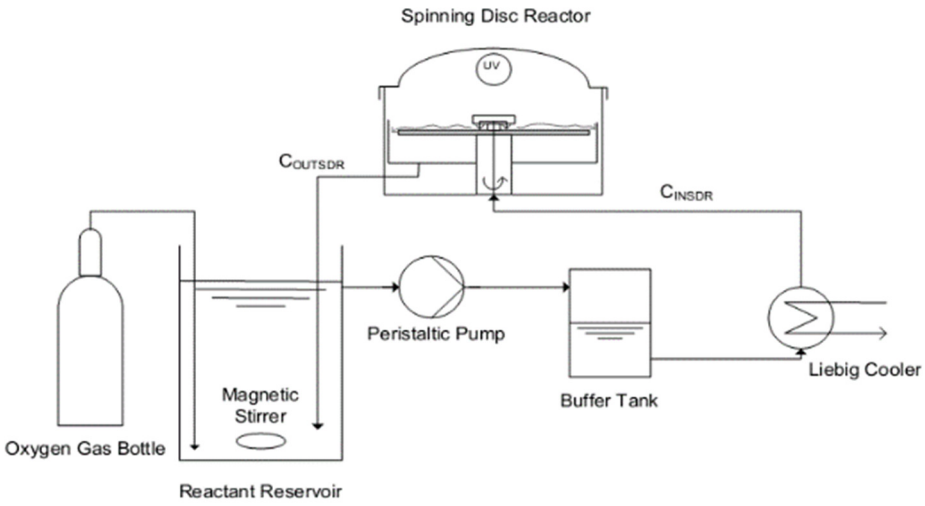

(a)

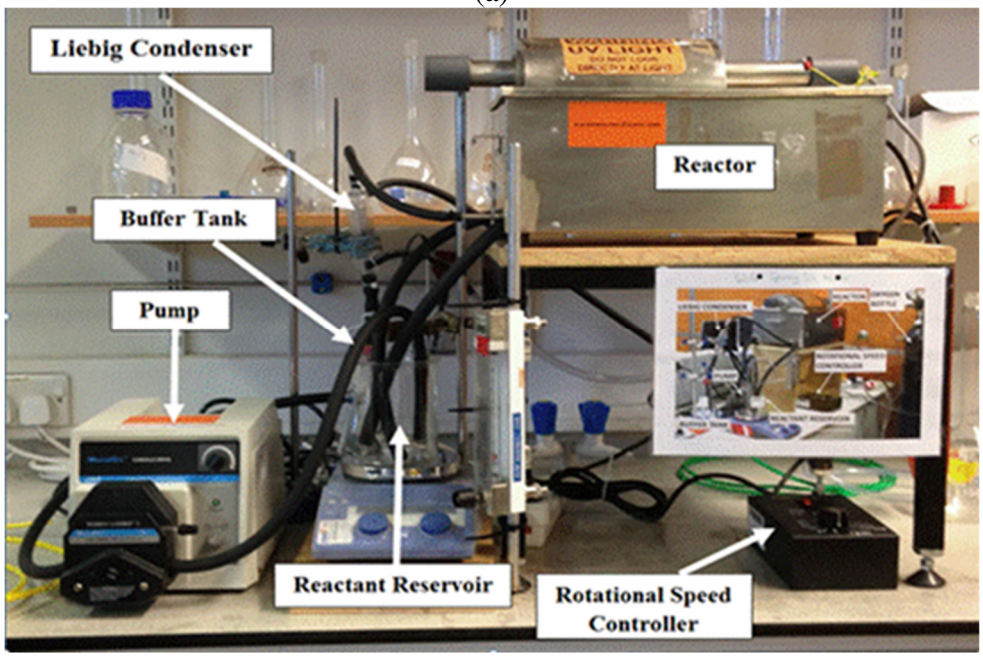

(b)

Figure 4.1: SDR experimental set up showing (a) process flow diagram of the SDR rig (Boiarkina, 2012) and (b) photograph of set up.

This work significantly extends the previous work on the pSDR (Boiarkina, 2012) through investigating the use of a range of different photocatalyst textured macrostructures (meshes and grooves in the photocatalyst disc) in order to increase the micromixing and photocatalyst surface area, to increase the overall degradation rate in the pSDR.

4.2 Catalyst Immobilisation

A sol-gel solution was prepared using the method used in Boiarkina (2012). A detailed preparation procedure can be found in Appendix A1.

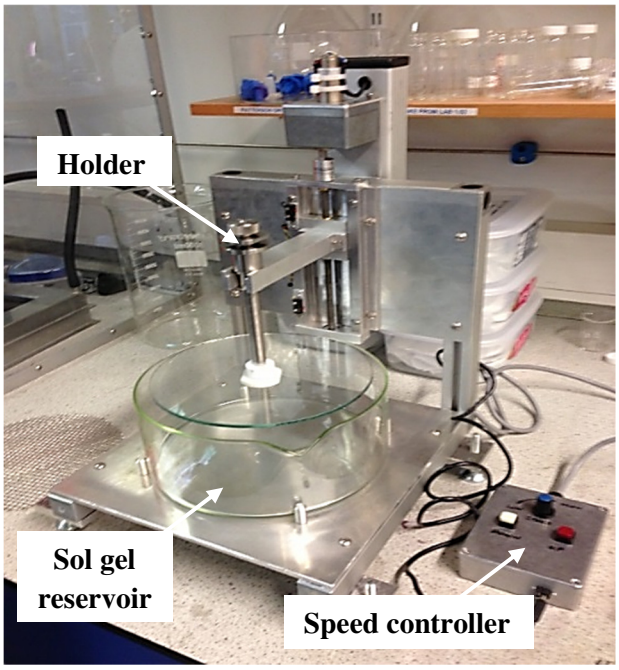

Figure 4.2: Dip coater

Glass and stainless steel mesh discs were first cleaned by water and detergent and brushed vigorously using a cleaning brush, rinsed using deionised water before being dried in an oven prior to dip coating. A special coating rig (Figure 4.2) was built for the coating of the glass and stainless steel mesh discs. A 1mm/s extraction rate was used as suggested in Boiarkina (2012) and Ling *et al.* (2004).

The dip-coated discs were allowed to air dry for 5 minutes in the fume-hood and then transferred to an oven at 100°C for 30 minutes. This process was repeated once more before the discs transferred to a furnace for calcination to obtain the photocatalytically active anatase crystal structure. This was confirmed with x-ray diffraction (XRD). The heat ramp up rate was 2°C/min, and the temperature was held at 500°C or 550°C for 1 hour before cooling down naturally to minimise cracking. The calcined discs were then taken out, cleaned and dried again, before applying another coating. The weights of the discs were taken using a balance before coating and after washing and drying, after calcination. The parameters for the heat treatment are suggested by Ling *et al.* (2004). Once the catalyst substrate had cooled, the process was repeated once more to obtain a total of four TiO_2 layers, with calcination every two layers.

4.4 Experimental Overview

The experiments were carried out in three sets, with each set following one another, investigating phenomena observed and characterised in the results of the previous set of experiments. Adsorption and photolysis studies are discussed separately, as they are relevant to all the experiments. The three sets of experiments and their purpose are summarised as follows:

Set 1 Experiments: The first set of experiments was carried out using smooth disc to test the effect of flow rate, rotational speed and flow regime on the degradation rate of pollutants, methylene blue and ibuprofen. Set 1 experiments are discussed in detail in Chapter 5.

Set 2 Experiments: The second set of experiments was carried out with mesh disc in order to investigate the increase of micromixing and photocatalyst surface area, to increase the overall degradation rate in the pSDR. The results of Set 2 experiments were no significant differences in MB degradation between different mesh sizes. Compared to the smooth disc, with a lower photocatalytic surface area, it can be seen that the meshes did not produce any process intensification. The reasons for and effects of these changes has been discussed in Chapter 6. All of these results drove the development of Set 3 Experiments.

Set 3 Experiments: The third set of experiments was carried out to determine if using a patterned disc appears to even out the flow across the surface of the disc, which would both increase local UV penetration onto the disc surface (less scattering) and provide more uniform volumetric utilisation of the catalyst. This results in an improvement of mass transfer properties due to the increased mixing.

4.5 Residence Time Distribution Studies

Distilled water was used as the test fluid which was continuously fed from a reservoir into the reactor at three different flow rates between 10 and 20 mL/s. Three different types of glass discs were used in this study: a smooth disc (Fig. 4.3a) and two grooved discs; with three square and mesh grooves (Fig. 4.3b and c).

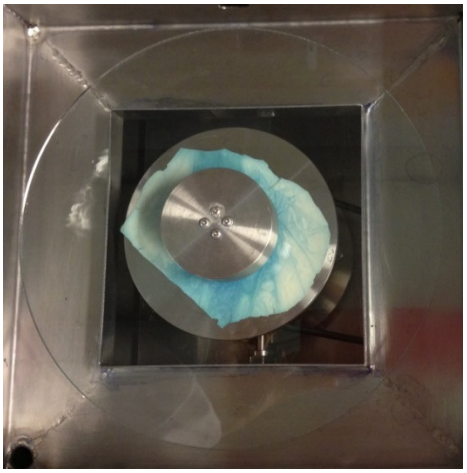

(a)

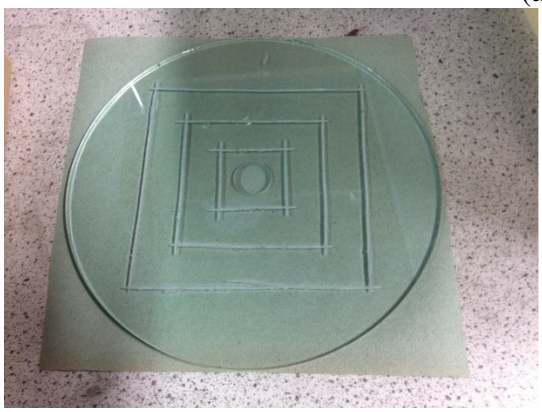

(b)

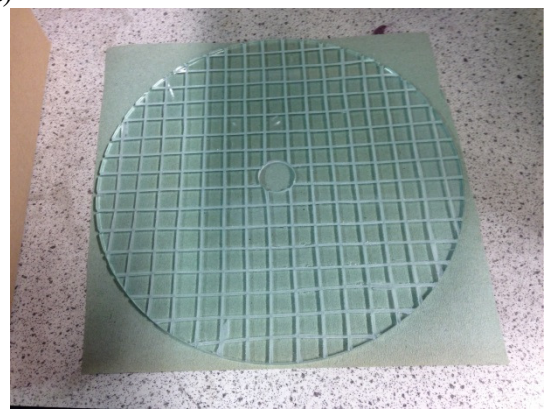

(c)

Figure 4.3: Disc surface: (a) Smooth disc surface. (b) Square grooved disc surface (20mm gap). (c) Mesh grooved disc surface (10mm gap).

The E61M014 conductivity probe with 4 mm diameter and 103 mm length was positioned inside the sampling shoe so that its tip was placed just above the liquid line in the sampling shoe (Mohammadi and Boodhoo, 2012; Feng et al., 2014). The sampling shoe was held to the base of the reactor and was located near to the edge of the disc so it can capture the fluid threw off the edge of the disc. When the fluid collected in the shoe, it made contact with the probe before exiting through the outlet. The set-up of the sampling shoe in the reactor and the probe within it is shown in Fig. 4.4.

1 ml of 0.5 M KCl solution (Sigma-Aldrich) was injected rapidly using a syringe into the system at the centre of the disc next to the nozzle. The data logger was started simultaneously with the pulse injection. Conductivity was measured and logged on a computer with a LabX direct software data logger.

A set of KCl solutions with different concentrations at a fixed conductance range of 40 mS/cm was used to calibrate the conductivity probe. The conductivity measurements from data logger can be directly used to find the age distribution functions, $E(t)$ or $E(\theta)$, as well as the mean residence time τ.

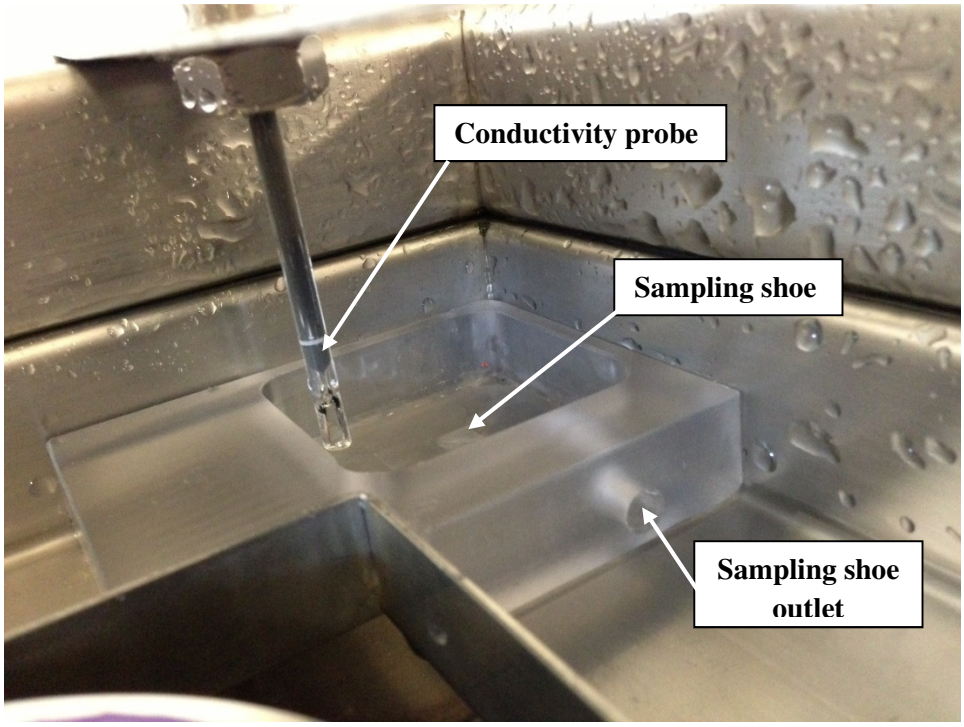

Figure 4.4: Set-up of probe and sampling shoe in reactor housing.

4.5.1 Residence Time Distribution Analysis

Residence time distribution (RTD) is the property of a reactor. Depending on the flow and mixing behaviour in the reactor, the molecules will have different residence times. The mean residence time is defined as (Levenspiel, 1999):

$$\tau = \frac{V_R}{\dot{V}} \tag{4.1}$$

where:

V_R = volume of reactor in operating condition [L]

$\dot{V}$ = Volumetric flow rate $\left[\frac{\mathrm{L}}{\mathrm{min}}\right]$

The residence time is designated by τ and describes the efficiency of the process in continuous reactors and is also referred to as space time. Furthermore, the mean residence time refers to the exiting volumetric flow, while the space time refers to the incoming flow. If the density does not change (which is the case with most liquid-phase reactions) and if both quantities are equal, space time and mean residence time are also identical.

The residence time of a chemical reactor is one of the most important reaction related parameters. The product of the rate constant, *k* of a first-order response and the mean dwell time, τ is the first number of Damkohler, DaI which essentially determines the conversion of a simple reaction in a reactor.

In order to be able to compare reactors with different volumes and times, the dimensionless time parameter θ is introduced. It is the quotient of the residence time *t* of a volume of fluid based on entrance conditions and the space time or average residence time τ. It is dimensionless (Fogler, 2016).

$$\theta = \frac{t}{\tau} \tag{4.2}$$

with:

t = time [min]

τ = mean residence time [min]

The values of the residence time distribution, for a plug flow (without backmixing), can be specified immediately without deriving, as there is only one residence time:

$$E = \infty \quad \text{for} \quad t = \tau \quad \text{or} \quad \theta = 1$$

$$E = 0 \quad \text{for} \quad t \neq \tau \quad \text{or} \quad \theta \neq 1$$

$$F = 0 \quad \text{for} \quad t < \tau \quad \text{or} \quad \theta < 1$$

$$F = 1 \quad \text{for} \quad t \geq \tau \quad \text{or} \quad \theta \geq 1$$

The distribution of the residence times is described by the residence time sums function *F(t).* It indicates the fraction of the compound which enter the reactor at time $t = 0$, and have left it at time $t > 0$.

$$F(t) = \int_0^t E(t)dt \tag{4.3}$$

with:

E(t) = age distribution functions [min^{-1}]

Furthermore, the exit-age distribution function *E(t)* can also be used to describe the residence time behaviour. It indicates how much fraction of exit stream have left the reactor exactly at time *t*:

$$\int_0^\infty E(t)dt \tag{4.4}$$

4.5.2 Determination of the Residence Time

In an experimental system, the residence time is usually determined with a marking substance (so-called tracer), which is injected into the inlet of the apparatus. The tracer should be quantitatively determined in the flow through the apparatus. Basically, the impact mark and a displacement mark are distinguished.

If the tracer concentration at the outlet of the apparatus is measured over time, the residence time density function *E(t)* is obtained during the impact marking. The integral over this function is defined by 1:

$$\int_0^\infty E(t)dt = 1 \tag{4.5}$$

In order to obtain the residence time function *F(t),* the distribution density function *E(t)* must be integrated:

$$F(t) = \int_0^t E(t')dt' \tag{4.6}$$

It represents the proportion of the volume elements which have left the reactor at time *t* after the addition at time 0 (Levenspiel, 1999).

4.5.3 Residence Time Behaviour of Reactor

In principle, the different type continuous reactors are distinguished, which also differ in their residence time behaviour.

For spinning disc reactor, it is assumed behave like the ideal flow tube (plug flow reactor), the distribution density function is a step function, since a so-called plug flow prevails and thus no backmixing takes place.

$$E(\theta) = \frac{N\cdot(N\cdot\theta)^{N-1}}{(N-1)!}\cdot \exp(-N\cdot\theta) \qquad \text{with} \qquad \theta = \frac{t}{\tau} \tag{4.7}$$

where N is the tank-in-series number and θ is the normalized residence time (Levenspiel, 1999).

4.6 Micromixing Study

The principle of the SDR based on the formation of a thin liquid film in magnitude between 20 and 300 µm on a rotating surface. This liquid film is formed due to high tangential and radial acceleration, which caused by shear and centrifugal forces on the disc surface. This provides a very good micromixing due to the high surface to volume ratio mass and heat transfer coefficients arise.

These properties are useful in a variety of reactions, such as homogeneous or heterogeneous-catalysed reactions, as well as precipitation processes, since the rapid dissipation of heat and the high degree of micromixing leads to an improved product

quality. The time of the reaction should be in the same order as the mixing time because the micromixing is one of the importance properties; if the reaction time is shorter than the mixing time, the reaction is carried out under inhomogeneous conditions, which may result in lower yield or undesirable side reactions.

4.6.1 Determination of Micro-Mixing Using the Villermaux-Dushman Reaction

The degree of micromixing is critically dependent on the diffusion processes between macroscopically non-mixed volume elements. Consequently, according to the Fick's second law, the magnitude of the non-mixed portions is decisive for the time that is required to produce a complete reaction by means of diffusion balancing. The influence of different process parameters of the SDR on the degree of micromixing is to be investigated by the Villermaux-Dushman reaction (Fournier, Falk and Villermaux, 1996). In this reaction, which also called iodide-iodate reaction, is a system of competitively parallel reactions. These described from the following equations:

$$H_2BO_3^- + H^+ \rightleftharpoons H_3BO_3 \tag{4.8}$$

$$5I^- + IO_3^- + 6H^+ \rightleftharpoons 3I_2 + 3H_2O \tag{4.9}$$

Reaction (4.8) takes place instantaneously, while reaction (4.9) is orders of magnitude slower. Consequently, iodine will only formed when insufficient mixing of excess local proton occurs. The amount of iodine formed is thus a direct measure of the quality of the micromixing. According to reaction equation (4.10), the iodine formed is then reacted with an excess of iodide to the Triiodide complex I^-_3, which can be detected by UV/Vis spectroscopy at a wavelength of λ = 286 nm and quantified using the Lambert-Beer law.

$$I^2 + I^- \rightleftharpoons I_3^- \tag{4.10}$$

For the quantitative determination of the degree of micromixing, segregation index, X_s is used. X_s is defined as the actual amount of iodine produced, Y compared to the amount of iodine at maximum yield, Y_{TS}:

$$X_s = \frac{Y}{Y_{ST}} \tag{4.11}$$

The results obtained are, therefore, initially presented in terms of the segregation index, X_S. Conceptually, X_S can assume values between 0 and 1:

$X_S = 0$ Perfect micromixing (4.12)

$X_S = 1$ Total segregation (4.13)

$0 < X_S < 1$ Partial segregation (4.14)

However, a comparison of the results should be noted that only the results of experiments can be compared with identical precursor concentrations. A better approach for comparison of reactors here provides the determination of the mixing time. The *Interaction by Exchange with the Mean* (IEM) model to determine the mixing time is based on the conceptual model that is based on the reactants of the Villermaux-Dushman reaction, an exchange between the acidic and the flow containing iodide-iodate-borate takes place. The time required for mass transfer between the two regions is called the mixing time t_m (Falk and Commenge, 2010).

In this study, the concentrations of the reactant solutions in Table 4.1 were chosen for the Villermaux-Dushman reaction so that a further evaluation of the experimental data based on Schneider *et al.* (2004) can be done.

Table 4.1: Reagent Concentrations Used in This Study

Feed 1 (r = 10mm)	**Concentration [mol/L]**
c(KI)	1.16×10^{-2}
c(KIO_3)	2.33×10^{-3}
c(NaOH)	9.09×10^{-2}
c(H_3BO_3)	1.82×10^{-1}
Feed 2 (r = 20mm)	**Concentration [mol/L]**
c(H_2SO_4)	4.2×10^{-2}

Experimentally, it is important to dissolve KI, KIO_3 and NaOH in water first before adding H_3BO_3 in order to prevent thermodynamic iodine formation. All solutions were prepared shortly before use. The ratio of the flow rate between feed 1 and feed 2 was

1:1 and is varied at 4.5 and 15.0 mL/s. Among the various process parameters, the speed from 100 to 500 rpm is varied in each case. After 40 s, which is about 10 times the retention time, steady-state conditions were achieved. After that, a sample was taken and analysed with a dual beam UV/vis spectroscope (Cary 100, Agilent) at a wavelength of λ = 353 nm (ε_{353} = 2606 m^2/mol).

4.7 Analytical Techniques

Several analytical techniques were used in this study: SEM and XRD on the coatings, HPLC, UV-Vis, LC-MS and others on the samples.

4.7.1 Scanning Electron Microscopy

Scanning electron microscopy (SEM) and x-ray diffraction (XRD) were used to characterise the immobilised catalyst. The SEM employed was a JEOL SEM6480 and all samples were coated with gold due to their semi-conductive nature using a sputter coater. An accelerative voltage of 10kV was used with typical magnifications ranging between 100× to 10,000×.

4.7.2 X-ray Diffraction

X-ray diffraction (XRD) was used to identify the crystal phases present in the TiO_2 coatings. A powder X-ray Diffractometer (BRUKER D8-Advance (Cu radiation)) was used with Cu-Kα radiation scanning at a 2θ angle from 20° to 80° at 0.02° steps operating at 30kV and 15mA.

4.7.3 High Performance Liquid Chromatography

The degradation of methylene blue (MB) and ibuprofen (IBU) was analysed using a Gilson High Performance Liquid Chromatography (HPLC). An Agilent Eclipse XDB-C18 column 4.6 × 150mm with 5μm packing was used. The analytical techniques used for the two chemicals were:

1. *Methylene Blue:* A gradient method was used where solvent A comprised of deionised water with 0.1(v/v)% trifluoroacetic acid (TFA) and Solvent B comprised of 0.01(v/v)% TFA, 80(v/v)% acetonitrile and 20(v/v)% deionised water. A detection wavelength of 665 nm was used. The gradient method employed was 95% solvent A at 0 minutes, 90% solvent A at 5 minutes, 10% solvent A at 40 minutes and 95% solvent A at 45 minutes. A flow rate of 1 mL/min was used with an injection rate of 50 µL, and total analysis time of 50 min. This method was based on the work of Boiarkina (2012).

2. *Ibuprofen:* Using a gradient method composed of two mobile phases: a) Pure acetonitrile and; b) De-ionised water acidified with 0.01 vol% TFA. A detection wavelength of 288 nm was used. The gradient method employed was 95% solvent A at 0 minutes, 90% solvent A at 5 minutes, 10% solvent A at 20 minutes and 95% solvent A at 45 minutes. A flow rate of 1 mL/min was used with an injection rate of 20 µL, and total analysis time of 30 min.

4.7.4 Ultraviolet-Visible Spectrophotometry

Ultraviolet-visible (UV-Vis) spectrophotometry is an analytical technique that measures the concentration of a component inside a solution by measuring the amount of absorbance of radiation at a particular wavelength. The equipment allows for measurement of absorbance and transmittance and can be used to analyse liquids and some solids. It is a very quick way of analysing pure compounds. For multiple component solutions, if the absorbance wavelength of two or more components are very similar, then the results from the UV-Vis is less accurate (there are no separation of components unlike that of HPLC). Another feature of the UV-Vis is the use of cuvettes, which are sample holders with a square cross-section. Plastic cuvettes are frequently used for absorbance measurements over 350nm while special fused quartz cuvettes have to be used for wavelengths under 350nm.

For this study, Cary 100, Agilent was used. Detailed operation including start-up procedures can be found in Appendix A: for MB, absorbance scan from 400-700nm (uses tungsten lamp and plastic cuvettes).

The machine was calibrated by analysing five samples of known concentrations. The concentration against absorbance plot should provide a straight line for direct relationship between absorbance and concentration.

4.7.5 Liquid Chromatography–Mass Spectrometry

Liquid Chromatography–Mass Spectrometry (LCMS) uses the HPLC to perform separation on the components of a solution followed by mass analysis via a mass spectrometry. It is mainly used to identify unknown components inside a solution by identifying the mass of the components in question. This was a method used to identify the reaction intermediates in the IBU degradation reactions via photocatalysis.

The equipment used was Bruker MicrOTOF electrospray time-of-flight mass spectrometer (ESI-TOF) coupled to an Agilent High Performance Liquid Chromatography (HPLC) unit for the separation of mixtures combined with accurate mass measurement in Chemical Characterisation and Analysis Facility (CCAF). The method used for LCMS analysis was the same for the HPLC method for IBU mentioned earlier with one difference: instead of acidified water using TFA, deionised water acidified with formic acid was used due to the incompatibility of the MS with TFA. Results from the analysis were used to identify possible reaction intermediates using computer software, in the form of empirical formula. One representative sample containing all the detected peaks from HPLC analysis were analysed using the LCMS due to availability of equipment and time.

4.7.6 Total Organic Carbon

The Total Organic Carbon (TOC) content gives information about the mineralization efficiency (carbon dioxide and water formation) of the organic pollutants. The measurements were carried out using TOC analyser (Shimadzu TOC-5000A), by following the amount of carbon dioxide released during the burning of the sample solutions at 1000°C in a high-purity oxygen-argon gas mixture. The calibrations were done using potassium hydrogen phthalate standard solutions in a 5-50 ppm

concentration range. The carbon content of the Milli Q water used for the preparation of the solutions was subtracted from the values of samples.

4.7.7 Dissolved Oxygen and pH Monitoring

If the dissolved oxygen (DO) or pH was measured during the reaction, the probes were inserted close to the inlet pipe and away from the oxygen source, to prevent interference from the oxygen bubbles. The pH was measured using a Hanna pH meter and the oxygen was measured using a Hanna dissolved oxygen meter.

CHAPTER 5 SPINNING DISC REACTOR CHARACTERISATION - HYDRODYNAMICS OF THE FLUID FILM, RESIDENCE TIME DISTRIBUTION AND MICROMIXING

5.6 Introduction

The use of a spinning disc reactor (SDR) has in a previous study proven to be a beneficial and superior operation compared to conventional batch reactors because of its unique operational characteristics (as outlined in Chapter 3). In addition, the advantage of a SDR is that there is a low risk of fouling or plugging. In the SDR, liquid is fed from the centre of a reactor consisting of a spinning disc. Although SDR flow is in theory characterised to be within the laminar regime (Burns and Jachuck, 2005), the rotational speed is usually high which generates thin, unstable and wavy liquid films. These cause the film surface to be covered with numerous ripples which may induce turbulence within the layers of the film beneath its surface and have an effect on its residence time distribution (RTD) and micromixing. Also, the liquid travels in plug flow in the film from centre to the edge. There are some studies that indirectly indicate that flow conditions within the SDR approach a plug flow regime(Mohammadi and Boodhoo, 2012; Feng *et al.*, 2014). The aim of this chapter is to investigate the RTD and micromixing efficiency of a SDR when varying process parameters such as rotating speed, surface structure of the disc and flowrate. All of the different disc structures are examined: smooth disc, meshes, the square groove disc (SGD) and the mesh groove disc (MGD). For this purpose, the influence of hydrodynamic conditions of the thin film flow and disc configurations on the RTD is studied so as to determine the optimum experimental parameters that allow close to plug flow behaviour to prevail on the spinning disc using both high speed photography to characterise the flow (Chapter 5.2) and the residence time distribution to quantify the overall fluid behaviour on the disc (Chapter 5.3). Additionally, the degree of micromixing is investigated (Chapter 5.4). Combined, these will provide a comprehensive characterisation of the hydrodynamics on the disc surface and the effect of the different process parameters on this, which will be used in subsequent chapters to understand the effect these same process parameters have on the reaction rates and mechanism.

5.7 Hydrodynamics of the Fluid Film

The aim of this section of work is to get insight into the hydrodynamic properties of the fluid film on the rotating disc. For this purpose, high-speed camera photographs of the fluid film at different rotational speeds and flowrate are taken and analysed. The fluid film on the disc flows at nearly the same tangential speed as the disc (Jacobsen and Hinrichsen, 2012). Neglecting the Coriolis force, the fluid dynamic properties can be calculated based on the Navier-Stokes equations with the Nusselt flow model. With the condition that the centrifugal force and the frictional resistance in the radial direction of the disc surface is in equilibrium, the local film thickness δ can be calculated (Emslie, Bonner and Peck, 1958).

As shown in Fig. 5.1 and 5.2, it can be seen with the increasing of rotational speed, increasing wave formation is observed. As observed by Charwat *et al*. (1972), more waves formed at certain distance from the disc centre and spread the spiral to the edge of the disc. The increasing number of waves results in a further improvement in the mixing of the fluid film and therefore improved the mass transfer (Aoune and Ramshaw, 1999).

Fig. 5.1 and 5.2 show increasing rotational speeds and volume flowrates to result in changes in wave formation and changes in flow pattern with methylene blue on TiO_2 coated discs.

In general, these figures show that:

- The film thickness gets thinner with increasing spinning speed and decreasing flowrate, which is what is expected and the fact at higher inlet flowrates more volume needs to be accommodated in the same area under the same shear rate removing the film.

- The accumulation at the end of the disc decreases with spinning speed (a thicker blue film is observable at lower spinning speeds at the edge of the disc) – this has not been reported previously and could be a major factor in light penetration to the surface of the disc and therefore an additional explanation as to why lower spinning speeds (which also have lower micromixing and mass transfer) are not be optimal for the photocatalytic spinning disc reactor. This

phenomena is directly related to the thicker film on the disc at lower spinning speeds.

- Higher spinning speeds in general produce more uniform, well distributed films – which are likely to produce less light reflection and therefore a higher intensity of light at the catalyst surface – which should increase overall reaction rate. This pattern is however disrupted by the 'standing wave' caused by the nozzle (as described in previous work by Boiarkina et al., 2013) which in this analysis also appears to be a function of liquid overload in the system at higher inlet flowrates.

- At the same spinning speed, increasing inlet flowrate increases the wave formation on the disc.

- Overall, lower spinning speeds and higher inlet flow rates (the lower right hand side of Figures 5.1 and 5.2) give the greatest non-uniform flow, with dry patches, thicker films that appear to 'flood' over the disc and build up significantly at the end of the disc (giving thick blue edges) – these are likely to be unfavourable hydrodynamic conditions for producing high reaction rates.

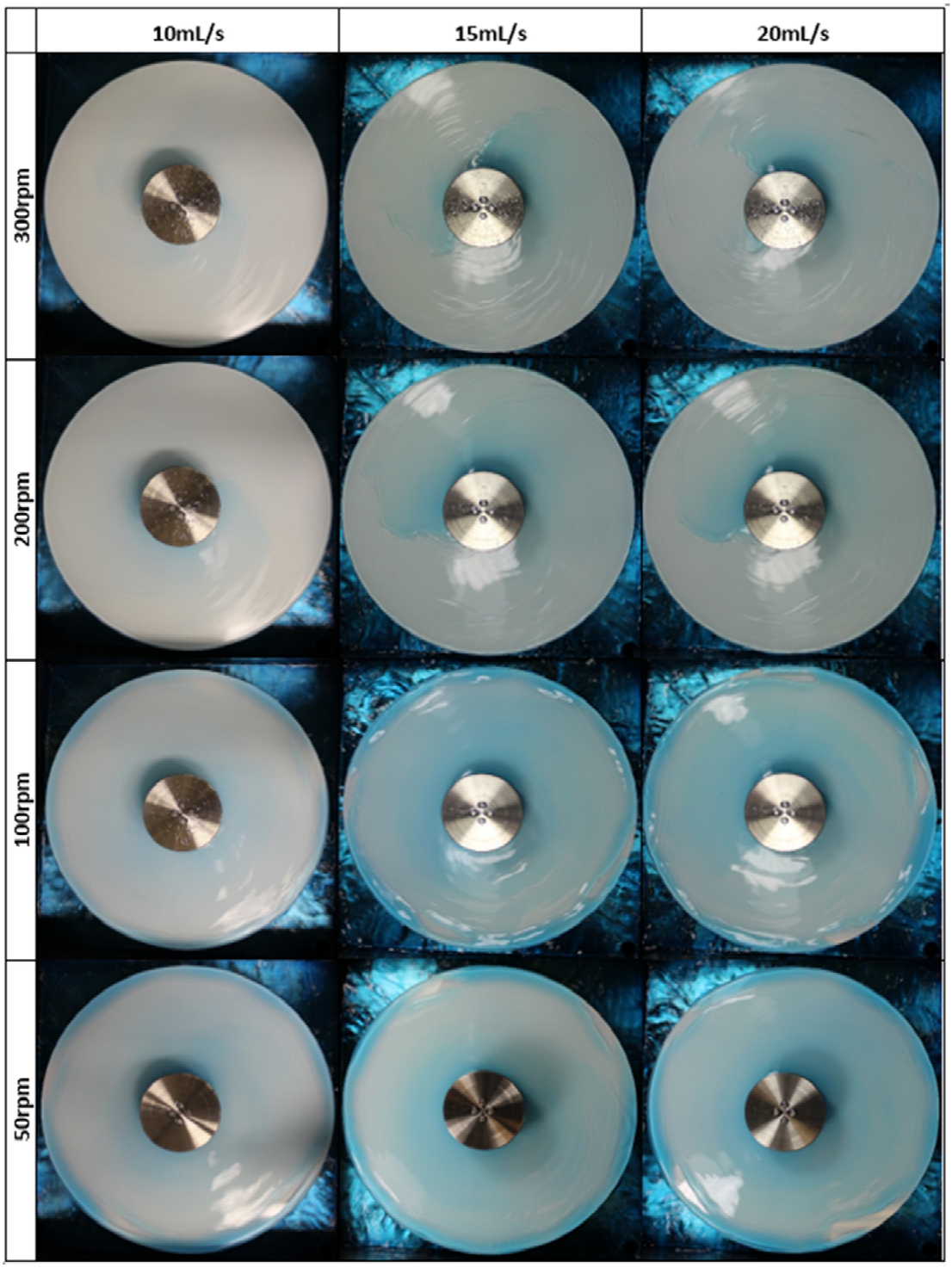

Figure 5.1: Photographs of the liquid film on the rotating smooth disc, taken at different spinning speeds and inlet flowrates.

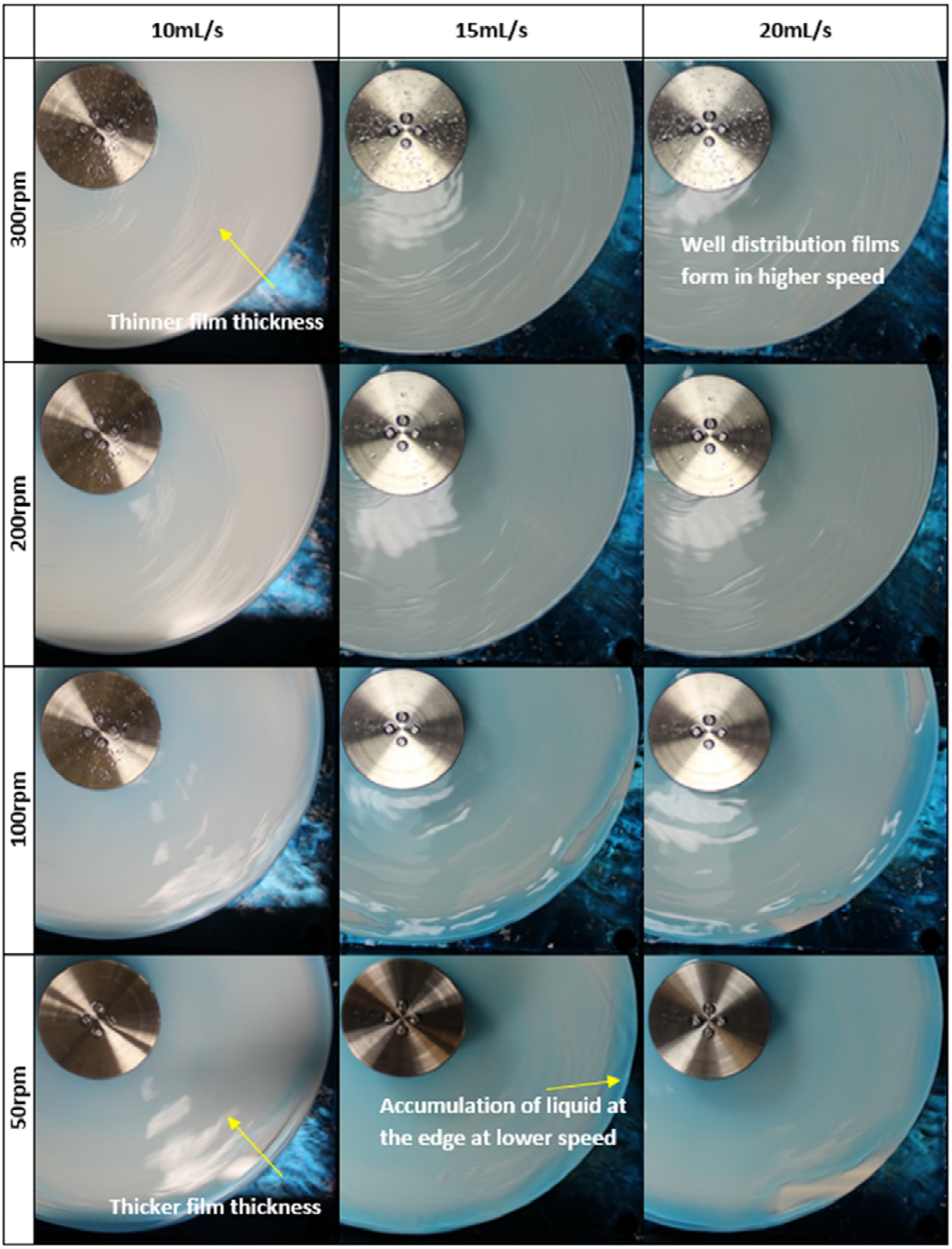

Figure 5.2: Photographs of the liquid film close-up on the rotating smooth disc, taken at different numbers of revolutions.

Note that although there are clear trends with increasing spinning speed and inlet flowrate, this may not have a significant impact on the overall degradation rate (or may not be easily correlated to it). For example, Boiarkina *et. al.* (2011) found that the

photocatalytic surface rate of reaction was independent of the flow regimes in the same SDR. However, this SDR thin film photocatalytic system has disadvantages if a thin film catalyst is coated directly onto the disc (Boiarkina, Pedron and Patterson, 2011), then the catalyst amount and surface area is largely limited to the surface area of the disc. To address these limitations, the development and optimisation of the SDR continues by introducing textured discs (meshes and grooves as a macrostructure) that will have more significant effects on the flow hydrodynamics than the changes outlined in Figures 5.1 and 5.2 and to increase the potential photocatalyst surface area on the disc as well as improve mixing. Textured discs in particular increase mixing through enhancing micro-mixing in the thin liquid film on the disc and changing the wave patterns compared to the smooth disc (Jachuck and Ramshaw, 1994).

In theory, the high surface area stainless steel meshes studied should both increase the surface area of photocatalyst present, as well as increase mixing due to interrupting the flow on the disc, which may result in an increased reaction rate compared to a smooth disc. A smaller mesh size would increase the photocatalyst surface area further, enhancing these gains.

However, as shown in Figure 5.3, the mesh disrupts the liquid film to a greater extent than expected, producing dry patches across the mesh surface, further reducing the effective surface area of the photocatalyst. At all inlet flowrates and spinning speeds, there is incomplete wetting of the disc (and therefore the photocatalyst on both the disc and the mesh) and increasing flowrate and spinning speed does nothing to improve this. This is likely due to the significant disruption of the thin film on the disc surface, causing incomplete flow and channelling the flow into streams that do not contact the rest of the disc. This strongly indicates that these meshes will make the SDR less effective than without them. Consequently, this all results in a less effective spinning disc photocatalyst surface and drove the development of grooves on the surface of the discs instead to overcome these issues.

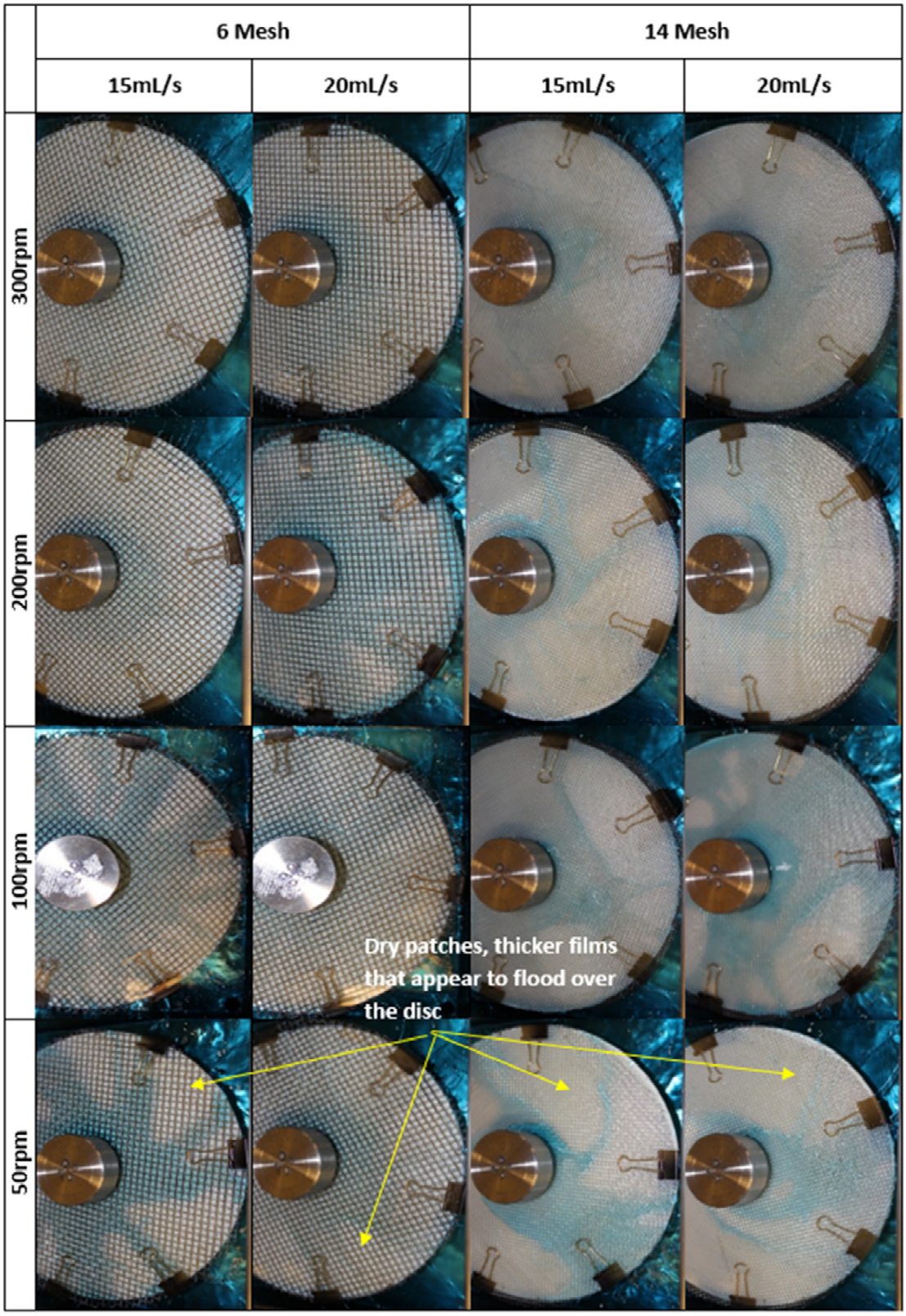

Figure 5.3: Photographs of the liquid film on the rotating mesh disc, taken at different numbers of revolutions.

Figure 5.4 shows the effect of spinning speed and inlet flowrate on the hydrodynamics of the disc thin film with two different grooved disc patterns – mesh and square grooves.

The same overall effects as observed in the flat discs can be observed for these, with two major differences.

Differences:

- Due to the additional surface area on the disc and the macrostructures disrupting the flow, lower spinning speeds and lower inlet flowrates produce an incomplete film on the surface of the disc. Therefore there is a critical spinning speed and inlet flowrate needed to produce a continuous film. For the meshes in Figure 5.3 above, this indicates that the critical flowrate and spinning speeds were not reached in the studied conditions. Here the critical conditions are:
    - Mesh groove disc: 200rpm and 15mL/s
    - Square groove disc: 20mL/s - it appears that the inlet flowrate is critical for this disc.
- The macro-texturing of the discs appear to have changed the wave patterns compared to the smooth disc, changing when waves appear at different spinning speeds and flowrates. So, for the square grooves - at the same spinning speed, increasing inlet flowrate decreases the wave formation on the disc. The flow appears to be smoother especially at higher flowrates. For the mesh groove disc, in general higher spinning speeds overcome the eddies formed by the grooves and create a smoother surface, which is needed to minimise reflection and enhance UV intensity on the disc surface.

Figure 5.4: Photographs of the liquid film on the rotating grooved disc, taken at different numbers of revolutions.

Overall, looking at all of the types of discs, it can be seen that for all types of discs (Fig. 5.1, 5.3 and 5.4) in general the amount of rivulets are reduced with increasing rotational speed. Furthermore, the formation of waves can be observed at higher rotational speed. The amount and the frequency of the ripples increase with increasing rotational speed. This should result in an improvement of mass transfer properties due to the increasing mixing, as described in the literature (e.g. Aoune and Ramshaw 1999). Using the grooved disc appears to also even out the flow across the surface of the disc at a wider range of conditions compared to the others, which would both increase local UV penetration onto the disc surface (less scattering) and provide more uniform volumetric utilisation of the catalyst. This sort of phenomena has been seen in related systems (Jachuck and Ramshaw, 1994).

Another possible affecting factor, which is related to the hydrodynamics just described and will affect the reaction rate on the disc surface is the residence time of the liquid within the reactor. This is quantified and analysed next section.

5.3 Residence Time Distribution Studies

The aim of this work was to investigate the Residence Time Distribution (RTD) of a SDR when varying process parameters like rotational speed, surface structure of the disc or liquid flowrate. The influence of the hydrodynamic conditions of the thin film flow and disc configurations on the RTD is studied to determine the optimum experimental parameters that close to plug flow behaviour prevails on the spinning disc.

RTD curves are expected to vary from very thin symmetric distribution when there is like ideal plug flow conditions occur to more asymmetrical and wider when significant deviations from plug flow arise. A thinner and symmetrical RTD is characterised by a low variance or dimensionless variance.

Experiments were repeated for five times at all operating conditions to examine the reproducibility of the data collected. The normalised RTD is used to compare directly the flow performance inside reactors at different conditions. The graph of normalised RTD (Fig. 5.5) at three different conditions (rotational speed and flowrates) show almost overlapping profiles for the repeated experiments.

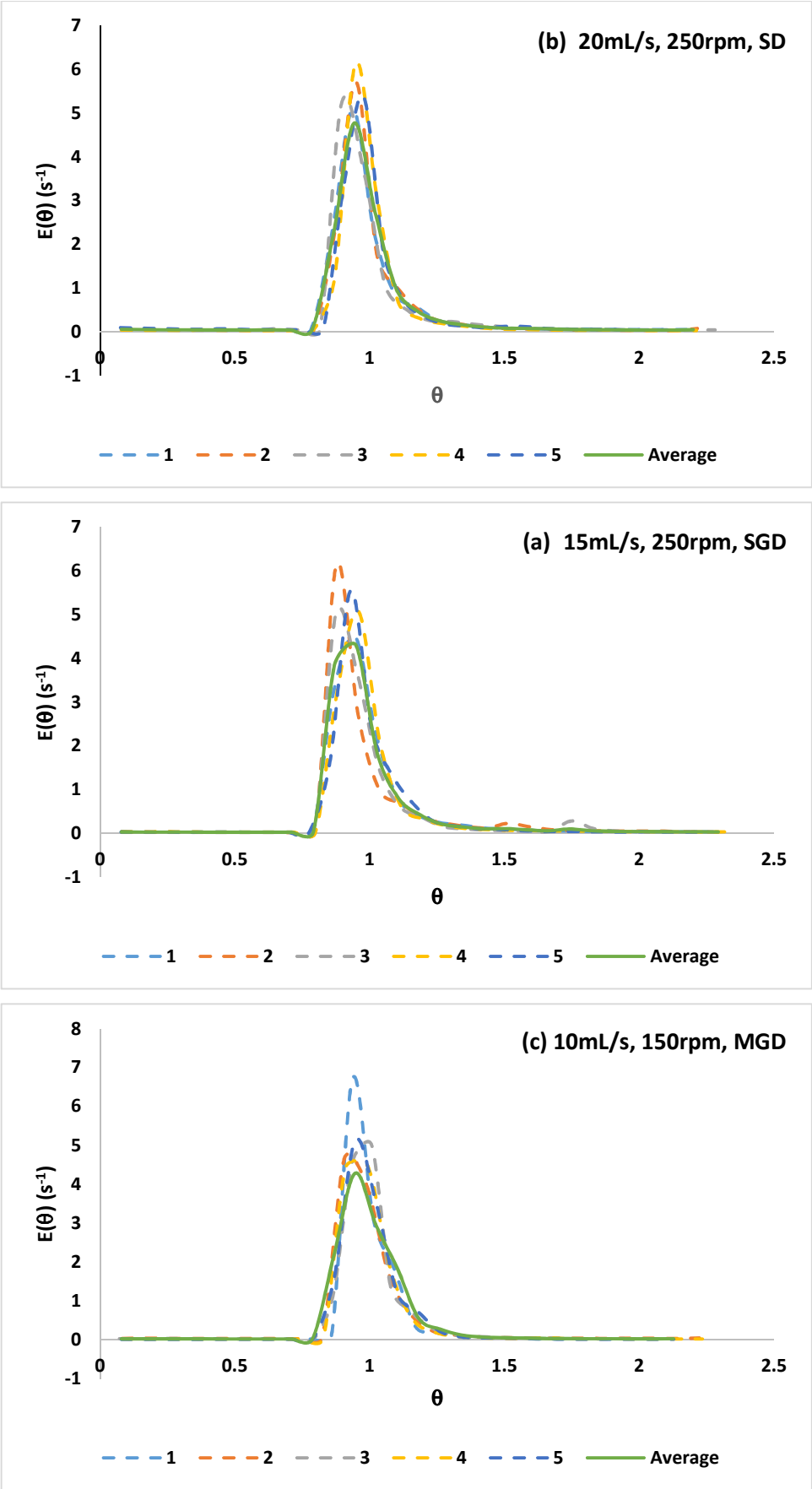

Figure 5.5: Reproducibility of experiments on different disc surface.

It is very common to compare RTDs by using their moments. The normally used moments are the mean residence time and the variance, or square of the standard deviation. The mean residence time for Figure 5.5(a) is 12.738 s (standard deviation = 0.336), Figure 5.5(b) is 12.651 s (standard deviation = 0.141) and Figure 5.5(c) is 12.729 s (standard deviation = 0.654). While the variance for Figure 5.5(a) is 0.057 s^2 (standard deviation = 0.007), Figure 5.5(b) is 0.057 s^2 (standard deviation = 0.008) and Figure 5.5(c) is 0.029 s^2 (standard deviation = 0.008). The magnitude of this moment is an indication of the spread of the distribution. The variances showed small values of moment for Figure 5.5, mean it has smaller distribution's spread. This is supported by the low standard deviation values which indicated that the data points tend to be close to the mean or the expected value. This indicated very good reproducibility of the data.

5.3.1 Effect of Flowrate and Rotational Speed

The general observation from Fig. 5.6 is that the lowest rotational speed of 100 rpm is associated with a slightly broader and relatively less symmetrical distribution compared to the higher disc rotational speeds. This is in particularly so at lower flowrates of 10 ml/s (Fig. 5.7). This observation is more evident from the higher dispersion numbers calculated at 100 rpm compared to the higher disc rotational speeds, as in Table 5.1. As the disc rotational speed increases, the dispersion number decrease for flowrates of 15 and 20 ml/s. Film breakdown at very low flowrates (as illustrated in Figure 5.1) has been shown to be responsible for decreasing mixing capability of the film (Boodhoo and Al-Hengari, 2012). While at higher disc rotational speed (as illustrated in Figure 5.2), shear rate within the film is enhanced (Vicevic, Boodhoo and Scott, 2007) and the depth of film surface wave formation is also extensively increased (Aoune and Ramshaw, 1999). Under conditions of higher disc rotational speeds in the SDR, RTD of the liquid film on the disc becomes tighter (Figure 5.6). This would give a consistent film as it travels over the disc surface. These disc rotational speed effects are expected to lead to improve the micromixing in the film (Section 5.3) (Boodhoo and Al-Hengari, 2012; Jacobsen and Hinrichsen, 2012).

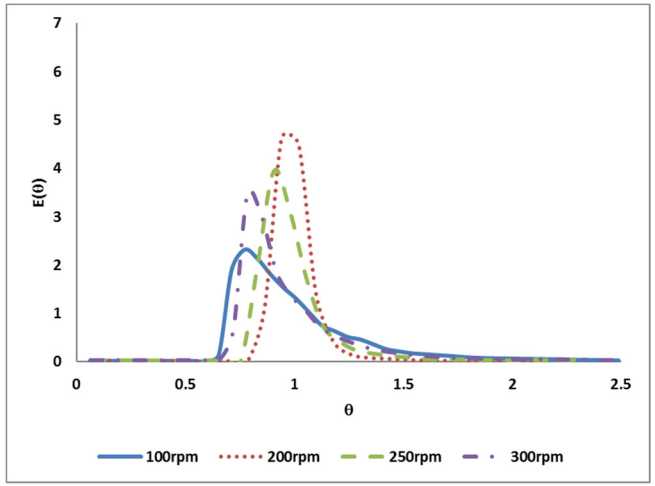

(a)

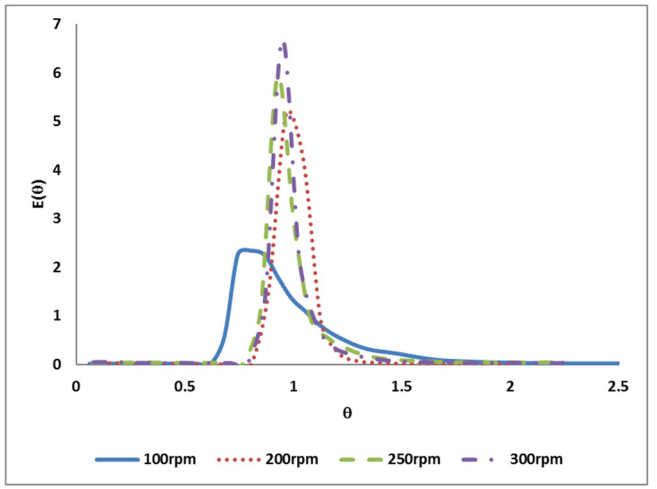

(b)

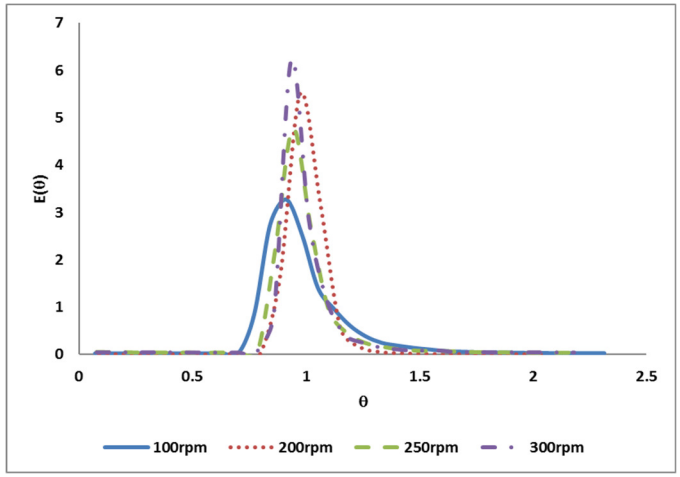

(c)

Figure 5.6: Influence of rotational speed on RTD on smooth disc, (a) 10 ml/s; (b) 15 ml/s; and (c) 20 ml/s.

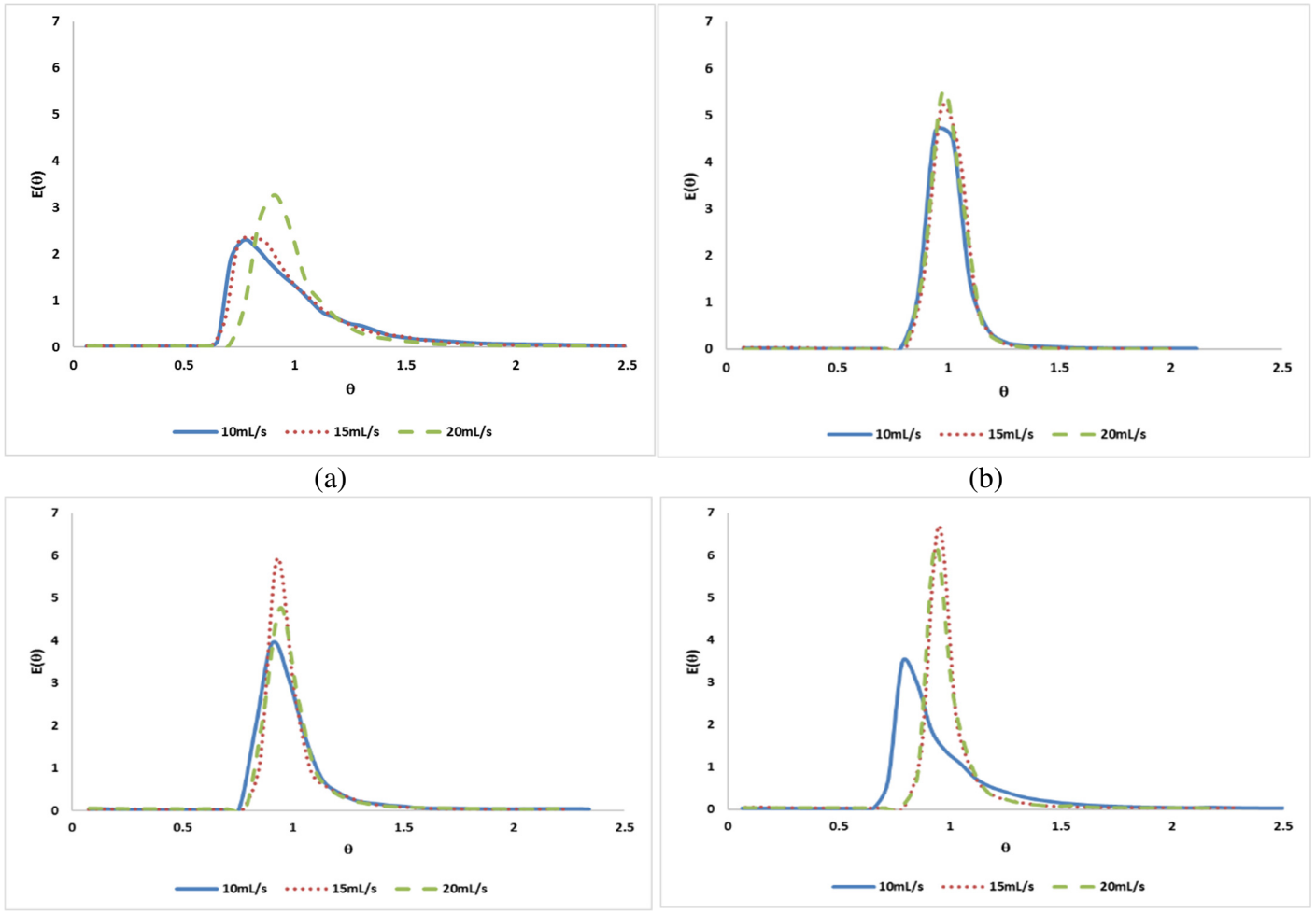

Figure 5.7: Effect of flowrate on RTD on smooth disc, (a) 100 rpm; (b) 200 rpm; (c) 250rpm and (d) 300 rpm.

Table 5.1: Dispersion parameters for water on smooth disc at different flowrates and rotational speeds.

Flowrate	**Dispersion number (=D/u_mR)**			
(ml/s)	**100 rpm**	**200 rpm**	**250 rpm**	**300 rpm**
10	0.112±0.006	0.051±0.006	0.084±0.005	0.107±0.021
15	0.114±0.008	0.046±0.003	0.078±0.003	0.079±0.008
20	0.087±0.006	0.036±0.003	0.085±0.007	0.076±0.005

Fig. 5.6 shows an increase in the flowrate from 10 to 20 mL/s induces in a narrower RTD. In terms of the hydrodynamic phenomena of the thin film flow, an increase in flowrate has a similar influence to an increase in disc rotational speed on the approach to plug-flow behaviour. Achieving this, it causes higher shear in the thin film and more surface ripples and hence better mixing, resulting in even and homogenous distribution of the reaction zones (Boodhoo and Al-Hengari, 2012; Mohammadi and Boodhoo, 2012). Previous work has noted that to achieve close to plug-flow behaviour, the flow needs to have a uniform velocity profile in the direction perpendicular to the flow direction and also simultaneously have negligible dispersion in the direction of flow (Boodhoo and Al-Hengari, 2012; Mohammadi and Boodhoo, 2012). Surface ripples (waves) are usually absent at low disc rotational speeds and low flowrates where a smooth thin film in the laminar flow regime prevails (as illustrated in Figure 5.1 .and 5.2). Boiarkina *et al.* (2011) demonstrated for the reactor used in this work using dye mixing in a water film that the dye followed the wave fronts with limited radial mixing without significant mixing in front, confirming that for this spinning disc reactor that the flow is likely to be plugflow as the streaklines were sharp and no significant dye mixing was observed. The results above appear to confirm this result (further analysis is presented in Section 5.2.2). However, any micromixing within the generated dye streaklines would not have been visible.

5.3.2 Effect of disc surface

The aim of introducing a macrostructured disc surface was to increase mixing and overcome the mass transfer limitations seen in previous work Boiarkina *et al.* (2011;

2012). This can in part be examined using RTD analysis. Only grooved discs were analysed, considering the poor wetting already seen in Section 5.1 in the visual analysis of these systems.

Fig. 5.8(a) and (b) show the RTD profile comparisons between the smooth and grooved discs at different operating conditions. Under same conditions of disc rotational speed and flowrate, it is observed that the grooved disc is generally associated with an overall narrower RTD compared to smooth disc at higher disc rotational speeds as shown in Fig. 5.8 (a) and higher flowrates (Fig. 5.8(b)). The flow profile was typically sharper than that for the smooth disc between these two extremities (Fig. 5.8). This result likely relates to one or more of the following:

1. A greater number of instabilities or turbulent eddies are generated in the film because it flows across the texture disc. The texture has been shown to govern the RTD and intensity of surface wave formation (Jachuck and Ramshaw, 1994; Mohammadi and Boodhoo, 2012). These occur as a results of film detachment on the surface and its subsequent re-attachment at the disc edge.

2. On gravity driven flows, studies have shown that rivulet flow may be overcome on textured surface. Rivulet flow as opposed to film flow would lead to more continuous film to form and propagate throughout the surface which can result in thinner films with higher surface coverage, specifically under strictly laminar flow conditions. Thus, the intensifying results of the grooved disc in this study may be related to the ability of the grooves to encourage more steady continuous film flow on the grooved disc than the smooth disc at different operating conditions. With the continuous film breakdown this may lead to rivulet flow occurring. A combination of these improvement factors exhibited by the grooved disc would be contributory to promoting good control of the RTD. This corroborates the results found in Section 5.1, where the grooved disc is observed to promote a more smooth film formation.

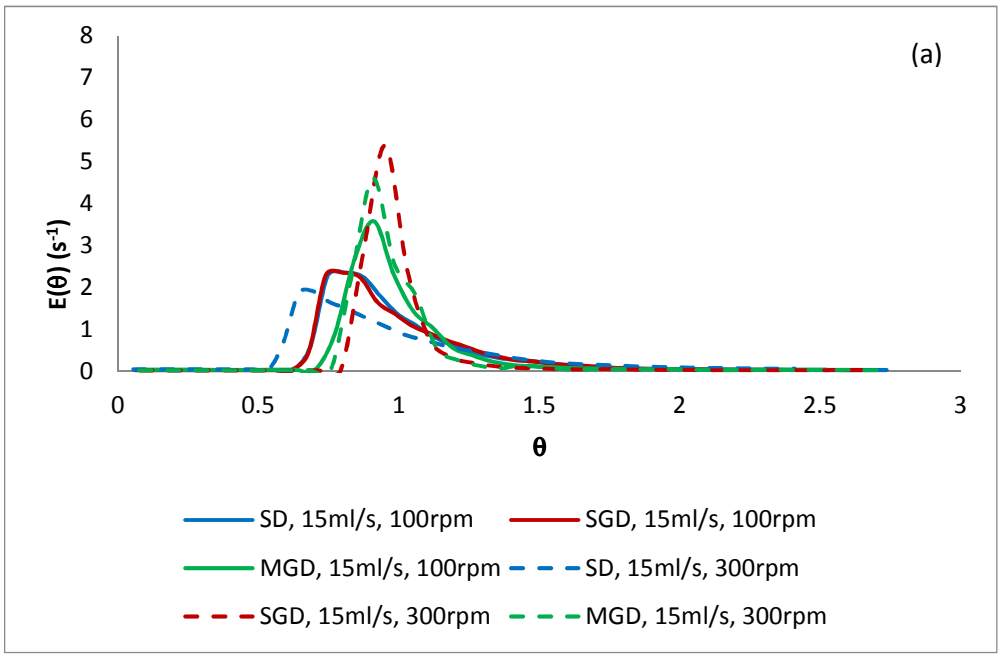

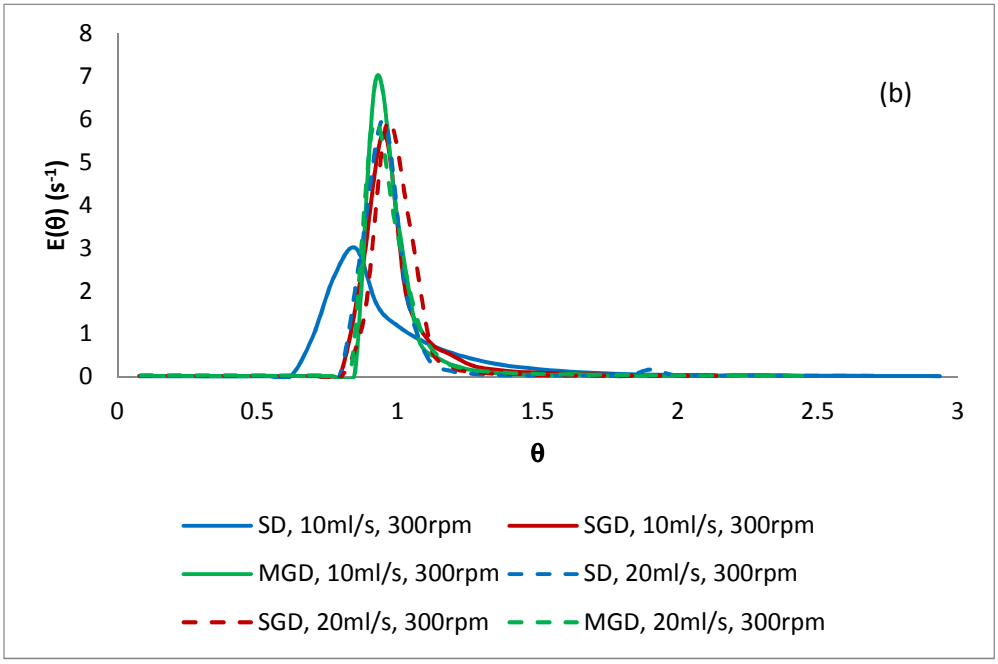

Figure 5.8: Influence of grooved disc on RTD curves (a) 100 rpm and 300 rpm at flowrate of 15 ml/s, (b) 10 ml/s, 20 ml/s at rotational speed of 300 rpm.

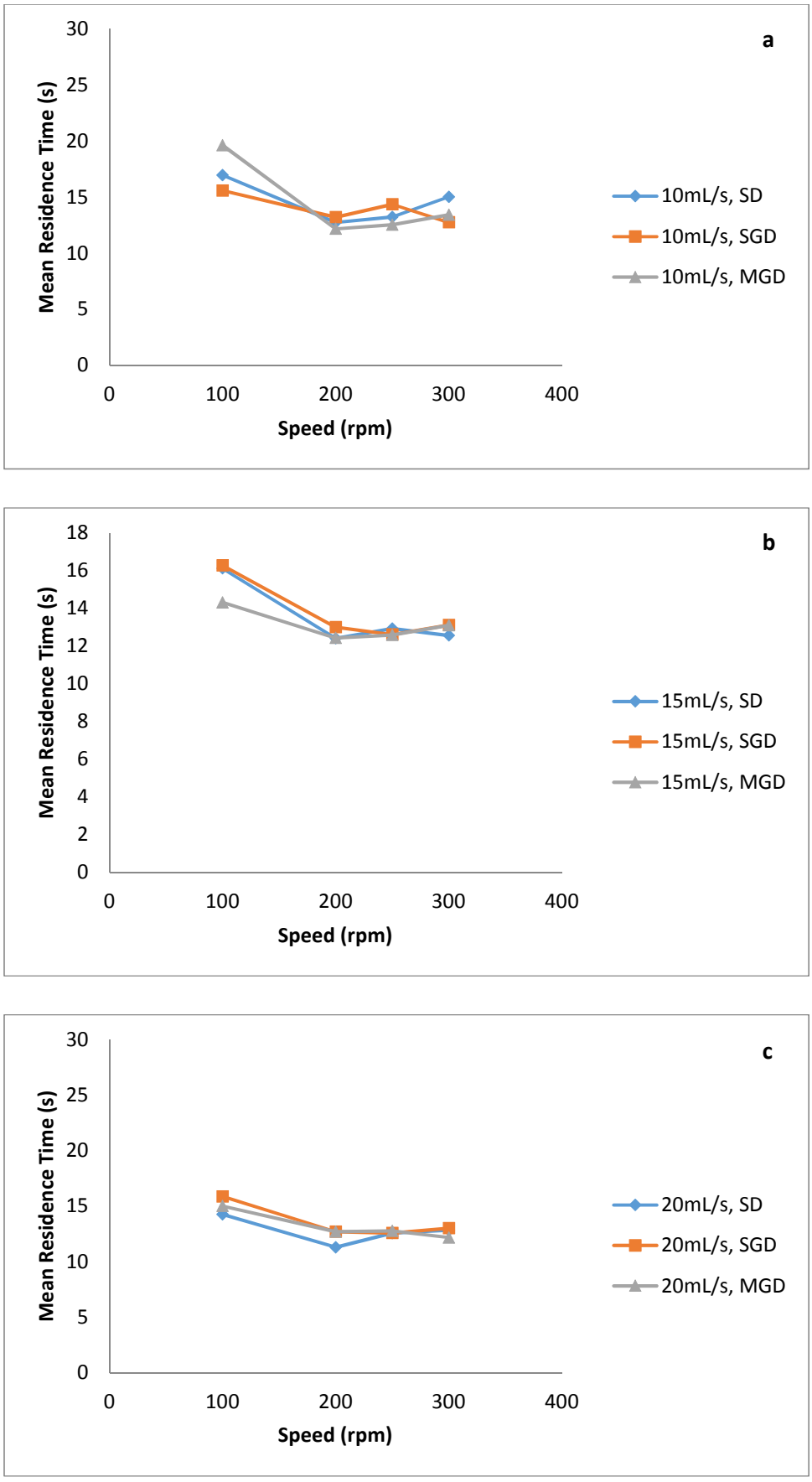

Fig. 5.9. The mean residence time at different spinning speeds and flow rates.

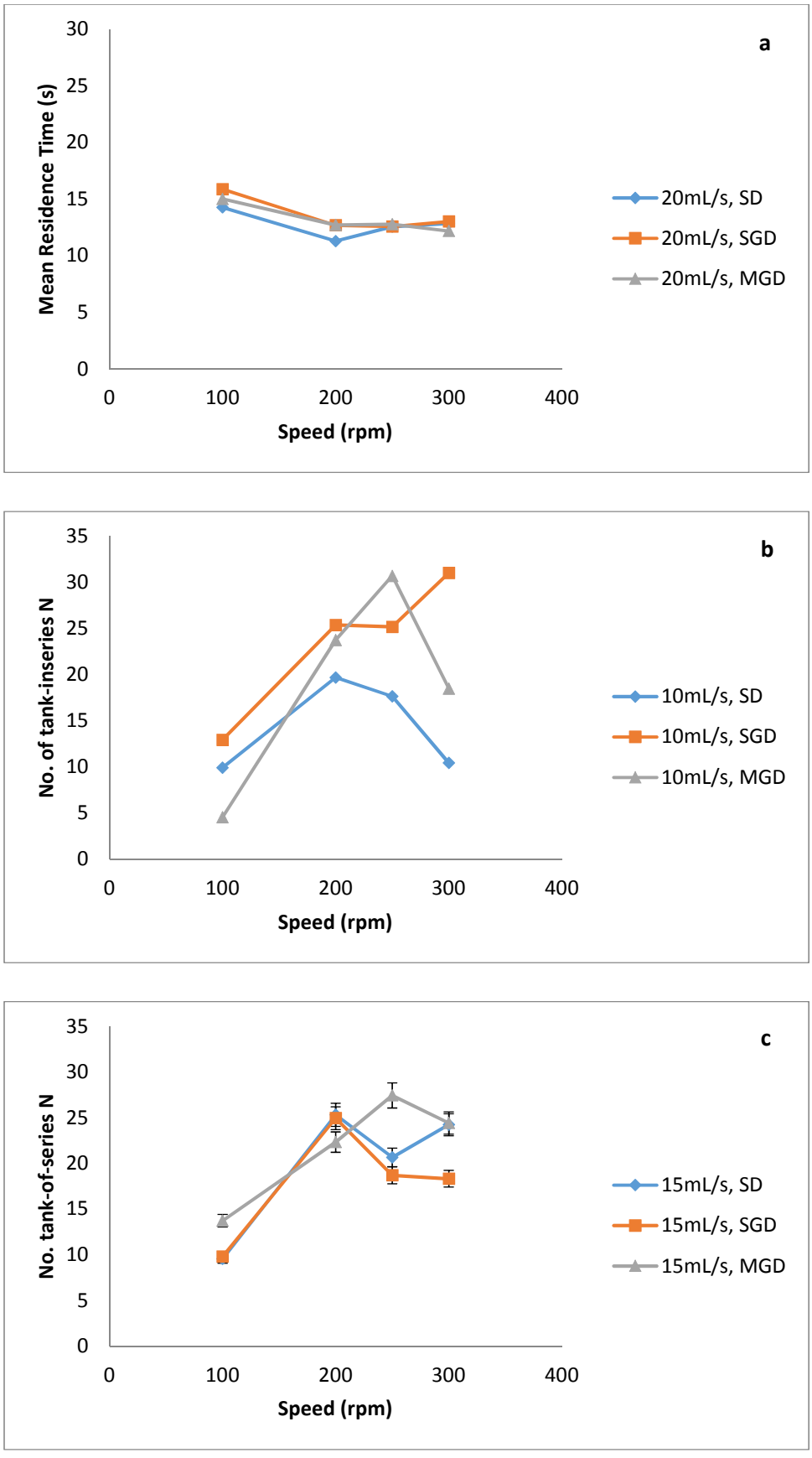

Fig. 5.10. The number of tanks-in-series (N) at different spinning speeds and flow rates.

Fig. 5.9 shows the mean residence time versus spinning speed of disc. In addition, as expected, the mean residence time decreased with the increase of spinning speed and flow rate. A large number of tanks-in-series (N) means that the flow pattern is close to plug flow (N > 50 is usually considered as a small deviation from plug flow). As can be seen from Fig. 5.10, N increased with an increase of spinning speed. At a spinning speed of 100 rpm, due to smaller centrifugal forces, the mixing efficiency on the disc was low; hence the residence time was longer. It was estimated N increased with the speed increase, but when the speed higher than 200 rpm the results are not consistent either the N lower or higher compare to 200 rpm. But still higher compare to 100 rpm. These possibly caused by less liquid in contact with the probe when speed increased.

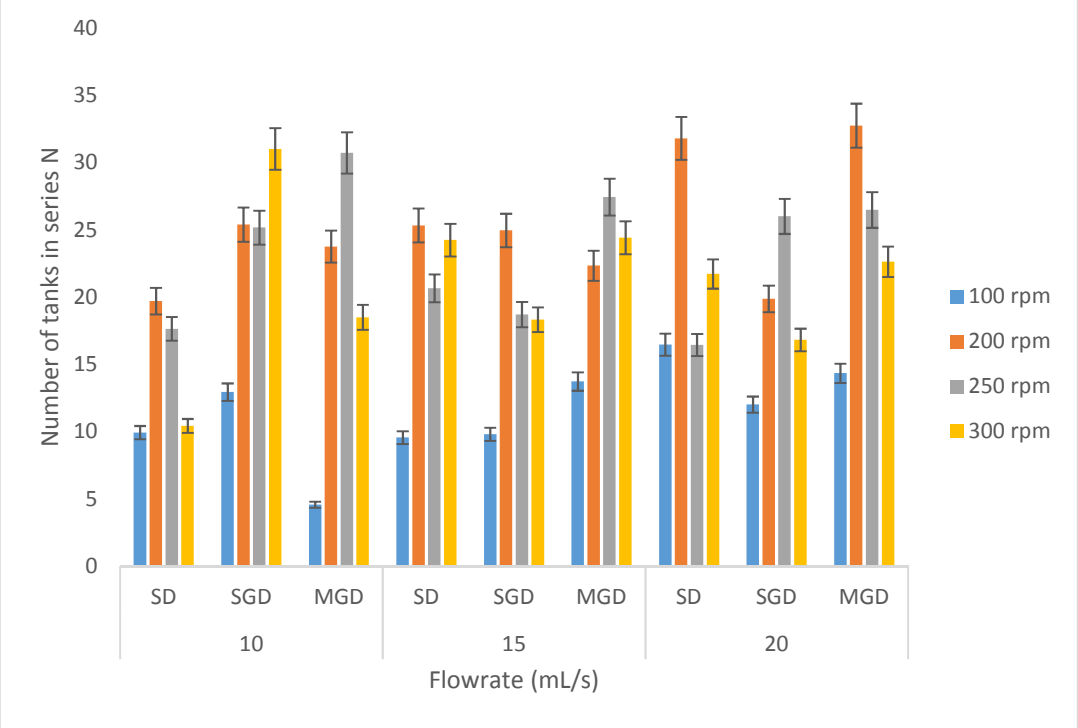

Figure 5.11: Number of tanks-in-series for smooth disc vs. grooved disc at different disc rotational speed.

The overall results for the number of tanks-in-series are illustrated in Fig. 5.10. It is seen that the number of tanks-in-series is generally higher with the grooved disc than with the smooth disc, with more pronounced increases in N from, for instance, 32 for the smooth disc to 33 for the grooved disc at the higher disc speed and flowrate of 200

rpm and 20 ml/s respectively. These data reinforce the beneficial effect of higher disc speed as explained above.

The RTD was demonstrated to be strongly influenced by rotational speed, liquid flowrate, and type of disc surface. The best operating conditions for obtaining narrower distributions are high rotational speeds, high flowrates and textured disc surface. Interaction effects particularly between the disc speed and flowrate on RTD have been demonstrated, which highlight the advantages of operating at the high disc speed of 200-300 rpm in this study. A grooved disc was also shown to be even more effective over a wider range of operating conditions, most likely due to the altered hydrodynamics which ensure that film breakdown is minimised. The MGD also shown higher no of tanks-in-series compare to SGD. This probably the ability of MGD having more grooves to encourage more steady continuous film flow compare to less grooved surface. In comparison with the smooth surface, the grooved surface can produce much narrower distributions.

5.4 Micromixing Studies

The aim of this work was to investigate the micromixing efficiency of an SDR when varying process parameters like rotating speed or surface structure of the disc, or volume flow. For this purpose, the iodide-iodate reaction (Villermaux–Dushman reaction) is carried out as a competitive parallel reactions system, which allows the quantification of the micromixing degree and mixing time, where a very fast, i.e., an instantaneous reaction competes with a slower but still fast reaction. (Fournier, Falk and Villermaux, 1996).

5.4.1 Micromixing Analysis Using the Iodide-Iodate Reaction – Examining the Effect of Rotational Speed and Volumetric Flowrate

The fluid dynamics of the fluid flow on the disc is decisively influenced by the rotational speed of the disc as demonstrated in previous work and in the work above. As shown in Eq. (5.1), the film thickness decreases on the disc with the increasing of rotational speed. The reason is that with the increasing of the rotational speed of the

disc the film thickness will decrease therefore the diffusion time is reduced. In addition, as described in Jacobsen and Hinrichsen (2012), a higher number of waves observed on disc surface (Fig. 5.1-5.4) when the rotational speed and the flowrates increases. This additional turbulence induced the mixing, whereby the micro-mixing can be positively influenced.

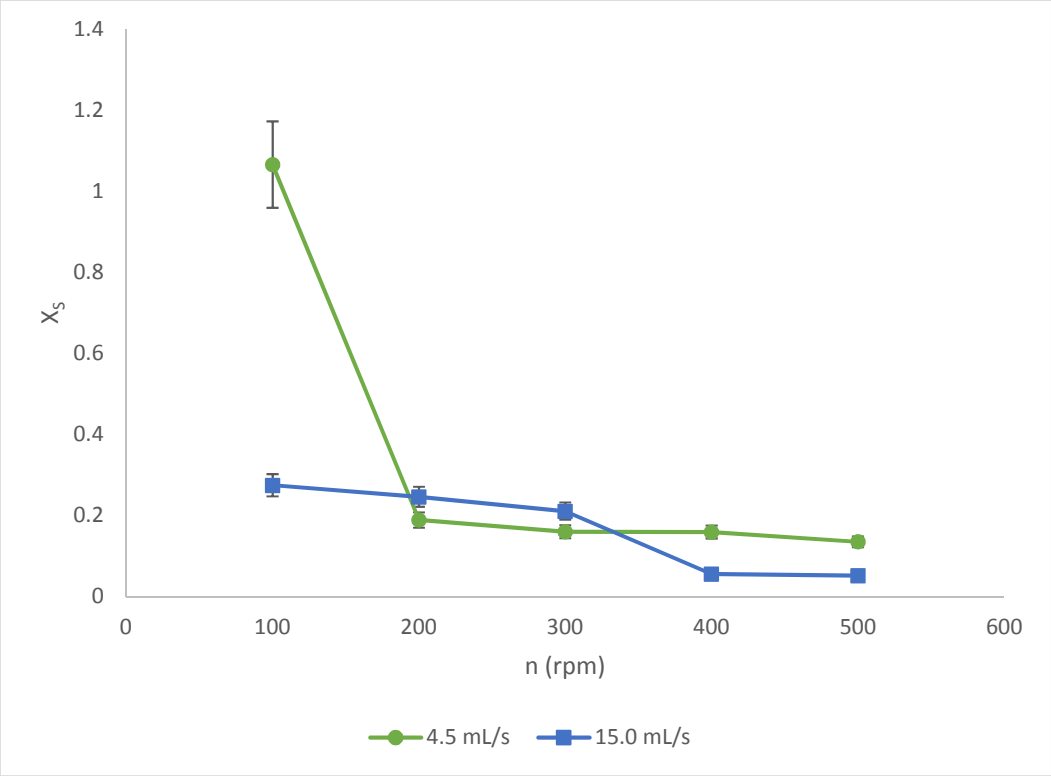

Figure 5.12: Segregation index dependent on the disc speed and the volume flow at a dosing distance of r = 10 mm.

Fig. 5.12 shows the Villermaux-Dushman reaction determined values of the segregation index as a function of the rotational speed and the total flowrate of the reactants. The dosage of sulphuric acid was each at 20 mm distance from the disc centre. The dependence of the film thickness of speed and volume flow according to the Synchronized flow model according to Eq. (5.1) is shown for comparison in Fig. 5.13. Both the segregation index and the film thickness decrease with increasing rotational speed. Initially both rapidly decrease and become flatter when the rotational speeds increasing. In the speed range n > 300 rpm only slightly influence the total

volume flowrate can be seen on the micro-mixing, which can be explained by the small difference in the film heights. At speeds from 100 to 200 rpm, however, an improvement of the micro-mixing is observed with decreasing of the volume flowrate. There is thus a direct dependence of the segregation index of the film thickness.

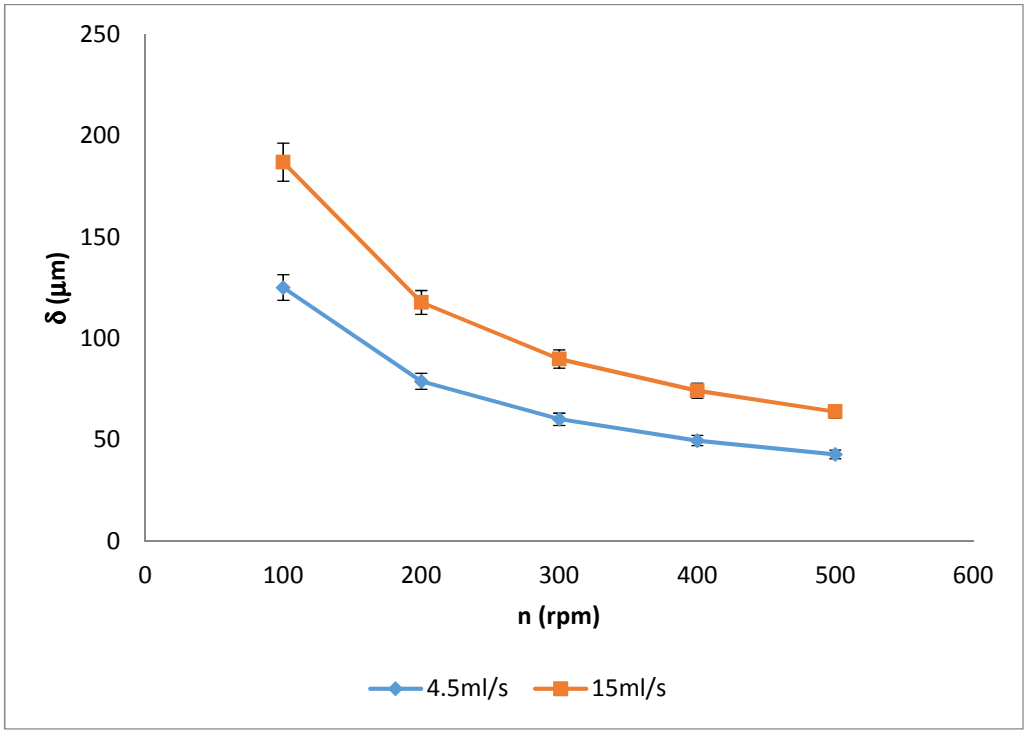

Figure 5.13: Calculated film thickness versus the rotational speed.

Furthermore, the influence of the volumetric flow rate on the mixing degree has been examined. Experiments have been performed at total volume flow rates of 4.5, and 15.0 mL/s with a feed ratio of 1:1. At a lower rotational speed, one may recognize that with increasing volumetric flow rates, better micromixing efficiency can be obtained. By comparing the measurement data (Figure 5.12) with the predicted film thickness of the Nusselt model (Figure 5.13), it can be seen that the obtained results support the assumption that the height of the liquid film is one of the decisive parameters for the degree of micromixing.

The expected influence of a better disc surface wetting at a volumetric flow rate of 15 mL/s in comparison with 4.5 mL/s at 100 rpm can be observed. It seems that the

increase in film thickness caused by the higher hold-up compensates for the worse mixing conditions due to dry areas on the surface at low flow rates.

5.4.2 Micromixing Analysis Using the Iodide-Iodate Reaction – Examining the Effect of Structure of the Disc

The usage of textured discs influences the hydrodynamics and formation of the waves. Ramshaw and Jachuck (1994) demonstrated that a grooved disc drastically improves the heat transfer caused by continual creation and breakdown of the boundary layer between the disc and liquid. This implies that micromixing should be improved.

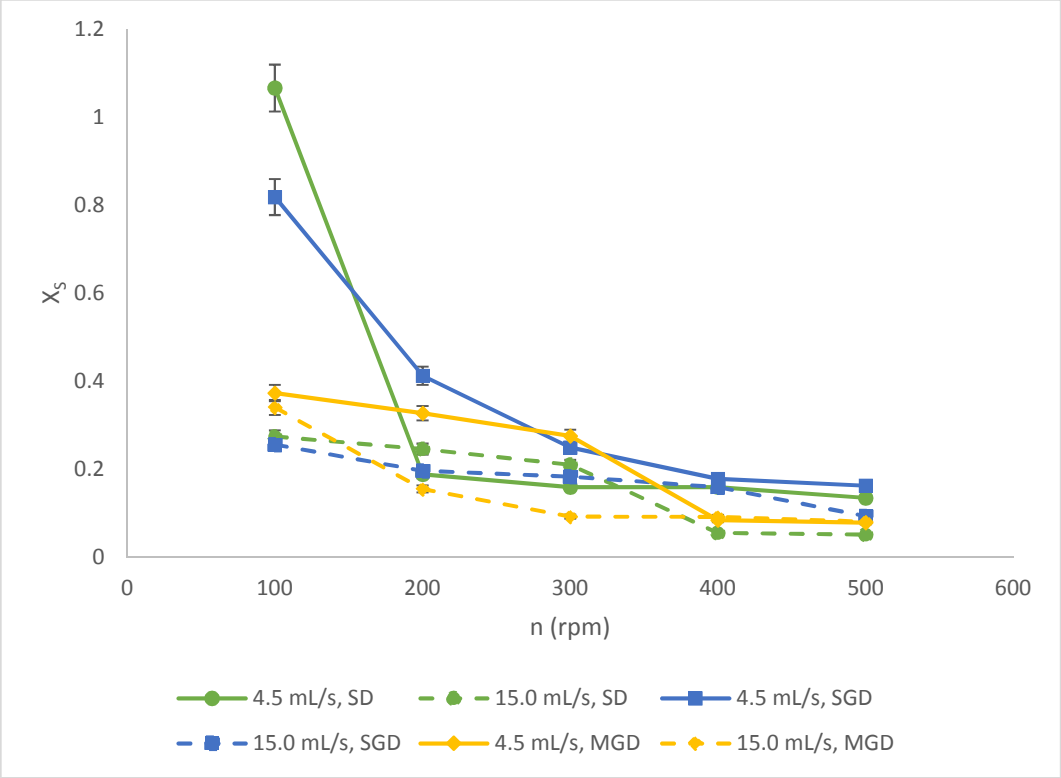

Figure 5.14: Influence of the disc texture on the mixing quality (Q_{tot} = 9 mL/s).

Section 5.1 and 5.2 have shown that the textured disc surface changes the hydrodynamic characteristics of the film like the intensity of surface wave formation. As shown in Figure 5.14, the grooved disc surface used in this work, especially the

MGD, provides an improved mixing efficiency compared to the smooth disc with spinning speeds of 200 to 500 rpm.

The increased formation of waves attributable to grooves induces instabilities in the liquid film, resulting in an improved mass transfer. Particularly at rotational speeds in the range of 300 – 500 rpm, the effect of the textures is maximized. It can be seen on the high-speed camera recordings and Figure 5.4 that in this range the grooved disc (SGD and MGD) allows a better wetting of the surface. At lower disc speeds, the smooth surface and SGD shows better micromixing efficiency compared to MGD. This is because the radial and tangential velocities of the liquid at lower speed are so small that the liquid remains in the grooving and is less mixed which caused film breakdown leading to rivulet flow occurring.

Overall, it is expected that the increased micromixing with the grooved discs should help overcome the mass transfer limitations noted in previous work with this SDR and result in higher overall reaction rates. This will be examined in the following experimental investigations.

5.8 Conclusion

Overall, the work in this chapter shows the effect of the operating conditions of the SDR on the hydrodynamics on the disc quantifying this in terms of the wave and flow patterns on the disc surface, the residence time distribution and the extent of micro-mixing varied with both disc spinning speed and inlet flowrate. This demonstrated the following:

1) From hydrodynamic studies, using a textured disc appears to even out the flow across the surface of the disc, which would increase the local UV penetration onto the disc surface (less scattering) and provide more uniform volumetric utilisation of the catalyst. This is an atypical need for most SDRs, where the typical characteristics of increasing disc rotational speed and feed flowrate show more complete film formation. However, since a more uniform film surface is needed for a photocatalytic SDR, the optimal film structures for enhanced reaction rates in other SDRs (that do not rely on high intensity of UV on the surface of the disc) may be different.

2) The RTD investigation provides a valuable insight into the operating conditions of the SDR which generate flow profiles approaching plug flow behaviour. RTD analysis showed that the flow pattern on the spinning disc became close to plug flow with the increase of spinning speed and flow rate. The textured discs in particular made the flow more plug flow – as quantified by a higher number of tanks in series. This indicates, as with the visual analysis/hydrodynamic studies that higher spinning speeds, higher inlet flowrates and a textured disc should result in conditions more favourable for higher reaction rates.

3) The Villermaux-Dushman experiment performed in the spinning disc reactor clearly show that the SDR is a device suitable for obtaining a high degree of micromixing efficiency. The mixing quality can be influenced by several process parameters such as the disc rotational speed, feed flowrate, and surface structure all proved to be important hydrodynamic parameters in determining the micromixing characteristics in SDR. The effect of the process parameters on the mixing efficiency has clearly been demonstrated by use of the iodide–iodate reaction. The best micromixing conditions were generally achieved at high disc rotational speeds, high feed flow rates and using textured discs.

CHAPTER 6: ENHANCING AND OPTIMISING THE REACTION RATE OF THE TiO_2 THIN FILM PHOTOCATALYST IN THE PHOTOCATALYTIC SPINNING DISC REACTOR FOR METHYLENE BLUE AND IBUPROFEN

6.1 Introduction

The experimental results are discussed in chronological order to illustrate the development of the results. Results are therefore ordered as such: Section 6.2 discusses the characterisation of the TiO_2 catalyst film using the XRD and SEM results. This is followed by a discussion of the UV irradiance profiles in the spinning disc reactor in Section 6.3, the results of which are used for photonic efficiency calculations later. This is followed by a discussion on the results of the performance of the SDR, and a discussion of the effects of operational parameters on its performance as a photocatalytic reactor for the degradation of methylene blue and ibuprofen.

6.2 Characterisation of the Titanium Dioxide Film

Glass discs were coated using the sol-gel method mentioned in Section 4.2 using a dip coating rig. An opaque white coating can be seen on the glass disc. A freshly calcined glass disc also had a layer of TiO_2 that was chalky and was removed easily. Application of soft brushing under flowing water completely removed the chalky layer leaving behind a far more cohesive layer of coating. This layer retained the white appearance and was only removable via scrubbing by steel wool.

An overall visual inspection of the coating revealed a non-uniform film. This was possibly caused by the uneven deposition of the sol-gel onto the disc surface during the extraction process resulting in several areas of the disc surface having a thicker coating. This situation improved by using the dip coating rig, which enabled a slower extraction rate and a lower viscosity sol to be used, so that the variation in film thickness around the disc was smaller. Note is that any unevenness was barely observable prior to calcination due to the sol being transparent.

6.2.1 Scanning Electron Microscopy Analysis of Glass Disc Coatings

The structure and morphology of the TiO_2 thin film before and after reaction was studied using Scanning Electron Microscopy (SEM), (Model: JEOL SEM6480). The SEM unit was operated at 10 kV accelerating voltage.

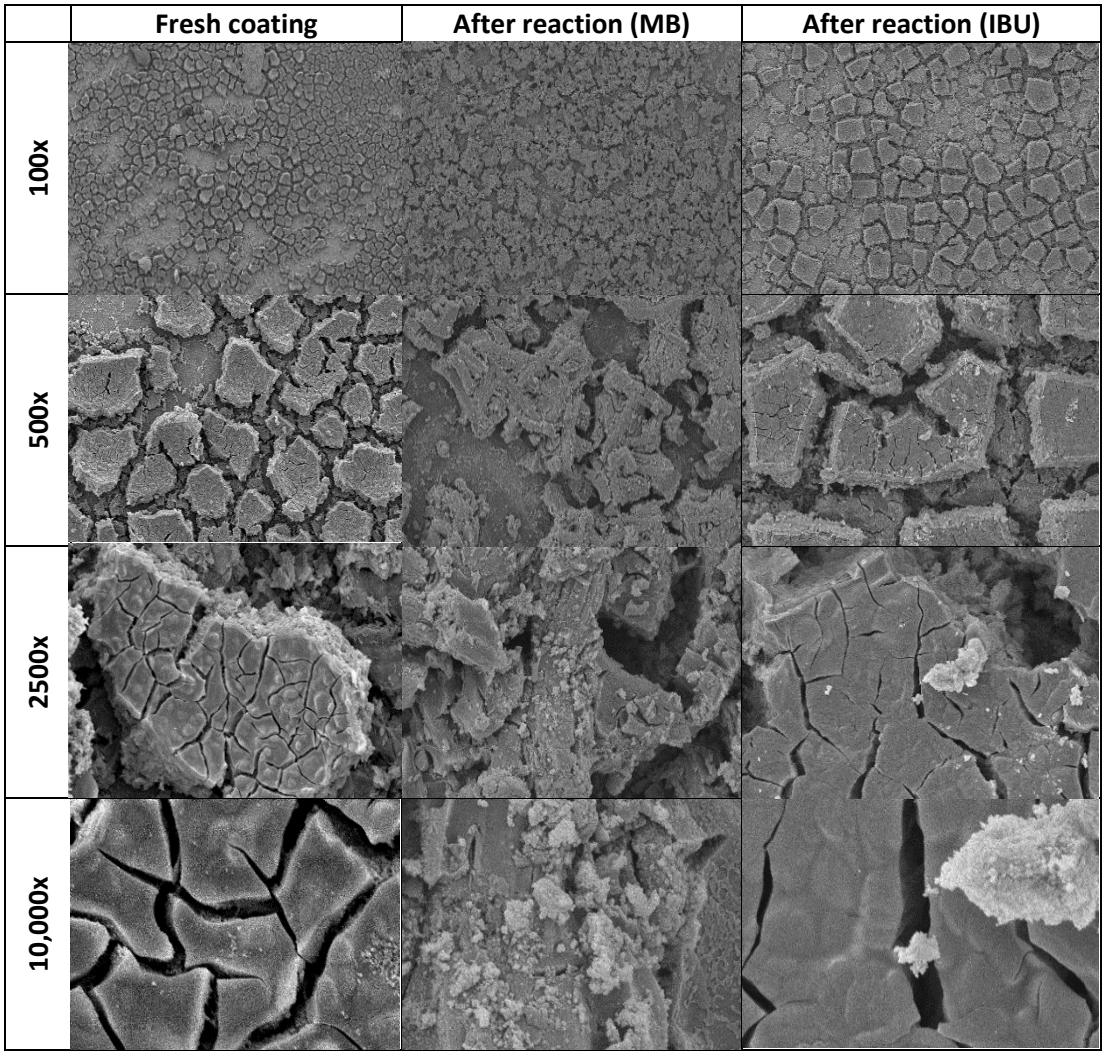

Figure 6.1: Surface morphologies of the TiO_2 thin films before and after photocatalysis (1μm).

Fig. 6.1 shows the SEM micrograph of the TiO_2 film coated on the glass disc under different magnifications. The picture shows a plain and smooth surface of TiO_2 film with few minor crack lines on the substrate. This indicated that the TiO_2 thin film layer was successfully coated on the glass disc with ultimate uniform and smooth appearance.

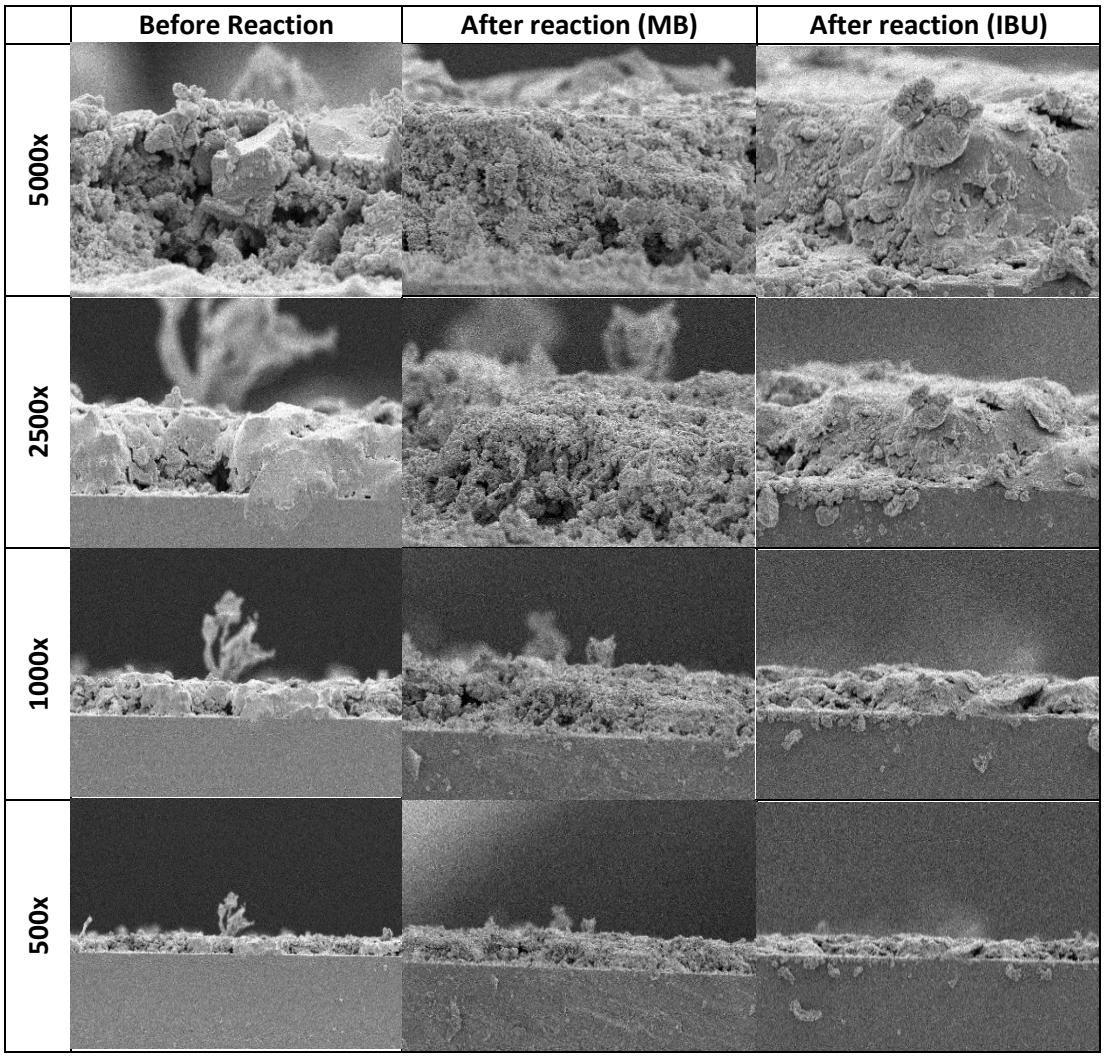

Figure 6.2: Cross-sectional view of the surface morphologies of the TiO_2 thin films before and after photocatalysis (1μm).

The film thickness obtained by dip coating was estimated to be 10 μm (Fig. 6.2). SEM analysis of the films showed a highly porous fractured appearance. The fracturing of the film is due to shrinkage and stress during drying (as the solvent from the sol gel is driven off and the material contracts during drying). Additional fracturing may have occurred throughout the annealing process due to the different thermal coefficients of expansion of the overlayer and the substrate.

6.2.2 X-Ray Diffraction Analysis

The photocatalyst was analysed with a Powder X-ray Diffractometer (BRUKER D8-Advance (Cu radiation)). Fig. 6.3 shows the X-ray diffraction (XRD) pattern of the

TiO_2 films at 550°C. The anatase peak, the most photocatalytically active crystalline form of TiO_2, was observed from discs calcined at 550°C. Calcination temperatures above 600°C, will convert anatase to the comparatively photoinactive rutile form. The excellent photocatalytic activity of the anatase phase has been reported by many researchers for the decomposition of organic pollutants (e.g. Houas, 2001). Thus, the temperature setting at 550°C was used to prepare all further TiO_2 photocatalyst films.

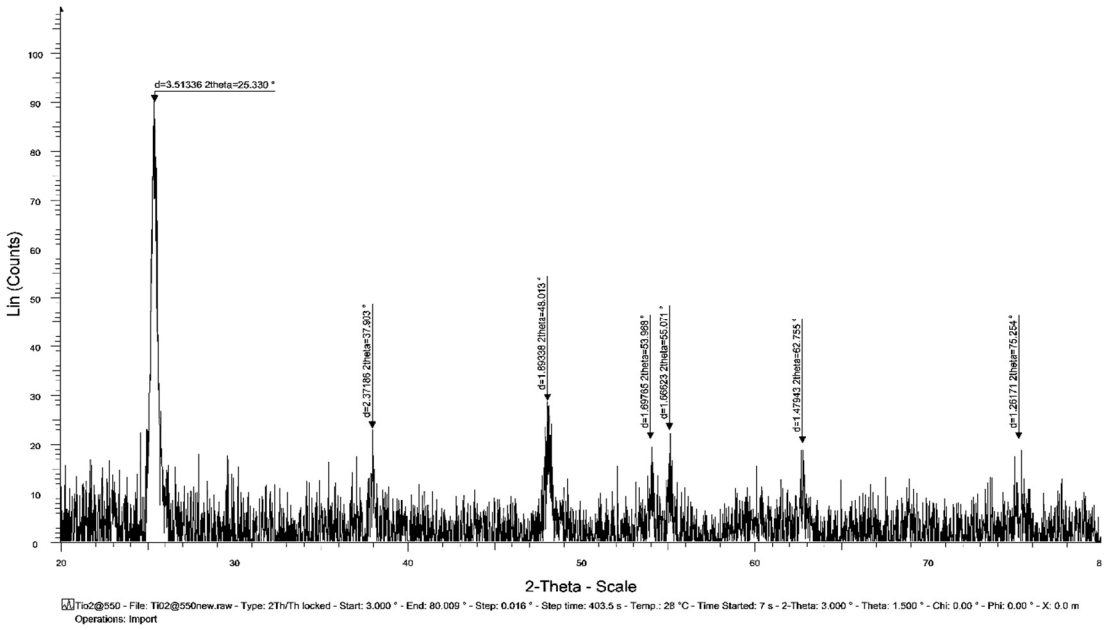

Figure 6.3: XRD pattern of the TiO_2 coated onto glass disc calcined at 550 °C.

6.3 Photon flux and photonic efficiency

The UV irradiance was measured at eight points inside the reactor level at the height of the glass disc's surface. Sigma Plot 12.3 was used to plot the irradiance distribution profile as shown in Fig. 6.4.

The irradiance profile is symmetric about the UV lamp axis with the maximum occurring at the centre of the disc. The irradiance profile is not completely homogeneous, with the measurements varying between 4 and 18 W/m^2. This compares well to a previous irradiance profile measured by Boiarkina *et al.* (2011, 2012, 2013b). Although unlike the results achieved in the work of Boiarkina et al.

which slightly higher the difference between the maximum and minimum still in the same order of magnitude.

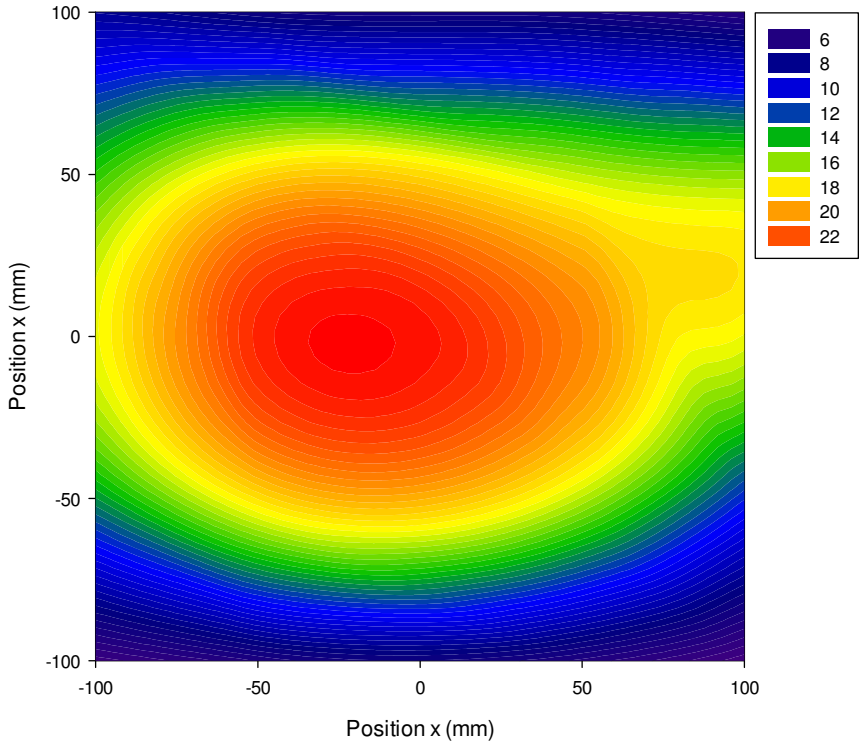

Fig. 6.4: UV light intensity distribution near the surface of the disc in the photocatalytic spinning disc reactor.

Fig. 6.4 and the reaction data were used to calculate the photon flux reaching the catalyst surface and hence the photonic efficiency of the process (Appendix C). The average photon flux was 2.05×10^{-5} Einsteins/m^2s.

6.4 Adsorption and Photolysis Experiments in the Spinning Disc Reactor for Methylene Blue

Experiments investigating the adsorption and photolysis of methylene blue in the reactor had to be carried out prior to any photocatalytic reactions in order to:

1. Specify the dark equilibration time for adsorption to take place so that any subsequent change in concentration of the substrate during the photocatalytic experiments are due to degradation only.

2. Evaluate if the substrate degrades significantly under UV light, without catalyst.

Figure 6.5a shows the adsorption of methylene blue with respect to time in the reactor and shows no decrease in the concentration of the substrate after 30 minutes. Based on this result, an adsorption time of 30 minutes was chosen prior to carrying out any reactions and this is also consistent with previous work using this reactor (Boiarkina, Pedron and Patterson, 2011; Boiarkina, 2012; Boiarkina, Norris and Patterson, 2013a, 2013b).

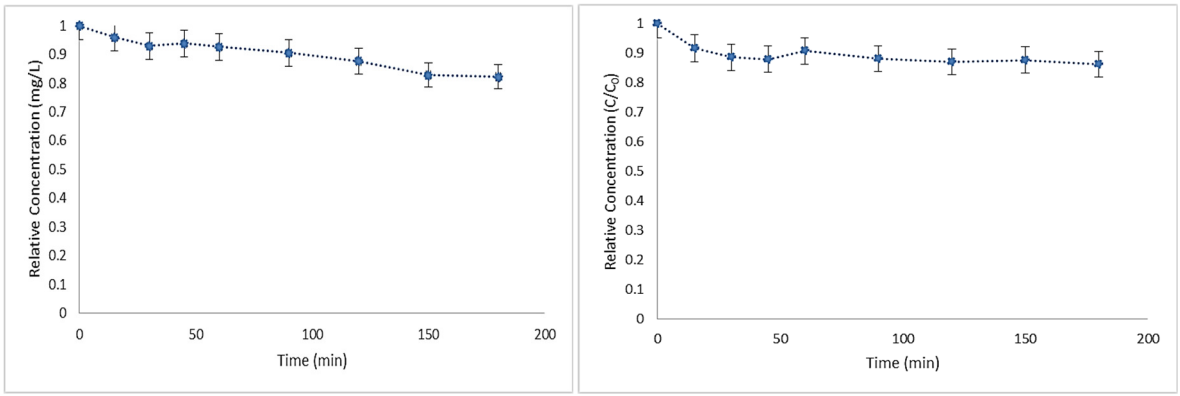

(a) (b)

Figure 6.5: Methylene Blue control experiments - adsorption and photolysis inside SDR (a) Adsorption on reactor; (b) Photolysis.

The photolysis results are given in Figure 6.5b. These results show that no degradation of methylene blue takes place over three hours due to exposure to UV light alone. Hence photolysis can be excluded as a degradation mechanism during the photocatalytic reactions and again this is also consistent with previous work using this reactor (Boiarkina, Pedron and Patterson, 2011; Boiarkina, Norris and Patterson, 2013a, 2013b).

6.5 Characterisation of the Photocatalytic Spinning Disc Reactor for Methylene Blue

The aim of this work was to investigate the effect of four key control parameters in the photocatalytic spinning disc reactor (pSDR): initial reactant concentration, feed

oxygenation, spinning speed and feed flowrate on the degradation rate, reaction kinetics and reaction mechanisms. Methylene blue (MB) was used as the benchmarking compound and was chosen since it has well established kinetics and reaction mechanisms in conventional photocatalytic reactors that can be used to benchmark the pSDR performance against and was used in previous investigations of the pSDR (Boiarkina, Pedron and Patterson, 2011; Boiarkina, Norris and Patterson, 2013a, 2013b).

6.5.1 Effect of Initial Reactant Concentration: Primary Degradation of Methylene Blue

The effect of initial MB concentration on the photocatalytic efficiency of the pSDR was examined. The photocatalytic degradation of MB was studied by varying the initial concentrations from 5 to 15 mg/L. The reaction profiles (normalised concentration versus time profiles) are presented in Fig. 6.6 and 6.7.

Figure 6.6 shows the expected results:

- A higher overall degradation for methylene blue solution with a lower starting concentration (and same oxygen feed environment), since with the same catalyst area (and mass) and supply of oxidant this lower total number of molecules will be degraded faster. At a fixed UV-light intensity, the decrease of degradation efficiency with increasing dye concentration may be attributed to the competition among dye molecules for degradation, inhibition of intermediates produced in degradation processes, and/or the reduction in the light intensity that reaches the TiO_2 surface by the scattering effect. In particular, at higher dye concentrations above 10 mg/L, more light was scattered by the dye solution and fewer photons are able to reach the TiO_2 surface. Thus, the generation of electron-hole pairs was greatly reduced, and in turn, the dye degradation was reduced due to absence of the oxidizing species. As Wang *et al.* (2000) reported that the deactivation of catalyst was observed since the adsorption of reaction intermediates on the TiO_2 surface (Guettaï and Ait Amar, 2005) In contrast, at lower concentration, the lower degradation efficiency may be attributed to the mass transfer resistance notwithstanding the mass-transfer intensified by disc rotation.

- For the smooth discs and for the degradation of methylene blue, a supply of oxidant increases reaction rate – indicating that at the conditions that these reactions were run at, there is insufficient mass transfer area and mixing (including micromixing) on the disc to supply the reaction with oxygen and this is likely the rate limiting factor in the reactions where oxygen is not supplied.

The highest degradation rate was for an initial MB concentration of 5 mg/L, a high extent of degradation was observed (96.6%) after 60 min of irradiation in pSDR.

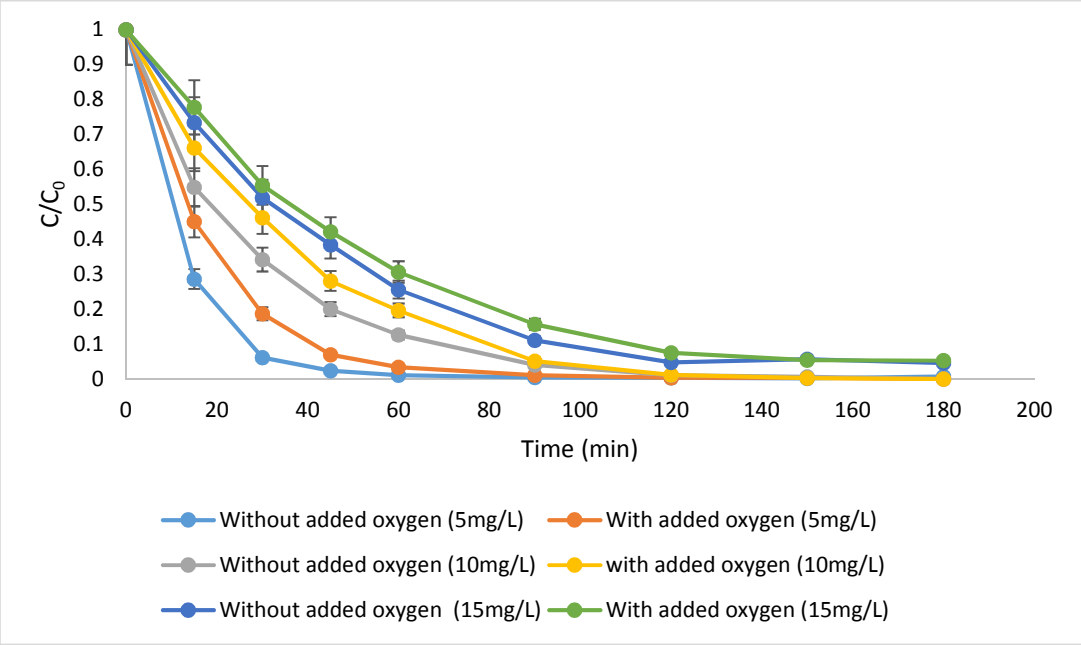

Figure 6.6: Effect of initial concentration of the photocatalytic degradation of MB in pSDR (UV-Vis) at different MB solution initial concentration: 5 mg/L, 10 mg/L, 15 mg/L.

Fig. 6.7 was the photocatalytic reaction kinetics of MB degradation efficiency based on the data plotted in Fig. 6.6. As shown in the figure, a fairly good correlation to the pseudo-first order reaction kinetics was found.

Therefore, it is reliable to conclude there are concentration effects and that a lower concentration is better since there are light absorption effects – which need to be accounted for. Due to the light absorption and scattering at concentrations of MB

above 10 mg/L, the inlet concentration of MB was limited to 10mg/L for all further experiments.

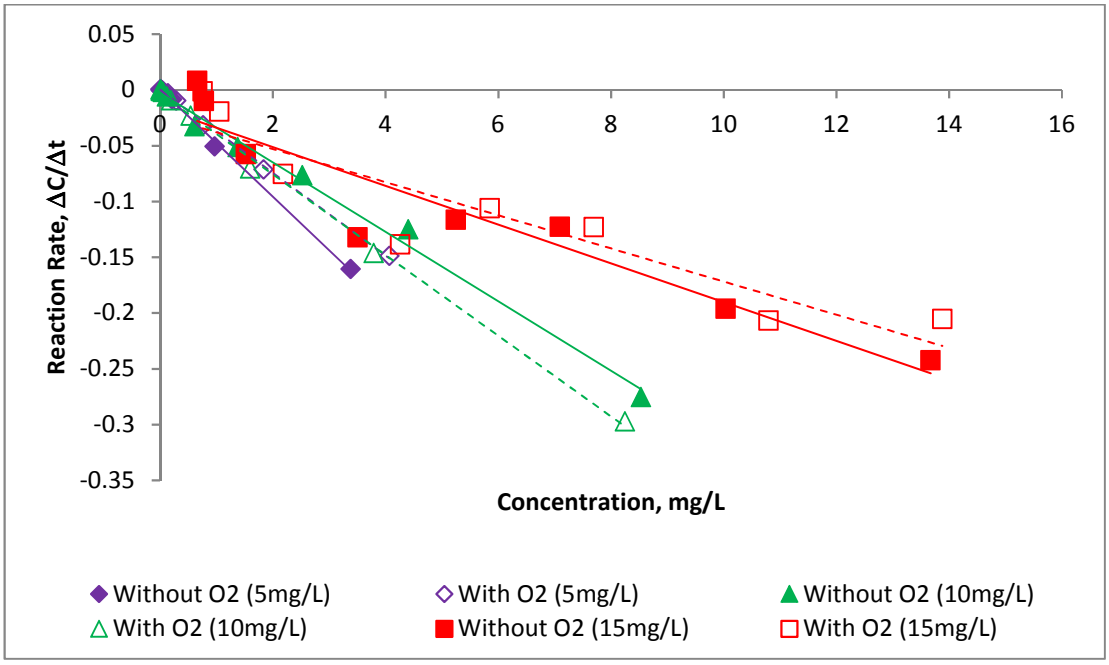

Figure 6.7: Kinetics of MB degradation in pSDR with different concentration.

6.5.2 Effect of Oxygen Feed, Rotational Speed and Feed Flowrates on Primary Degradation (Methylene Blue)

The results above indicate that there are several effects on overall MB degradation in the pSDR – including the effect of oxygen feed. Therefore, the degradation rate with and without oxygen added to saturate the feed with oxidant was investigated as a function of the two main tuneable parameters in the pSDR: the feed flow rate and spinning disc rotational speed.

Several experiments were performed to evaluate removal efficiencies and photocatalytic reaction rates MB using the pSDR. The area of the disc coated with titanium dioxide was calculated to be 0.03m^2 (and this is considered to be the active and irradiated surface area of the disc) – this was used for all reaction rate calculations, since rate needs to be reported on a surface area basis considering that photocatalysis is a surface area based catalysed reaction. All experiments were performed under UV

radiation unless otherwise noted. Photocatalytic degradation of MB in the pSDR was investigated at an influent concentration of 10 mg/L (26.74 µmol/L).

The degradation of MB is shown in Figure 6.5. In the pSDR, MB maybe degraded or removed under various pathways such as TiO_2 adsorption, photodegradation and photocatalysis. In Section 6.5.1 (and again here), there is a small amount of adsorption of MB in the reactor, however photolysis is negligible at these conditions, which is likely due to the light intensity being too low at the surface of the disc (which also indicates that the pSDR utilises this UV light intensity for photocatalysis – making it more efficient that other photoreactors that propagate photolytic reactions, such as annular photoreactors). So, Fig. 6.5 shows that under photocatalytic conditions, 99%+ degradation is achieved and this is likely due to photocatalysis only (no photolysis).

Three effects were examined:

- The effect of spinning speed at constant flowrate
- The effect of inlet flowrate at constant spinning speed
- The effect of feeding oxygen (fed to produce oxygen saturation in the feed or not fed, so that the only oxygen supply is through the surface area of the liquid on top of the spinning disc) at both of the above conditions.

Figures 6.8 and 6.9 shows the effect spinning speed at constant flowrate. This shows that at the conditions considered:

- Higher spinning speeds increase reaction rate. From Chapter 5, Section 5.4.1 it was shown that higher spinning speeds increases micromixing which is likely part of the explanation. The imaging studies (Section 5.4.1) show that the film surface under these conditions becomes smoother and therefore there is less UV scattering and higher UV penetration.
- At 300rpm, the reaction without oxygen being fed at saturation has the highest reaction rate. This is not expected and indicates that perhaps excess oxygen is detrimental to this reaction. Increased micromixing at these higher spinning speeds (Section 5.4.1) would enable a higher mass transfer of oxygen away from the top surface of the liquid film on the disc and therefore enhance mass transfer of oxygen into the pSDR – perhaps enabling sufficient (but not too

much) oxygen to be available for MB photocatalytic degradation to occur. This will be examined further below.

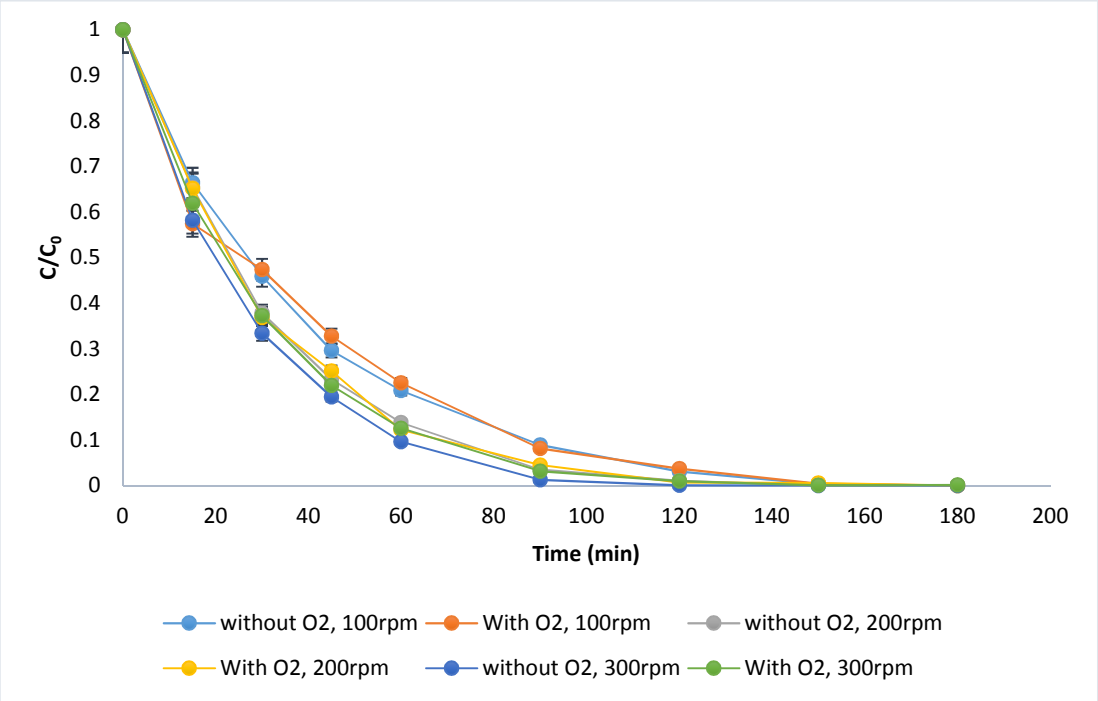

Figure 6.8: Effect of spinning speed and oxygen feed (with and without) at 10mL/s flowrate (UV-vis).

With the effect of absorption and scattering of photons eliminated through using a lower MB concentration (10 mg/L), the kinetics of these reactions approximate a pseudo-first order reaction (Fig. 6.9 and 6.11), with an adsorption period in the dark of 30 min. The apparent first order kinetics is in agreement with a generally observed Langmuir–Hinshelwood mechanism, with the rate *r* being proportional to the coverage θ which becomes proportional to *C* at low concentrations

$$r = k\theta = \frac{kKC}{1+KC} \approx kKC = k_{app}C \qquad 6.1$$

The derived fitted apparent first order reaction rate constants are given in Table 6.1 and 6.2. Table 6.1 rate constants bear out the same trends as discussed above with respect to spinning speed and oxygen feed.

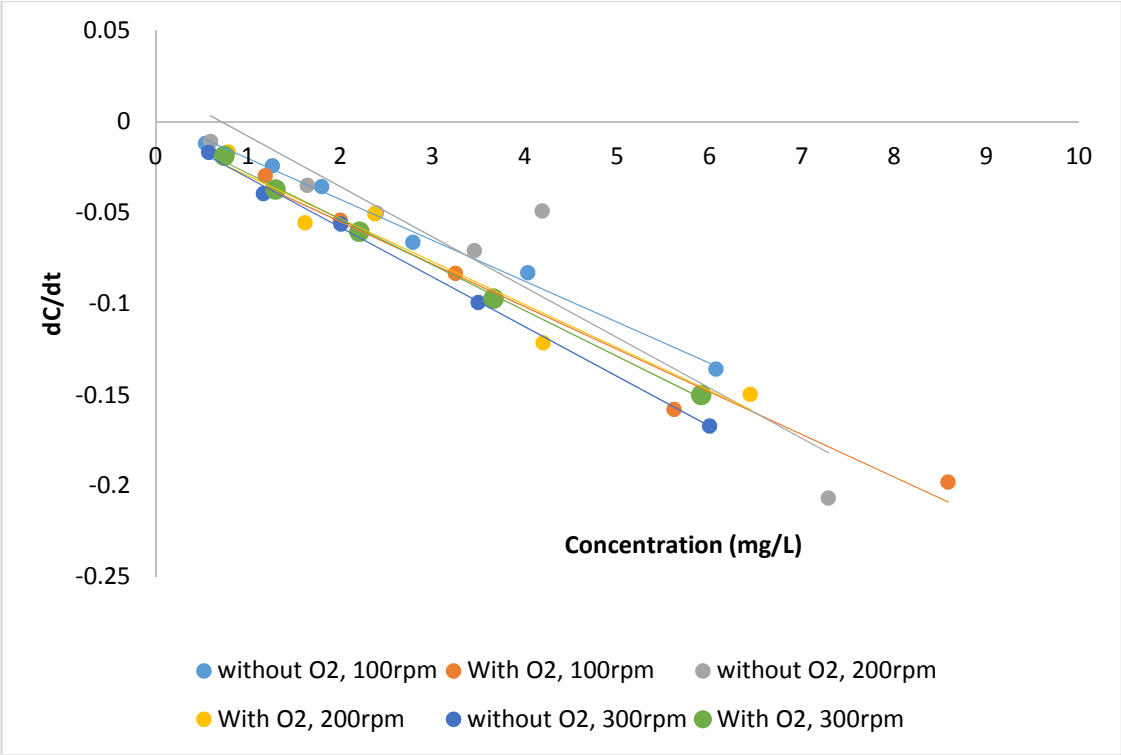

Figure 6.9: Reaction rate versus concentration for the results in Figure 6.8 showing that an apparent first order kinetic fit is appropriate now.

Table 6.1: Reaction rate constants for MB reactions at 10mL/s

Oxygen	Speed (rpm)	k_{app} (min^{-1})	$k_{app,S}$ ($min^{-1}m^{-2}$)
Without	100	0.0225	0.0764
With	100	0.0234	0.0795
Without	200	0.0277	0.0941
With	200	0.0236	0.0801
Without	300	0.0273	0.0927
With	300	0.0251	0.0852

Examining the effect of inlet flow rate and added oxygen for these experiments (Figure 6.10, 6.11 and Table 6.2), the following can be observed:

- When oxygen is supplied, there is no significant difference between the degradations at the different flow rates. This indicates that the differences in residence times (and the overall recirculation times associated with these in this

circulating batch photoreactor) do not make a difference in the overall degradation at these conditions.

- There is no significant difference seen at the lower flowrate (10 mL/s) between adding oxygen or not which indicates that the rate of oxygen mass transfer into the surface of the liquid film on the disc is sufficient to keep the reaction going – it does not become limiting.

- However, at the higher flowrate (15 mL/s), adding oxygen increases the rate to be comparable to those at the lower flowrate (10 mL/s). This indicates that the rate of mass transfer through the liquid film surface is limiting at the higher flowrate. At the higher flowrate, the residence time of the liquid on the disc is smaller (see Chapter 5, Section 5.3.1), therefore the contact time on the surface of the disc is insufficient to oxygenate the feed sufficiently to keep the photocatalytic oxidation/degradation supplied with oxidant.

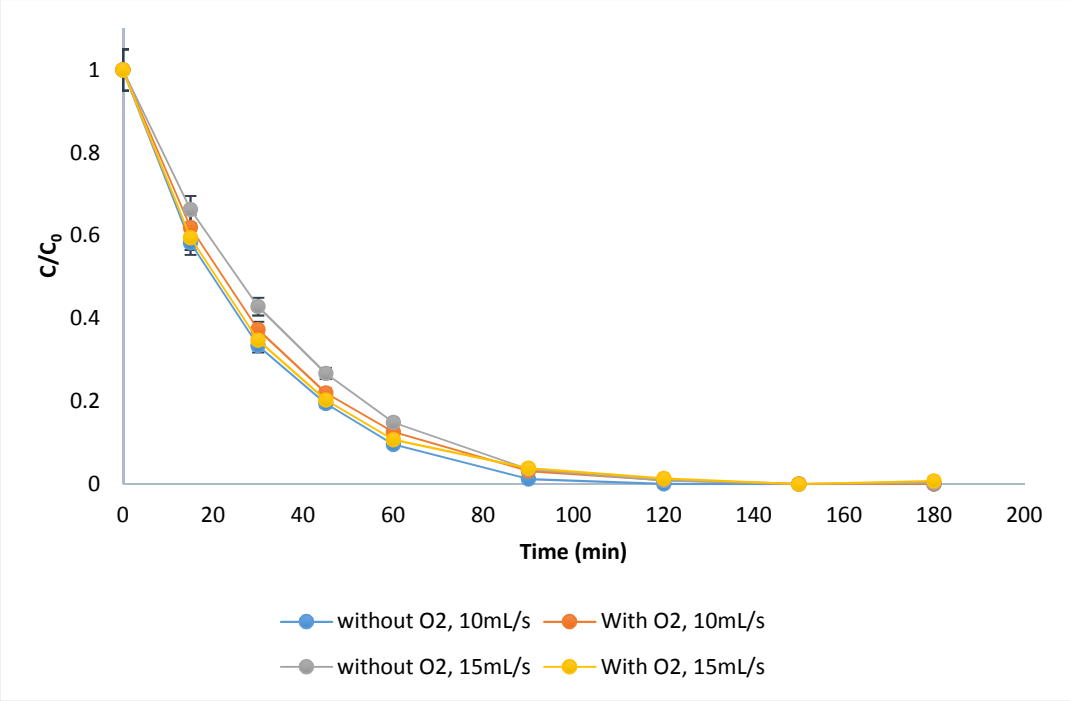

Figure 6.10: Effect of added oxygen and inlet flow rate on the primary degradation of MB at 300rpm spinning speed.

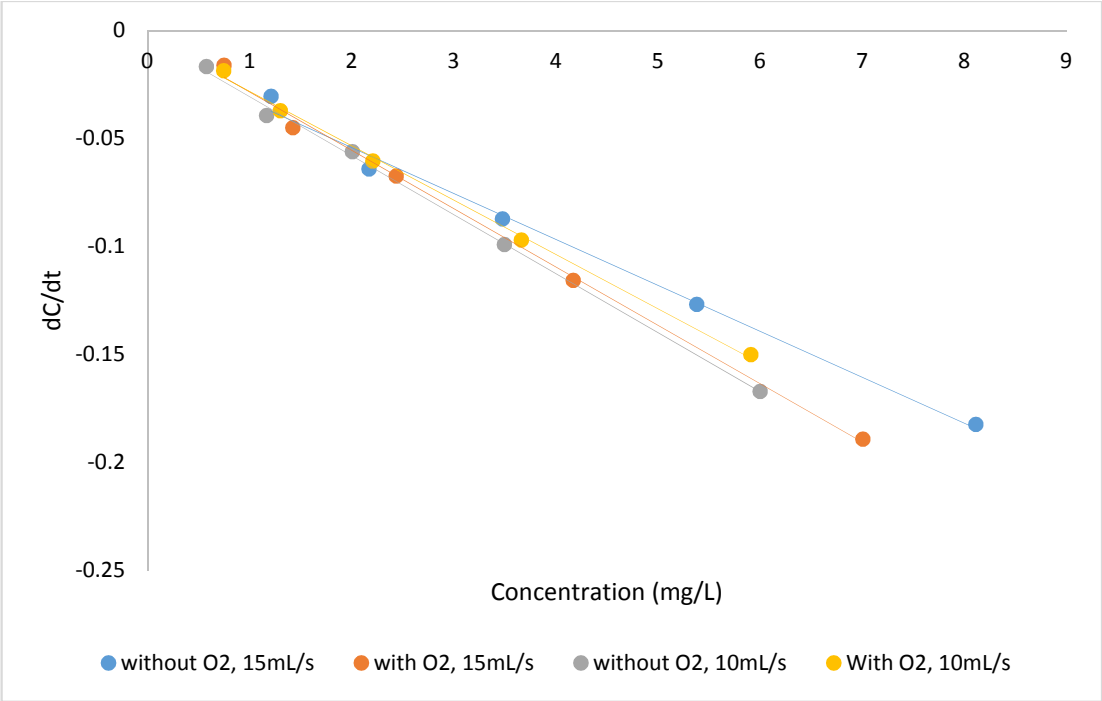

Figure 6.11: Plot on the reaction rate at 300rpm speed

Table 6.2: Reaction rate constants for MB reactions at 300rpm speed

Oxygen	**Flowrates (mL/s)**	k_{app} **(min^{-1})**	$k_{app,S}$ **(min^{-1}m^{-2})**
Without	15	0.0213	0.0723
With	15	0.027	0.0917
Without	10	0.0273	0.0927
With	10	0.0251	0.0852

Combining all of this data to look at the combined effects in general - the overall reaction rates and kinetic constants are summarised in Table 6.3. The meta-analysis shows that for the conditions studied, the maximum primary degradation rate of MB occurs at a flow rate of 15 mL/s and 200 rpm, **without added oxygen**. This is a significant result – it indicates that the added oxygen may be detrimental to the overall mechanism (perhaps excess oxygen blocks active sites and/or contributes to increased UV absorption).

Table 6.3: Effect of oxygen presence, spinning speed and feed flowrate on reaction rate and rate constant.

Oxygen	Feed Flowrate (mL/s)	Spinning Speed (rpm)	Reaction Rate		First order rate constant	
			$r_A \times 10^7$ (mol L^{-1} s^{-1})	$r_A'' \times 10^5$ (mol m^{-2} s^{-1})	$k_{app} \times 10^2$ (s^{-1})	$k''_{app,S}$ ($s^{-1}m^{-2}$)
Without	10	100	6.02	2.04	2.25	0.76
With	10	100	6.26	2.12	2.34	0.80
Without	10	200	7.41	2.52	2.77	0.94
With	10	200	6.31	2.14	2.36	0.80
Without	10	300	7.30	2.48	2.73	0.93
With	10	300	6.71	2.28	2.51	0.85
Without	15	100	4.65	1.58	1.74	0.59
With	15	100	5.56	1.89	2.08	0.71
Without	15	200	8.24	2.80	3.08	1.05
With	15	200	5.80	1.97	2.17	0.74
Without	15	300	5.70	1.93	2.13	0.72
With	15	300	7.22	2.45	2.70	0.917

Figures 6.12a, 6.12b and 6.12c show the initial rates of reaction rates on a surface area basis plotted against flow rate and rotational speed in a 3D scatter graph and in a surface plot.

Two observations:

1. For the reactions with added oxygen, there is a greater reaction rate with increased spinning speed (as discussed above) and a slightly higher reaction rate with increased flowrate. This bears out the trend seen in previous data (Boiarkina, Norris and Patterson, 2013a). Boiarkina expected that there would be an increasing surface rate of reaction at an increasing rotational speed and flow rate, due to increasing shear, but such a trend is not visible on the graph (Boiarkina, Norris and Patterson, 2013a).

2. For the reactions without added oxygen, there are limited data points, but there does not appear to be a trend with the data without oxygen – it appears to be a bit scattered. This is likely because the determinant factors that give a high or low rate are not well represented in the plot – this is all about mass transfer of oxygen to the fluid, which is determined by mixing, micromixing, residence time of the liquid etc.

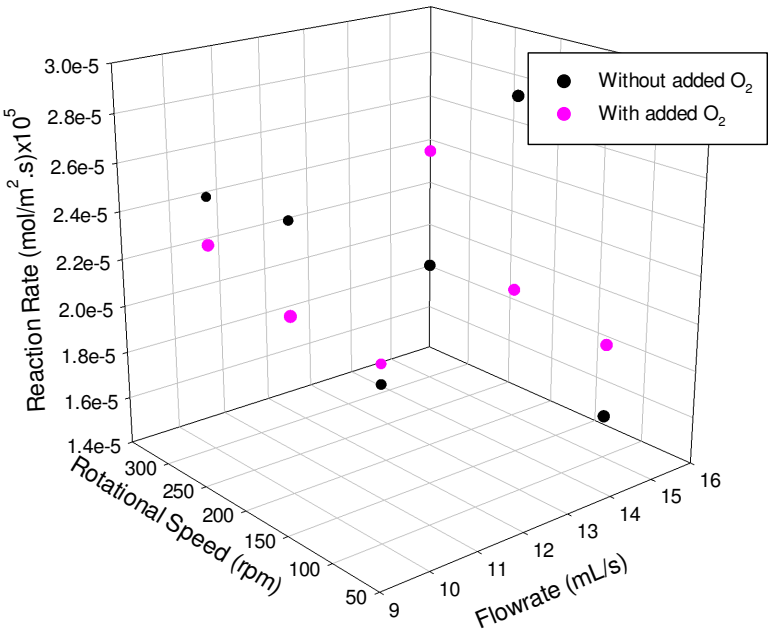

(a)

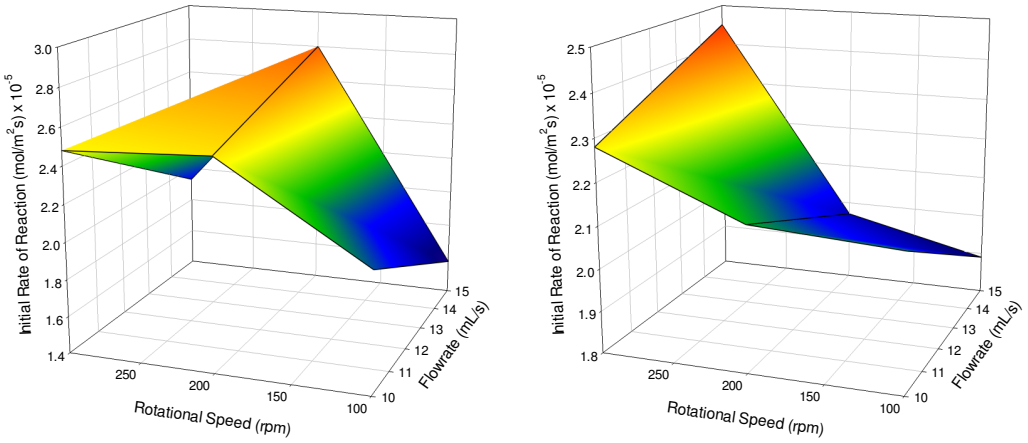

(b) (c)

Figure 6.12: (a) Effect of flow rate and rotational speed on the surface rate constants of the degradation of methylene blue, (b) without added O_2 average initial reaction rate surface plot and (c) with added O_2 average initial reaction rate surface plot.

Evidence for involving oxygen transfer through the free surface of the liquid can be easily found in continuous operations rather than in batch operations. Increase in the liquid flow rate does not have a great influence on the formation of a liquid film on the disc surface, but sufficiently alters the fluid motion (Section 5.2). That is, if the main

mechanism of oxygen transfer from the atmosphere is via the entrained thin film, the rate of oxygen transfer will not be significantly changed with the liquid flow rate.

A more plausible explanation is that the intensity of turbulence near the free surface of liquid increases with the flow rate. The mixing of liquid results from the interaction of the flow in continuous liquid flow operations and the rotating flow due to the disc rotation. These two flows complement each other to some extent, so the effect of disc rotation is latent at a high flow rate and that of flow rate is small when the disc rotates rapidly (Fig. 5.1).

Additionally, there are pH changes and trends in this study as this adds to what happened and can indicate if acid intermediates were formed or not. The pH of the reactant mixture is something that may require attention in photocatalysis due to its effect on the surface charge of the semiconductor (Mills and Le Hunte, 1997). The initial pH is between 7.0 to 7.4, while after reaction is between 5.0 to 6.4.

The initial pH has multiple effects on the photocatalytic reaction system that can significantly affect the yield and reaction rate. TiO_2 has a zero point of charge (zpc), which is the pH of the solution with the surface of TiO_2 is neutrally charged. The zpc for TiO_2 is 6.25, so when the pH below zpc the surface of the catalyst is positively charged. If the pH of the solution is over 6.25, then the TiO_2 surface is negatively charged. The surface charge of the catalyst determines whether a component of interest in the solution will be adsorbed onto the surface or be repelled (Ray, 1998; Robert and Malato, 2002). Many organic compounds are adsorbed to a positively charged catalyst surface. The higher the pH, the lower the initial adsorption rate of the component of interest onto the catalyst surface (Yang *et al.*, 2001; Wang *et al.*, 2009). Redox reactions in general are sensitive to pH and surface charge. The presence of excess H^+ (low pH) or OH^- (high pH) ions can affect the bonding of some compounds, altering their charge and ultimately increase or decreasing their susceptibility to hydroxyl radical attack (Yang *et al.*, 2001).

The exact effect of the pH on the reaction rate and yield of a reaction system, however, will ultimately be dependent on the compound being oxidized. For example, methylene blue prefers high pH (above 7) (Ling, Mohamed and Bhatia, 2004).

An important point to observe about photocatalytic reactions of many organic substances is that the pH of the reaction system will not remain constant throughout

the path of the reaction due to the formation of intermediate organic and/or inorganic acids. Again, whether this decrease in pH will result in an increase or decrease in reaction rate will depend on the reactants and intermediates. In general, due to the theory of zpc of TiO_2, having a lower pH will be preferable for anionic compounds while a higher pH preferable for cationic compounds. The appearance of such drops in pH was observed by Černigoj *et al.* (2007) in not only pure photocatalysis reactor systems, but also hybrid systems (Černigoj, Štangar and Trebše, 2007).

6.5.3 Examination of the reaction pathway – reaction intermediates analysis

To fully understand the photocatalytic degradation of MB in the pSDR, the reaction pathway and reaction intermediates need to be examined to determine if secondary degradation and mineralisation of the reaction intermediates occurs. This would indicate if the photocatalyst is useful beyond decolourisation and primary degradation of azo dyes like methylene blue.

Figure 6.13 shows the main azo dye related reaction intermediates that form at the different spinning speeds and flowrates above. The results suggest that a spinning speed of 200 rpm with added oxygen is the best for the degradation of these azo dye related intermediates. This therefore shows that although no added oxygen is more optimal when considering the primary degradation of MB, that sufficient and available oxidant is required for the degradation of the degradation products of MB, which may be more recalcitrant to photodegradation. This indicates that the whole reaction pathway and not just the primary degradation must be considered when determining the efficacy and efficiency of a reactor systems like the pSDR.

Overall, these results suggest the formation of intermediate products which were less amenable to photodegradation. In a study for the photocatalytic degradation of MB complete mineralization of the initial compound, and Azure A, Azure B and Azure C as intermediate products (Fig. 6.14). The overall degradation pathway and formation of intermediates will be discussed further in Chapter 7.

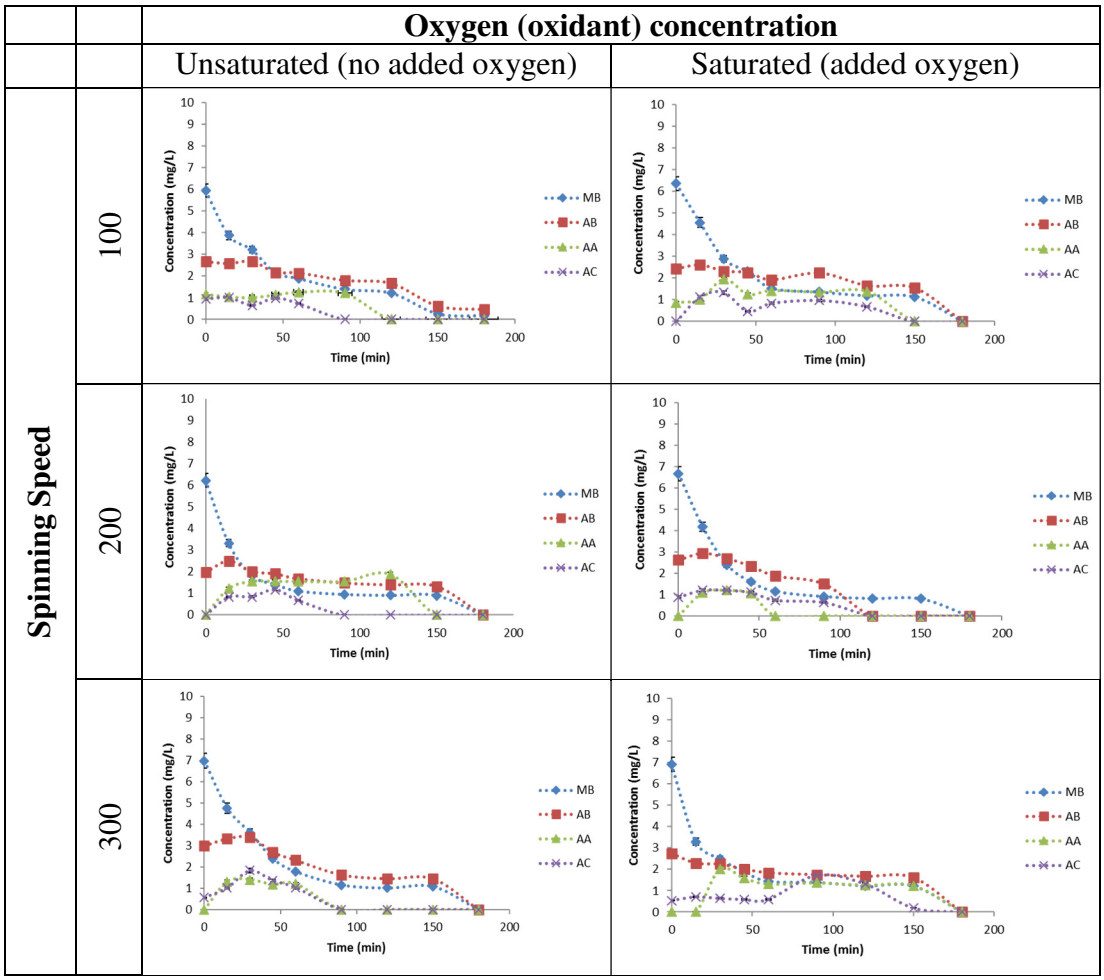

Figure 6.13: Reaction profile comparison of the reaction intermediates from methylene blue photocatalysed (15mL/s).

6.5.4 Reusability of the thin films

In addition to make sure the thin films have a sufficiently large UV exposed surface area and appropriate morphology to maximise photocatalytic activity, a key property of any thin film catalyst is that it needs to be mechanically and chemically stable, maintaining a high catalytic activity on an extended duration over use and reuse.

Figure 6.14 and 6.15 show no significant difference for the degradation rate of MB, although the thin film was used 10 times for reactions in order to determine the effect of these repeated uses on the photocatalytic activity and film morphology (Section 6.2.1). This is despite the observed adsorbed/absorbed species on the film surface. Overall, this is so that use is viable: once it is coated on a support material within a reactor, it can remain there for an economically and practically viable time for the operation.

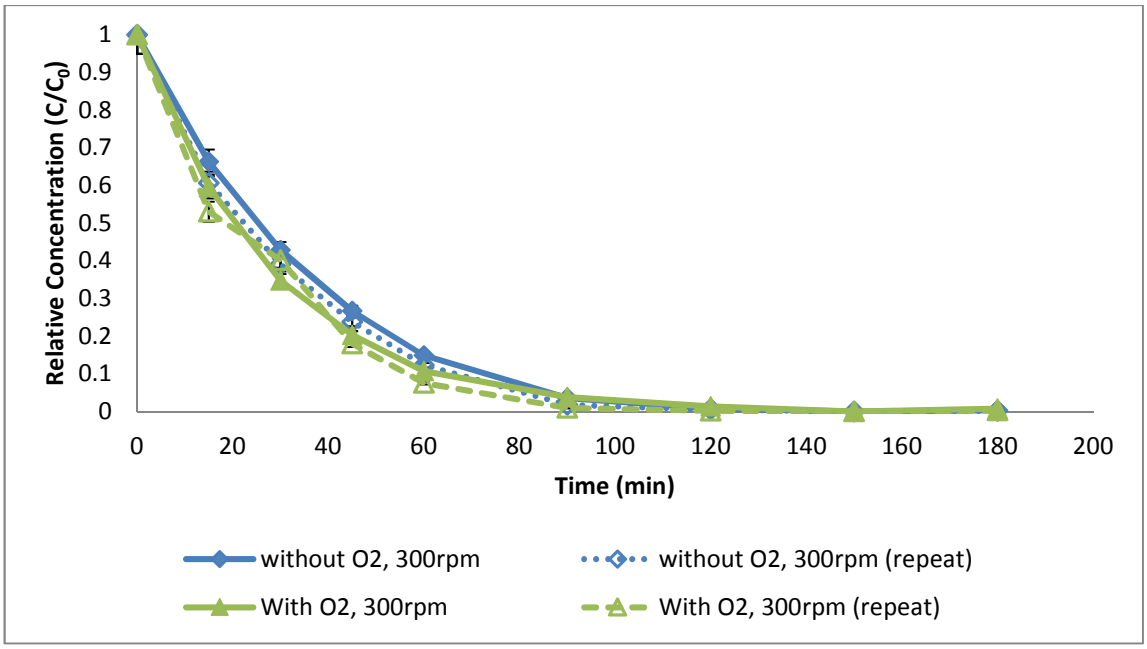

Figure 6.14: Relative Concentration of MB reduction with UV and with photocatalyst (15mL/s) (after reuse for 10 times).

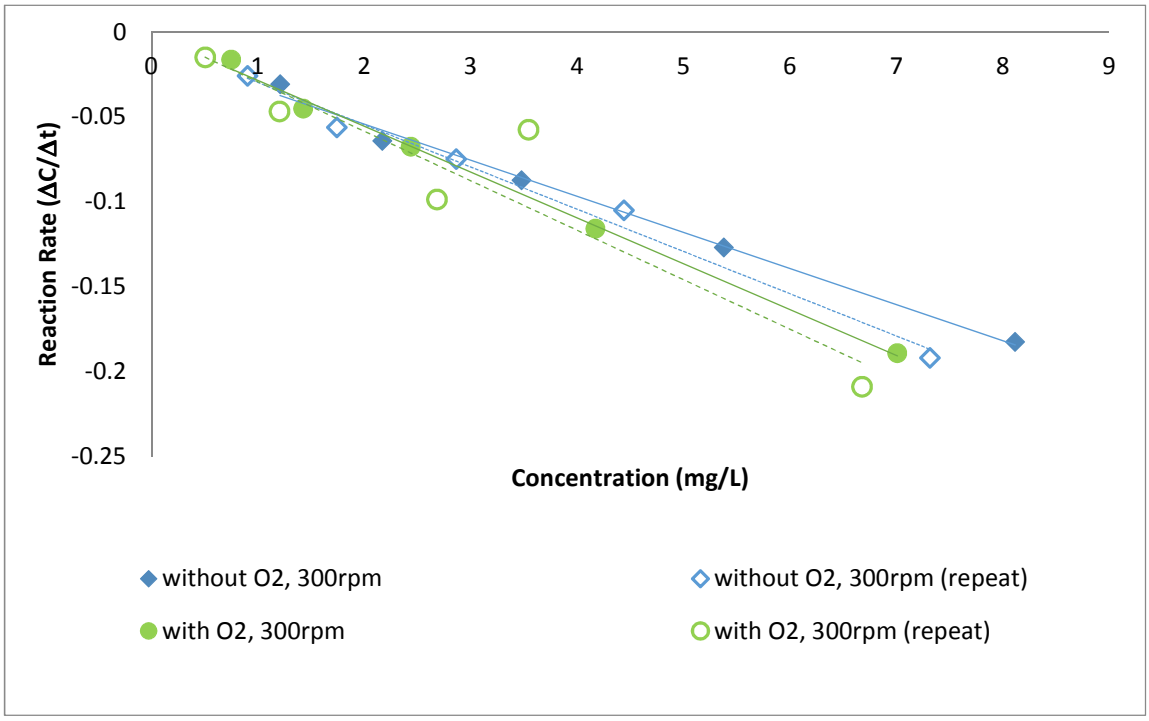

Figure 6.15: Plot of reaction rates examining photocatalyst disc reuse.

6.6 Adsorption and Photolysis Experiments in the Spinning Disc Reactor for Ibuprofen

Experiments investigating the adsorption and photolysis of ibuprofen in the reactor had to be carried out prior to any photocatalytic reactions in order to:

1. Specify the dark equilibration time for adsorption to take place so that any subsequent change in concentration of the substrate during the photocatalytic experiments are due to degradation only.

2. Evaluate if the substrate degrades significantly under UV light, without catalyst.

Figure 6.16a shows the adsorption of ibuprofen with respect to time in the reactor and shows no decrease in the concentration of the substrate after 30 minutes. Based on this result, an adsorption time of 30 minutes was chosen prior to carrying out any reactions and this is also consistent with previous work using this reactor (Boiarkina, Pedron and Patterson, 2011; Boiarkina, 2012; Boiarkina, Norris and Patterson, 2013a, 2013b).

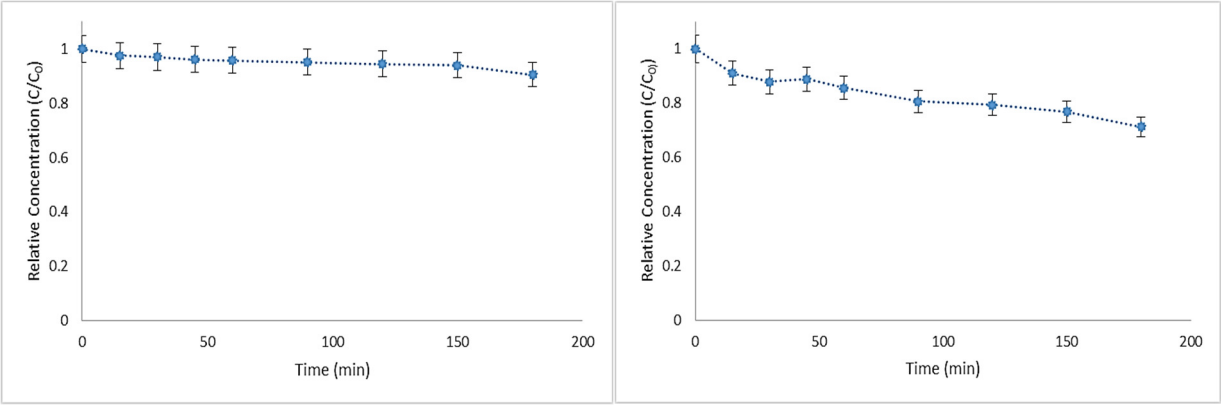

(a) (b)

Figure 6.16: Ibuprofen adsorption and photolysis inside SDR (a) Adsorption on reactor. (b) Photolysis

The photolysis results are given in Figure 6.16b. These results show that ibuprofen does undergo some degradation due to UV alone, with minimal degradation in the first hour. However, this degradation is significantly less than that observed with a photocatalyst. Hence photolysis can be excluded as a degradation mechanism during

the photocatalytic reactions and again this is also consistent with previous work using this reactor (Boiarkina, Pedron and Patterson, 2011; Boiarkina, Norris and Patterson, 2013a, 2013b).

6.7 Characterisation of the Photocatalytic Spinning Disc Reactor for Ibuprofen

The aim of this work was to investigate the effect of three key control parameters in the pSDR: feed oxygenation, spinning speed and feed flowrate on the degradation rate, reaction kinetics and reaction mechanisms. The degradation of IBU, one of the most consumed pharmaceuticals worldwide, in aqueous medium by pSDR was investigated herein. It was verified that the system was able to cause an almost complete degradation of IBP after a reaction time of 180 min.

The results below indicate that there are several effects on overall IBU degradation in the pSDR – including the effect of oxygen feed. Therefore, the degradation rate with and without oxygen added to saturate the feed with oxidant was investigated as a function of the two main tuneable parameters in the pSDR: the feed flow rate and spinning disc rotational speed.

Several experiments were performed to evaluate removal efficiencies and photocatalytic reaction rates IBU using the pSDR. Photocatalytic degradation of IBU in the pSDR was investigated at an influent concentration of 25mg/L (121 µmol/L).

The degradation of IBU is shown in Figure 6.17a and 6.18a. In the pSDR, IBU maybe degraded or removed under various pathways such as TiO_2 adsorption, photodegradation and photocatalysis. In Section 6.6 (and again here), there is a small amount of adsorption of IBU in the reactor, however photolysis is negligible at these conditions, which is likely due to the light intensity being too low at the surface of the disc. So, Fig. 6.17a and 6.18a shows that under photocatalytic conditions, 80%+ degradation is achieved and this is likely due to photocatalysis only (no photolysis).

Three effects were examined (as in MB):

1. The effect of spinning speed at constant flowrate
2. The effect of inlet flowrate at constant spinning speed

3. The effect of feed oxygen (fed to produce oxygen saturation in the feed or not fed, so that the only oxygen supply is through the surface area of the liquid on top of the spinning disc) at both of the above conditions.

Figures 6.17a, 6.18, 6.19a and 6.20 show the effect of spinning speed at constant flowrate. This shows that at the conditions considered:

- Higher spinning speeds increase the reaction rate. From Chapter 5, Section 5.4.1 it was shown that higher spinning speeds increases micromixing which is likely part of the explanation. The imaging studies (Section 5.4.1) show that the film surface under these conditions becomes smoother and therefore there is less UV scattering and higher UV penetration.

- At 300rpm, the reaction without oxygen being fed at saturation has the highest reaction rate. This is not expected and indicates that perhaps excess oxygen is detrimental to this reaction. Increased micromixing at these higher spinning speeds (Section 5.4.1) would enable a higher mass transfer of oxygen away from the top surface of the liquid film on the disc and therefore enhance mass transfer of oxygen into the pSDR – perhaps enabling sufficient (but not too much) oxygen to be available for IBU photocatalytic degradation to occur. This will be examined further below.

Examining the effect of inlet flow rate and added oxygen for these experiments (Figure 6.17a, and 6.19a), the following can be observed:

- When oxygen is supplied, there is no significant difference between the degradations at the different flow rates. This indicates that the differences in residence times do not make a difference in the overall degradation at these conditions.

- There is no significant difference seen at the lower flowrate (10 mL/s) between adding oxygen or not which indicates that the rate of oxygen mass transfer into the surface of the liquid film on the disc is sufficient to keep the reaction going – it does not become limiting.

The reduction of the IBU concentration seems to be strongly influenced by the rotational speed compare to flowrate investigated. Ibuprofen removal monotonically

decreases with time, and the higher the rotational speed the higher the IBU degradation.

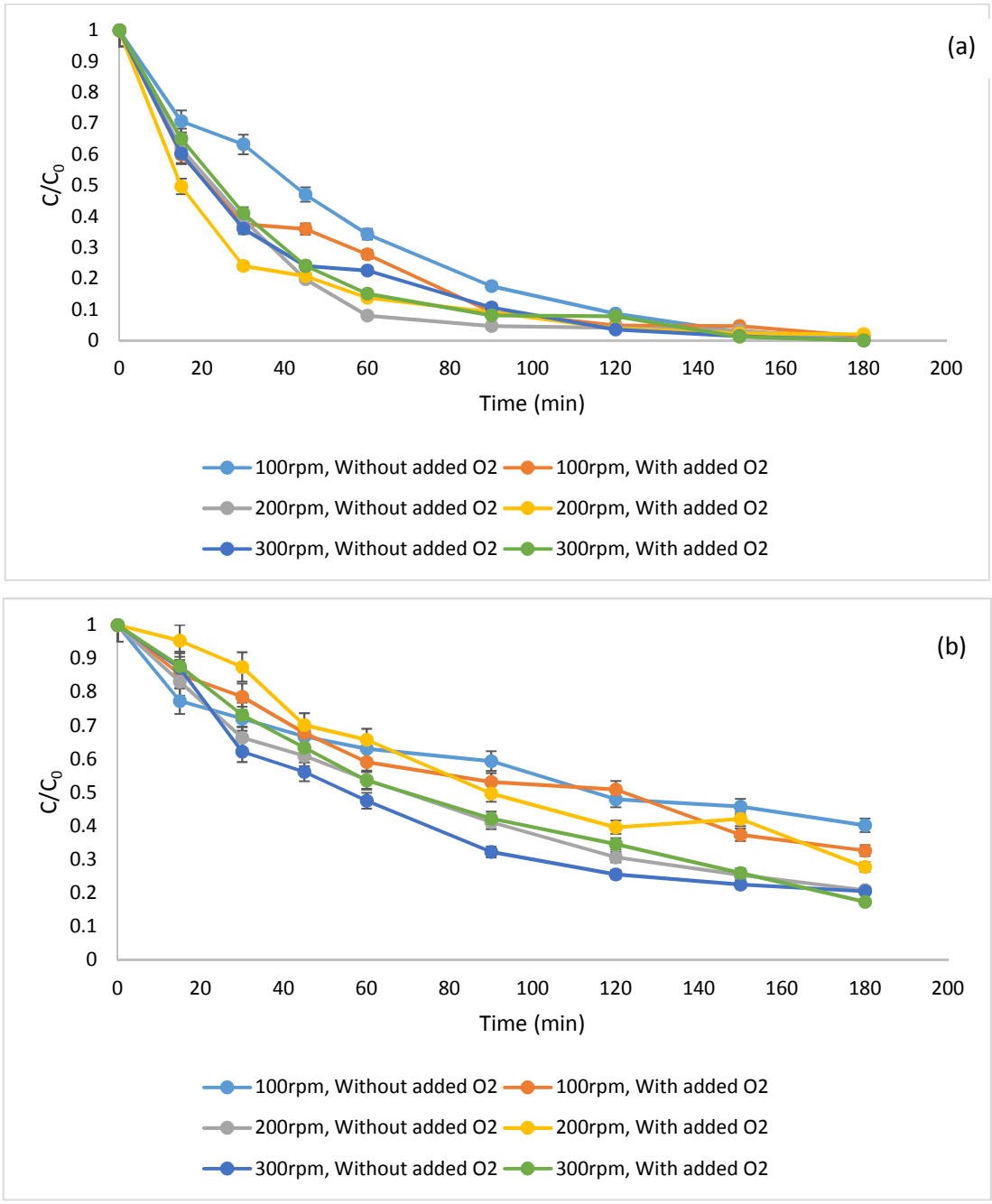

Figure 6.17: (a) Ibuprofen and (b) TOC degradation of 25 mg/L Ibuprofen at 10mL/s.

The photocatalytic degradation rate of organic compounds is commonly described in terms of the Langmuir-Hinshelwood model (Eq. 6.1). It has been demonstrated in many reports (Dimitrakopoulou *et al.*, 2012; Khuzwayo and Chirwa, 2015) that

photocatalytic reactions can be adjusted to this pseudo-first order model in a low-concentration solution under direct irradiation of light.

Figures 6.17b and 6.19b shows the TOC decay values for photocatalytic experiments, at the times of 0, 15, 30, 45, 60, 90, 120 and 180 min; it can be observed that a higher mineralization percentage (85%) is achieved with rotational speed 300pm, in contrast with the mineralization percentage reached with lower rotational speed (60 - 70%). During the photocatalytic degradation of IBU at 25mg/L within 60 min the TOC concentration (Fig. 6.17b and 6.18b) did not decrease so rapidly, indicating a fast transformation but not a fast mineralization. It is clearly seen that there is no significant improvement in the TOC removal for the degradation at different rotational speed for 60 min of reaction time. This may be cause by the formation of more stable intermediates in the degradation process in the first 60 min. After 180 min, a marginal increase in the mineralization was observed.

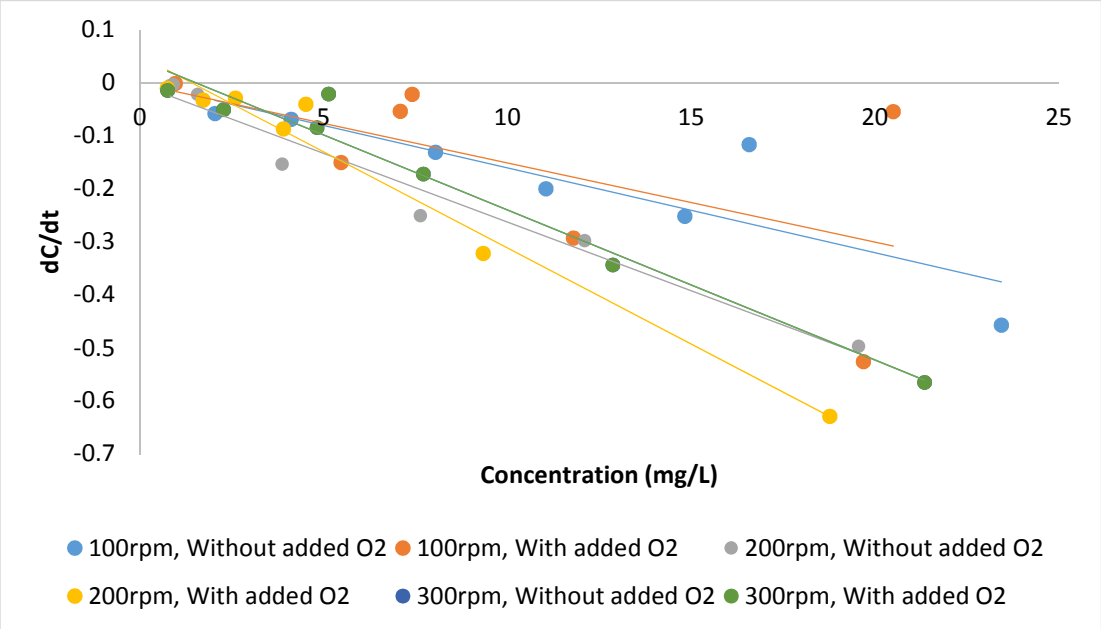

Figure 6.18: Reaction rate versus concentration for the results in Figure 6.18a showing that an apparent first order kinetic fit.

In Fig. 6.17b and 6.19b the concentration of IBU and its degradation are given as TOC. The sum of the quantified degradation products (Fig. 6.17b and 6.19b) showed that there was still an amount of non-identified intermediates, which contribute to the

measured TOC. This higher mineralization percentage could indicate that, the route for the ibuprofen decomposition yields organic molecules with lower molecular weight and better solubility than ibuprofen, such as decarboxylated and hydroxylated metabolites, as well as organic acids (Mendez-Arriaga, Gimenez and Esplugas, 2010).

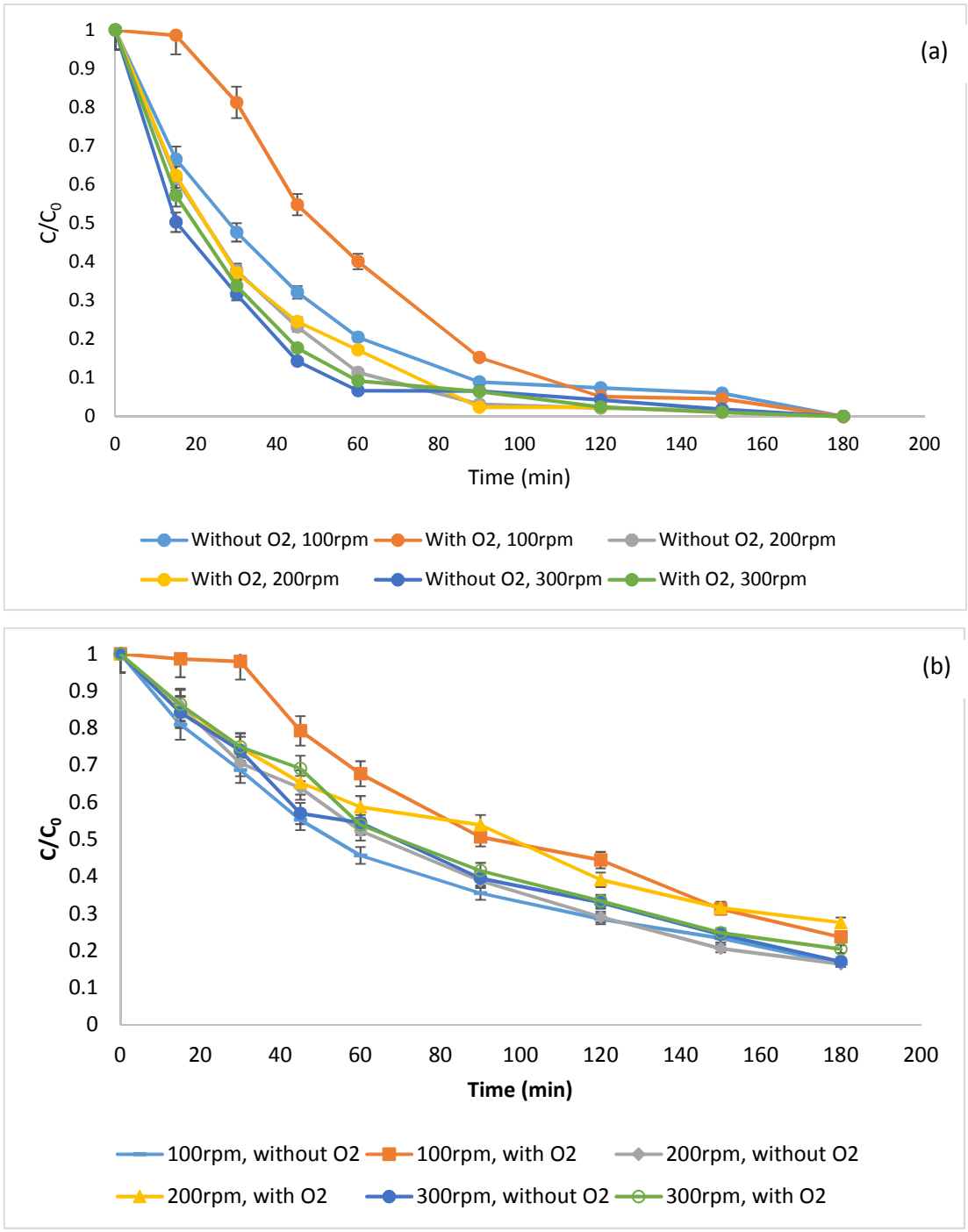

Figure 6.19: (a) Ibuprofen and (b) TOC degradation of 25 mg/L Ibuprofen at 15mL/s.

The degradation compounds which were not identified or quantified via standards above the retention time and their corresponding UV spectra were characterised by high-resolution MS. This allowed the detection and characterization of 9 by-products, many of them persistent even after an exposure of as long as 180 min. A possible photocatalytic degradation pathway scheme of IBU consisting of a few steps is proposed in Chapter 7. This indicates the complexity of the photocatalysis process and suggests the existence of various reductive and oxidative degradation routes resulting in multi-step or interconnected pathways. This work points to the necessity of extended knowledge of the successive steps in light-assisted photocatalytic degradation processes.

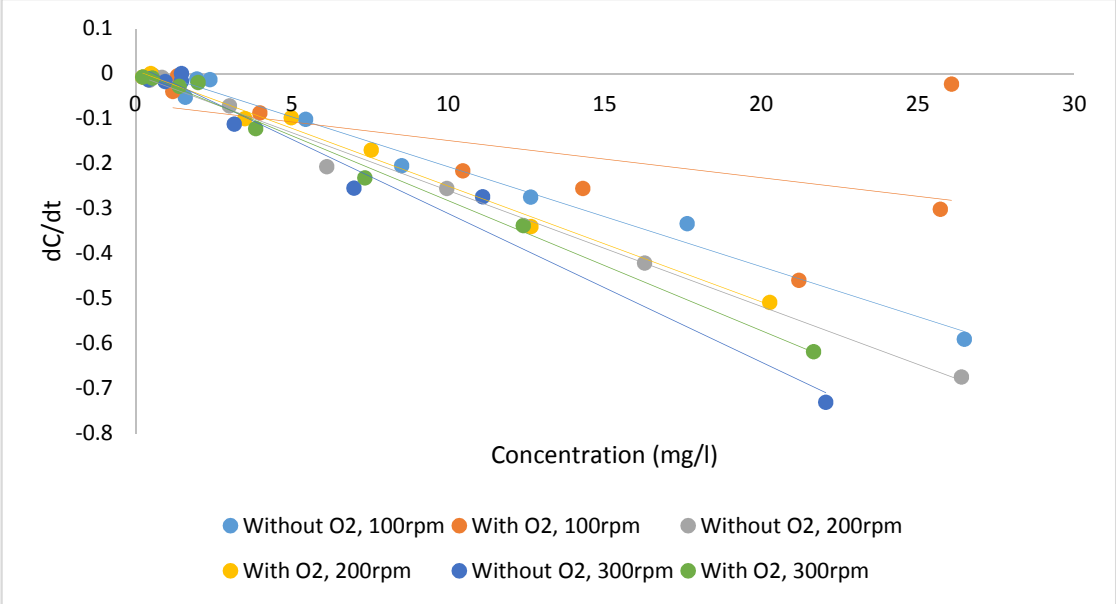

Figure 6.20: Plot on the reaction rate of 25 mg/L Ibuprofen at 15mL/s.

Figures 6.21a show the initial rates of reaction rates on a surface area basis plotted against flow rate and rotational speed in a 3D scatter graph. This shows:

1. There is a sure trend with the data with added oxygen – there is a greater reaction rate with increased spinning speed (as discussed above) and a slightly higher reaction rate with increased flowrate.

2. There are limited data points, but there does not appear to be a trend with the data without oxygen – it appears to be a bit scattered. This is likely because the

determinant factors that give a high or low rate are not well represented in the plot – this is all about mass transfer of oxygen to the fluid, which is determined by mixing, micromixing, residence time of the liquid etc.

3. As indicated in Figure 6.21, different rotational speed accelerated the IBU decomposition process. The fastest reaction rate was 0.0145 mmol/L.s obtained under the condition of 300 rpm and 15mL/s.
4. Figures 6.21 revealed that the presence of additional O_2 did not accelerated the photochemical decomposition of IBU. Furthermore, it was clear that the reaction rate without additional O_2 were greater than those with additional O_2, because higher oxidant level resulted in a higher concentration.
5. In this study, saturated O_2 resulted in lower degradation rates. However, it is noteworthy that some researchers observed that the addition of O_2 did not necessarily enhance the photodegradation (Turchi and Ollis, 1990).

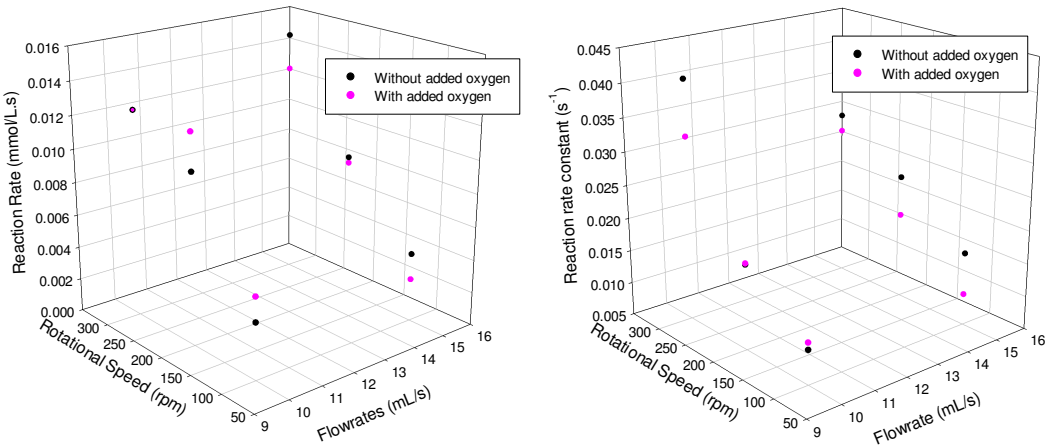

(a) (b)

Figure 6.21: Effect of flow rate and rotational speed on the rate of reaction of ibuprofen a) ibuprofen degradation b) TOC degradation.

Figure 6.21 summarises all of the results for ibuprofen. For ibuprofen degradation and mineralisation (TOC degradation), the following conclusions can be made:

- The TOC removal rate was much less than that of the degradation process under the same experimental conditions
- Higher rotational speeds were quite efficient for the degradation of IBU, but complete mineralization was not achieved over the time range examined which may be due to the high polarity of the intermediate products
- Photocatalysis at 300 rpm showed higher selectivity for the mineralization of IBU as it showed about 74% mineralization in 180 min of light irradiation.
- Rotational speed at 300 rpm achieves higher IBU and TOC reaction rate than lower rotational speed.

These results again indicate that primary degradation and secondary degradation/mineralisation conditions are not the same. Although impressive IBU degradation rates (over 90%) were achieved by the employment of the TiO_2, the TOC data revealed that IBU was not mineralized to a similar extent. Moreover, the mineralization rates derived from direct photolysis were negligible. These findings indicate that whereas most of the original IBU was not mineralized, recalcitrant by-products were generated under these conditions. The fact that the direct photolysis processes are unable to reduce the TOC content in solution strongly indicates that such refractory by-products did not absorb UV radiation. It is also evident that the highest rates of mineralization obtained by the photocatalytic systems can be attributed again to their superior ability to promote the in-situ generation of hydroxyl radicals upon exposure of the TiO_2 catalyst to UV radiation.

6.8 Conclusions

Two model compounds were investigated for the photocatalytic degradation in a SDR, methylene blue (MB) and ibuprofen (IBU) and the following conclusions were made regarding the performance of the SDR:

- A higher overall degradation for model wastewaters with a lower starting concentration 5 mg/L, will be degraded faster. In particular, at higher dye concentrations above 10 mg/L, more light was scattered by the dye solution and fewer photons are able to reach the TiO_2 surface. Thus, the generation of

electron-hole pairs was greatly reduced, and in turn, the dye degradation was reduced due to absence of the oxidizing species. In contrast, at lower concentration, the lower degradation efficiency may be attributed to the mass transfer resistance notwithstanding the mass-transfer intensified by disc rotation.

- For the smooth discs and for the degradation of methylene blue, a supply of oxidant increases reaction rate – indicating that at the conditions that these reactions were run at, there is insufficient mass transfer area and mixing (including micromixing) on the disc to supply the reaction with oxygen and this is likely the rate limiting factor in the reactions where oxygen is not supplied.

- At 300rpm, the reaction without oxygen being fed at saturation has the highest primary degradation reaction rate. When oxygen is supplied, there is no significant difference between the degradations at the different flow rates. This indicates that the differences in residence times do not make a difference in the overall degradation at these conditions.

- There is no significant difference seen at the lower flowrate (10 mL/s) between adding oxygen or not, which indicates that the rate of oxygen mass transfer into the surface of the liquid film on the disc is sufficient to keep the reaction going – it does not become limiting. However, at the higher flowrate (15 mL/s), adding oxygen increases the reaction rate. This indicates that the rate of mass transfer through the liquid film surface is limiting at the higher flowrate.

- The influence of different parameters on IBU degradation was evaluated. Moreover, a reaction mechanism was proposed and the reaction rate constants were estimated. A reduction of IBU concentration higher than 60% and up to 90% was reached in an hour of treatment time. The best results were obtained for the experiments performed at 300rpm rotational speed and 15 mL/s without added additional oxygen.

CHAPTER 7 PROCESS INTENSIFICATION IN THE PHOTOCATALYTIC SPINNING GROOVE DISC REACTOR

7.1 Characterisation of the Photocatalytic Spinning Mesh Disc Reactor for Methylene Blue: Stainless Steel Mesh Discs

The use of a spinning disc reactor (SDR) has proven to be a beneficial and superior operation compared to conventional reactors. In addition, the advantage of a SDR is that there is a low risk of fouling or plugging. However, this SDR thin film photocatalytic system has disadvantages because the catalyst amount and surface area is largely limited to the surface area of the disc. To address these limitations, the development and optimisation of the SDR continues by introducing meshes discs that will have more significant effects on the flow hydrodynamics (Section 5.2).

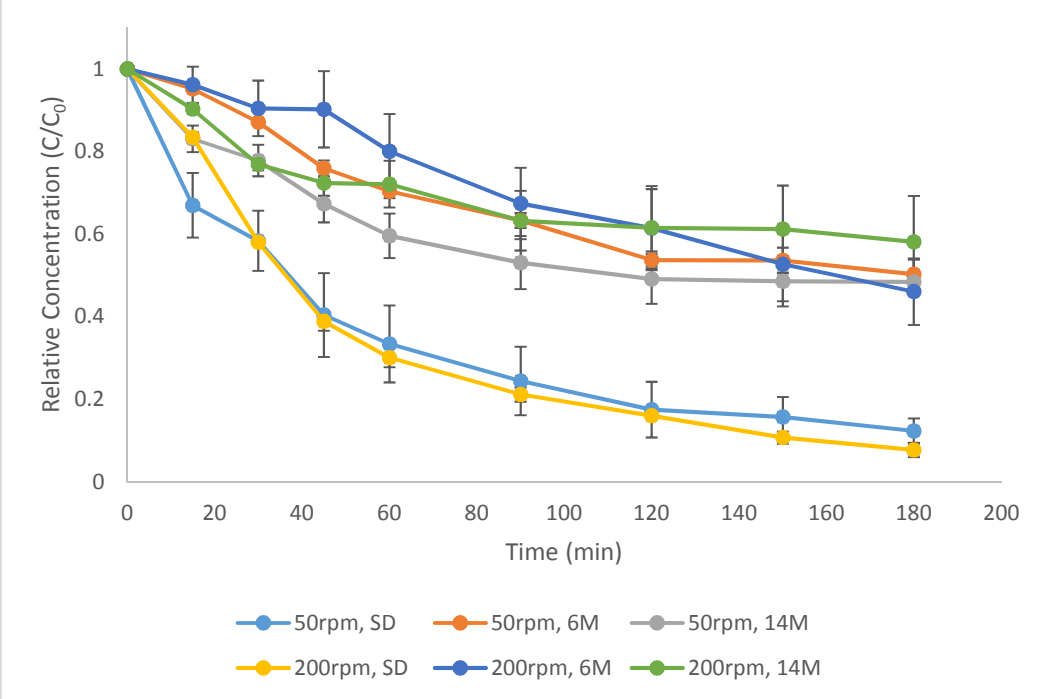

Figure 7.1. Relative concentration of MB degradation (SD = smooth disc; 6M = 6 meshes size; 14M = 14 meshes size).

In theory, the high surface area stainless steel meshes studied should both increase the surface area of photocatalyst present, as well as increase mixing due to interrupting the

flow on the disc, which may result in an increased reaction rate compared to a smooth disc. A smaller mesh size would increase the photocatalyst surface area further, enhancing these gains.

However, as shown in Figure 7.1, there were no significant differences in MB degradation between different mesh sizes. Compared to the smooth disc, with a lower photocatalytic surface area, it can be seen that the meshes did not produce any process intensification. It is hypothesised that this is due to two factors: firstly, there is a shadowing on glass disc by the meshes, reducing the light exposed surface area and therefore reducing the effective surface area of the photocatalyst. High speed camera analysis of the flow on the top of the disc (Figure 5.3) also show that the mesh disrupts the liquid film to a greater extent than expected, producing dry patches across the mesh surface, further reducing the effective surface area of the photocatalyst.

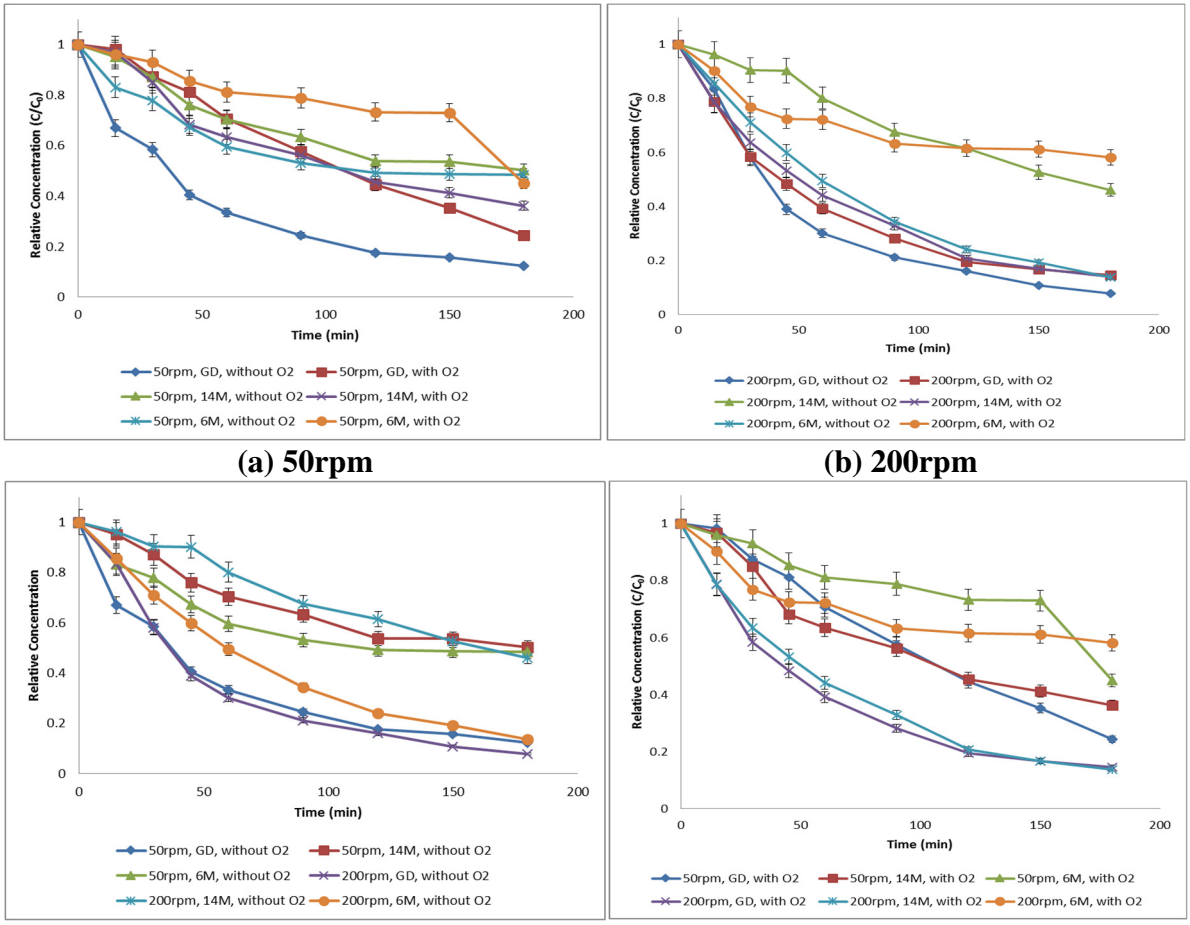

(a) 50rpm **(b) 200rpm**

(c)without added O_2 **(d) with added O_2**

Figure 7.2: Relative concentration MB degradation at C_i=25mg/L.

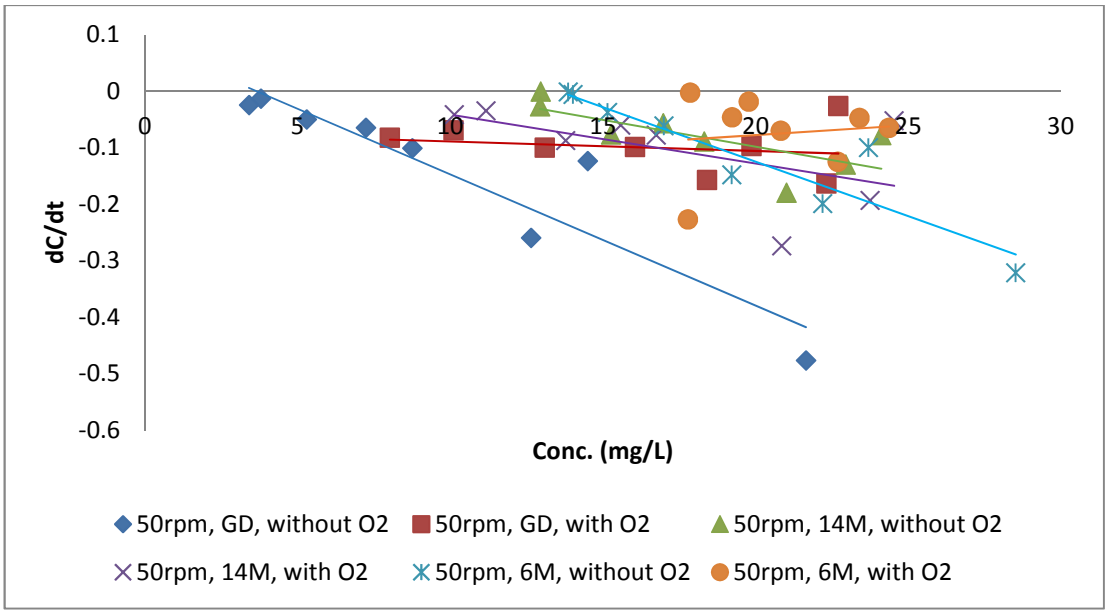

(a)

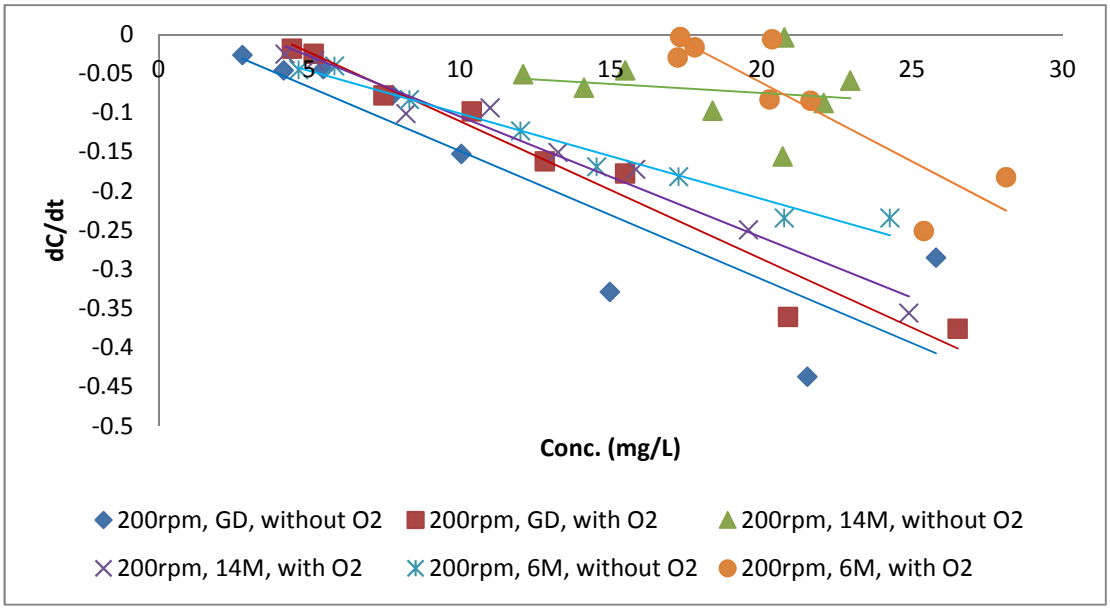

(b)

Figure 7.3: Reaction rate versus concentration for methylene blue degradation (a) 50 rpm; (b) 200rpm.

Figure 7.2(a) and (b) show that there are higher degradation rates when oxygen is not added to the feed except for 14 Mesh. It also again shows smooth disc give the best result compare to meshes. This can be explained by the UV exposed coated surface area – where the significant area of photocatalyst is on the glass disc rather than the meshes and therefore the UV shadowing effect on glass disc by the meshes reduced the effective UV exposed surface area. Furthermore, the meshes were not properly

attached to the glass disc, and this also can affect the mixing of the MB and wetted area of the meshes (Figure 5.3). Considering the effect of disc speed, Figure 7.2(c) and (d) shows that higher spinning speeds of 200rpm produce a higher degradation compared to 50 rpm. Therefore, although the meshes did not increase photocatalyst surface area, they do enhance mixing (and reaction rate as a result) confirming part of the hypothesis. This is despite that at high spinning speeds the meshes are not wetted well (Figure 5.3 at 200-300 rpm for 6M and 14 M meshes).

Although mesh disc result show less effective result compare to smooth disc, like many photocatalytic reactions of dilute pollutants, Figure 7.3 show that the kinetics which should be first order, are significantly affected by the poor wetting on the disc producing scattered kinetic data that cannot be resolved since it is not purely reaction based.

This all results in a less effective spinning disc photocatalyst surface and drove the development of grooves on the surface of the discs to preserve the concept but instead to overcome the shadowing issues.

7.2 Characterisation of the Photocatalytic Spinning Grooved Disc Reactor for Methylene Blue

In the development of grooves on the surface of the discs to overcome meshes issues; two types of grooved were produced as previously outlined in Chapter 5: the square grooved disc (SGD) and mesh grooved disc (MGD).

7.2.1 Effect of Disc Surface

The SGD and MGD are compared at different spinning speeds and flowrates in Fig. 7.4 – 7.7. For the SGD (Figure 7.4), changing spinning speed, inlet flowrate and oxygen addition has a small effect on the overall degradation. Increasing spinning speed and inlet flow rate have the largest effect in increasing extent of oxidation – this can be attributed to increased micromixing (Section 5.4) and a smoothing of the surface of the disc increasing UV penetration to the photocatalyst surface as discussed in Section 5.2.

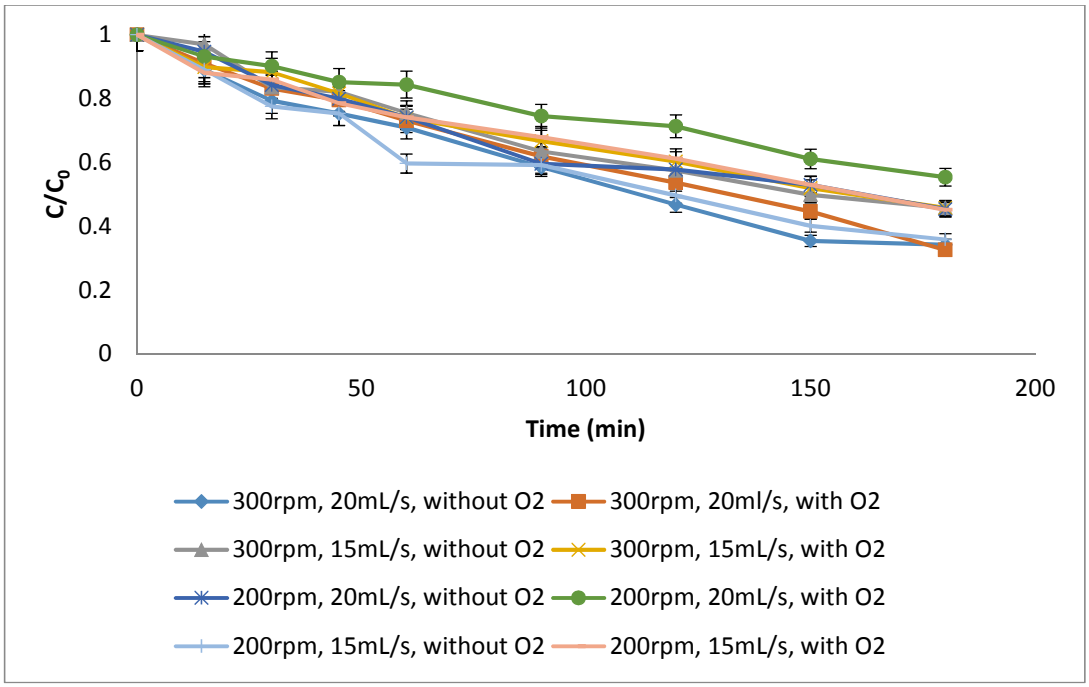

Figure 7.4: Relative concentration of methylene blue degradation for SGD, C_i = 15mg/L.

For the MGD, the highest degradation rate occurs at the highest spinning speed (300rpm) and inlet flowrate (20 mL/s) without oxygen. This indicates that sufficient oxidant is being mass transferred into the pSGDR through the mixing and micromixing at the higher spinning speeds and that when oxygen is added, the additional oxygen from mass transfer through the surface of the disc is detrimental (perhaps blocking access to active sites and/or reducing light intensity) (Dionysiou *et al.*, 2002). Again, these more optimal conditions can be attributed to increased micromixing (Section 5.4) and a smoothing of the surface of the disc increasing UV penetration to the photocatalyst surface as discussed in Section 5.2.

Directly comparing the SGD and MGD (Figures 7.5) shows that, considering only the grooved discs, the SGD provides the higher extent of degradation (and therefore reaction rate). From Fig 7.4, the SGD degraded 67.4% of MB in 3 hours at optimal conditions, rotational speed of 300 rpm, flowrate of 20 mL/s and with added oxygen. The optimal degradation with the MGD (Fig. 7.15) is 51.5% (3 hours) at a rotational speed of 300rpm and flowrate of 20 mL/s and without added oxygen.

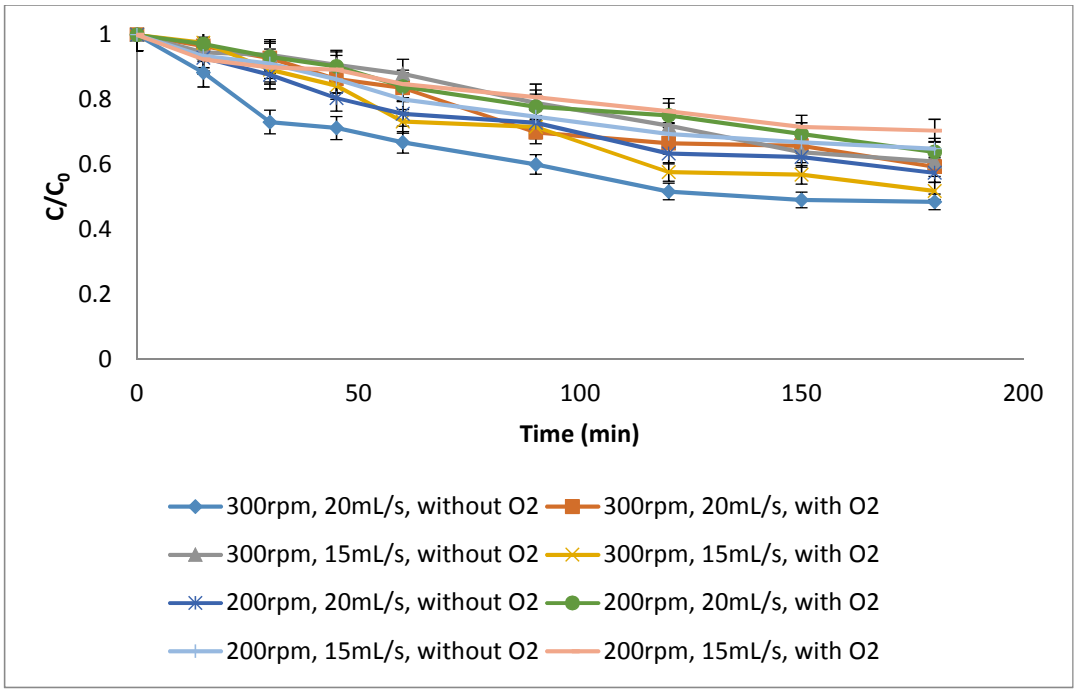

Figure 7.5: Relative concentration of methylene blue degradation for MGD, C_i = 15mg/L.

7.2.2 Effect of Inlet Flowrate

Figures 7.6 and 7.7 show that higher degradation rate occurs at the highest inlet flowrate (20 mL/s). At lower inlet flowrate (15mL/s) the grooved discs are not wetted well compare to inlet flowrate 20mL/s (Figure 5.4) this also can affect the mixing of the MB and liquid-catalyst contact. Again, these more optimal conditions can be attributed to increased micromixing (Section 5.4) and a smoothing of the liquid thin film on the disc surface as discussed in Section 5.2.

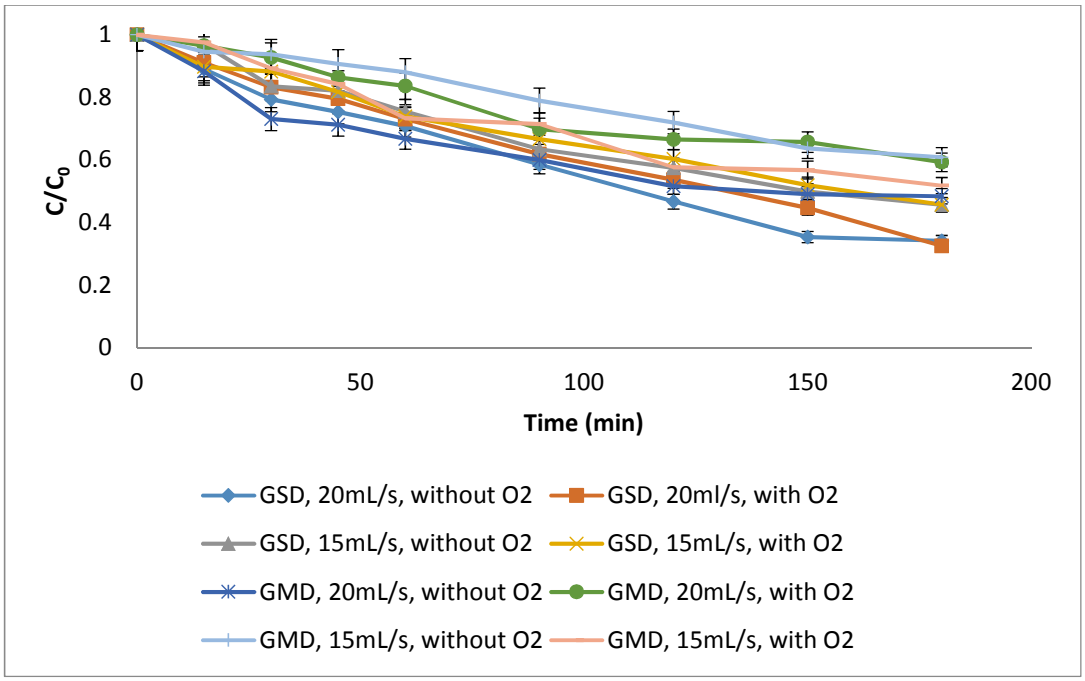

Figure 7.6: Relative concentration of methylene blue degradation at 300rpm, Ci = 15mg/L.

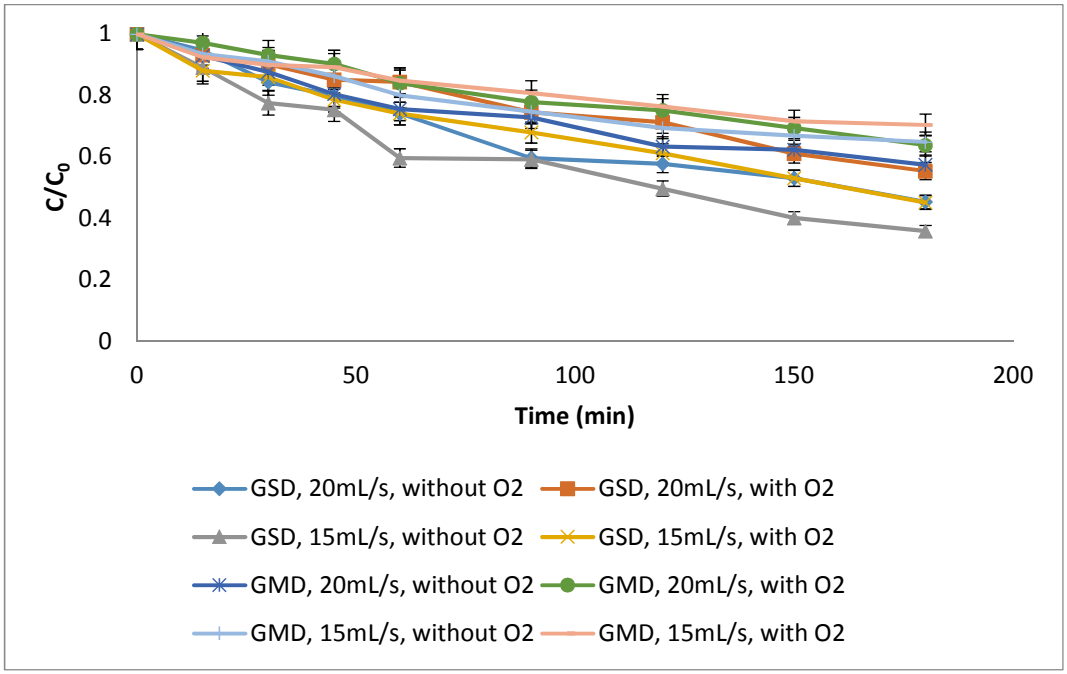

Figure 7.7: Relative concentration of methylene blue degradation at 200rpm, Ci = 15mg/L.

7.2.3 Effect of Spinning Speed

Figure 7.4 – 7.7 show that MB degradation is higher at 300rpm for 20mL/s and at 200rpm for 15mL/s. This reason is that with increasing rotational speed of the disc and therefore a decrease in the film thickness. The increase formation of waves due to grooves induces instabilities in the liquid film, supposed to resulting in an improved mass transfer (Figure 5.3, Section 5.2). But for MGD at 300rpm and 200rpm the radial and tangential velocities of the liquid are so small that the liquid remains in the groove and is less mixed. These are totally different results compared to previous study by Boodhoo and Al-Hengari (2012); and Jacobsen and Hinrichsen (2012) because they using rotational speed higher than 1000rpm. Degradation is also better without added oxygen for both grooved square disc and grooved mesh disc. It may be caused by the excess oxygen that blocks active sites and/or contributes to light scattering. This will cause the reactor to become less effective.

7.2.4 Overall comparison: SD, MGD and SGD

As shown in Figure 7.8, the square grooved disc surface used in this work provides an improved in reaction rate compared to the smooth disc and mesh grooved disc. This result supported by studies from Chapter 5 (hydrodynamic studies, RTD studies and Villermaux-Dushman experiment). From hydrodynamic studies, using a textured disc appears to even out the flow across the surface of the disc, which would increase the local UV penetration onto the disc surface (less scattering) and provide more uniform volumetric utilisation of the catalyst (Section 5.2). While, the RTD investigation (Section 5.3) provides a valuable insight into the operating conditions of the SDR which generate flow profiles approaching plug flow behaviour. The textured discs in particular made the flow more plug flow – as quantified by a higher number of tanks in series. This indicates, as with the visual analysis/hydrodynamic studies that higher spinning speeds, higher inlet flowrates and a textured disc should result in conditions more favourable for higher reaction rates. The Villermaux-Dushman experiment (Section 5.4) performed in the spinning disc reactor clearly show that the best micromixing conditions were generally achieved at high disc rotational speeds, high feed flow rates and using textured discs.

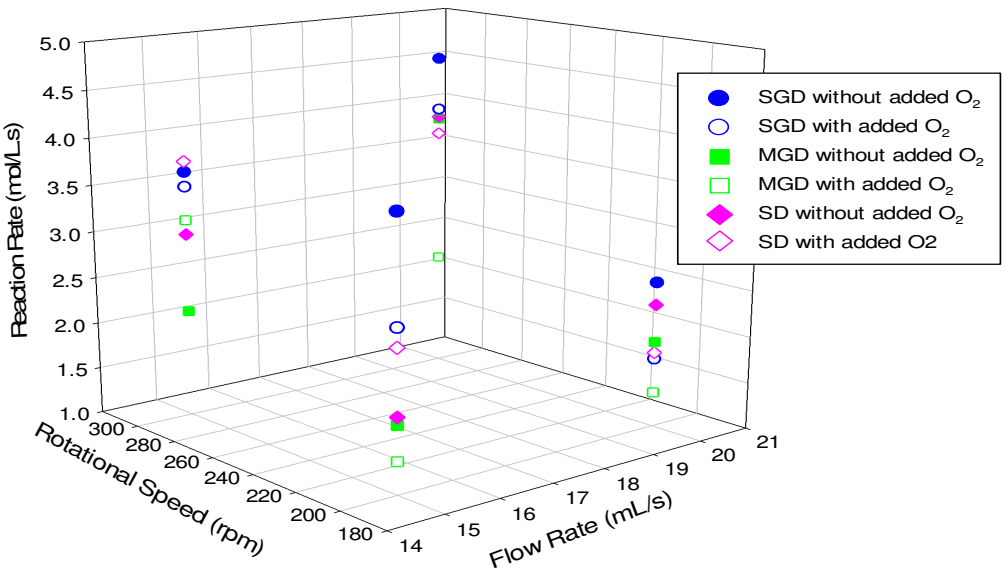

Figure 7.8: Volumetric reaction rates comparing effect of rotational speed and inlet flowrate for the square grooved discs, mesh grooved discs and smooth disc.

Investigating the effect of the two main pSDR control parameters (spinning speed and inlet flowrate), it was found that the optimal (highest reaction rate) was at 300 rpm and 20 mL/s for the square grooved disc without added oxygen, indicating that the self-aeration of oxygen by the pSDR spinning liquid film contacting air produces sufficient and more optimal oxidant input.

7.2.5 Intermediate Analysis

HPLC was used to identify the different reaction intermediates and products formed during the photocatalytic reaction. The three major identified reaction species were Azure B (AB), Azure A (AA), and Azure C (AC). Methylene Blue (MB) was used since it has a well characterised reaction product spectrum making differences in reactions between catalysts more reliably determined. It is therefore expected that these results match with previous MB photocatalysed reaction studies (Ali, 2011, Boiarkina *et. al.*, 2012) and they do. This analysis shows that for all reactions, the parent molecule methylene blue was fully oxidised in the reaction time studied.

Figure 7.9 – 7.11 shows the formation and degradation of the intermediates AB, AA, and AC at different flow rates, rotational speed and surface structure. It is clear from

Figure 7.9 – 7.11 that all of the identified intermediates could be degraded as well as the MB (although degradation was not complete).

7.2.2 Smooth disc reaction intermediates

Figure 7.9 – 7.11 in particular shows the formation of AA, AB and AC as the start of the reaction, indicated by the rise in peak area detected by the HPLC. This confirms findings by (Zhang *et. al*, 2001; Calza *et. al*., 2005; Ali, 2011) who proposed the formation of AB, AA, AC and Th as the reaction intermediates of MB in photocatalysis.

The intermediates identified during the photocatalytic degradation were the same as found by Ali, Emanuelsson and Patterson (2011): Azure A, Azure B and C. Figure 7.9 – 7.11 shows the total relative formation of Azure A, Azure B and Azure C, across the different operational parameters used in the reactor. It can be seen that for the majority of the reaction parameters, the relative concentration of intermediates increases. It remains constant and only starts to decrease slowly at the end of the reaction. This indicates that a true degradation of methylene blue is taking place, not simply reduction of methylene blue to leuco-methylene blue, which would otherwise show no formation of intermediates. The reactions at 15mL/s and 200rpm (without oxygen) show a significantly different reaction profile to that found at the other operational parameters with greater degradation of intermediates. As in chapter 6, this is not the optimal spinning speed and flowrate for primary degradation because of the different concentration used (10mg/L for Chapter 6; 15mg/L for Chapter 7) (different to the optimal of 20 mL/s and 300 rpm, without added oxygen square disc for just MB degradation). This again confirms that the entire reaction species spectrum needs to be considered to determine optimal reactor conditions.

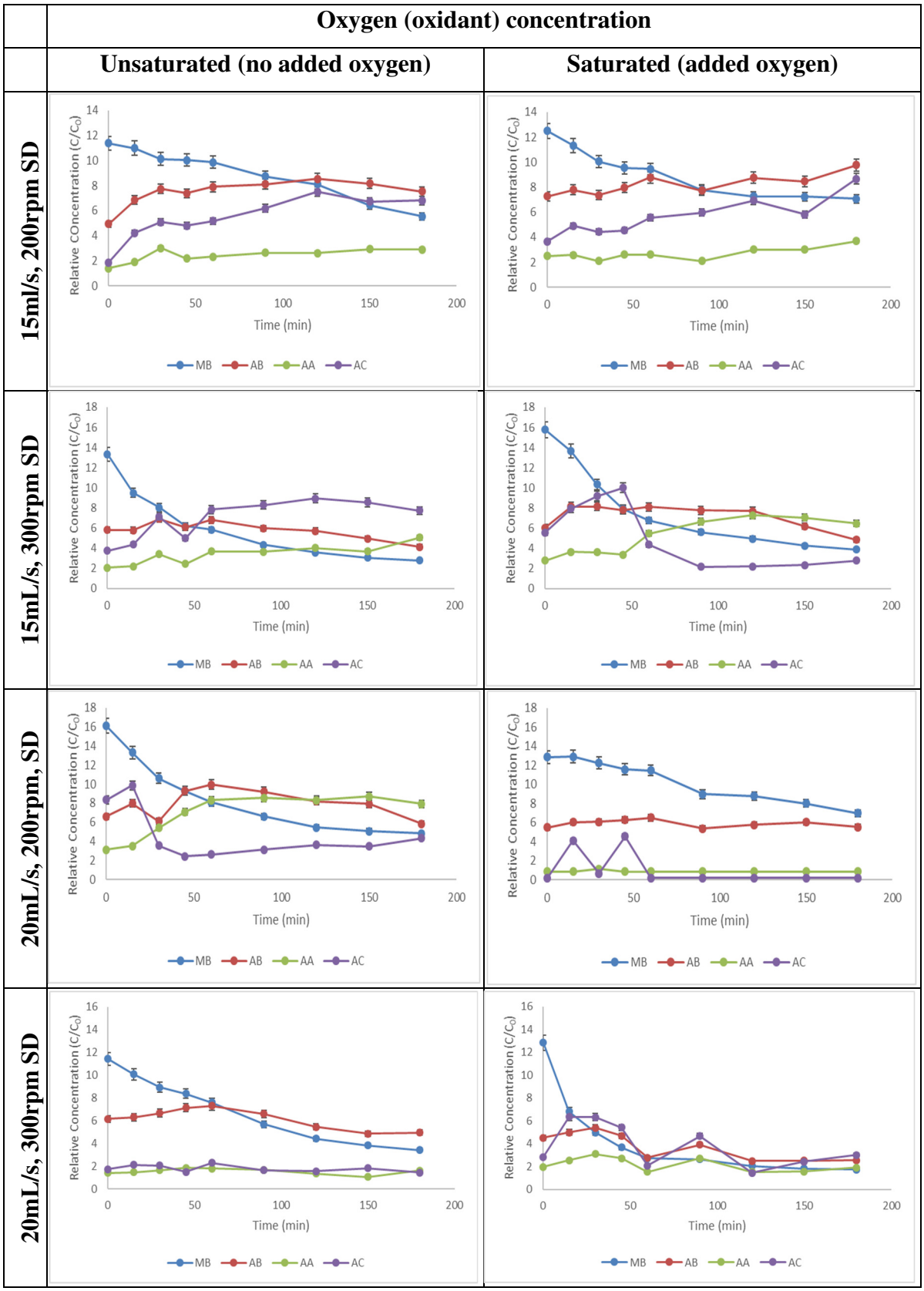

Figure 7.9: Reaction profile comparison of the reaction intermediates for methylene blue photocatalysed on the smooth disc – SD (initial concentration = 15mg/L) (MB = methylene blue; AB = azure B; AA = azure A; AC = azure C).

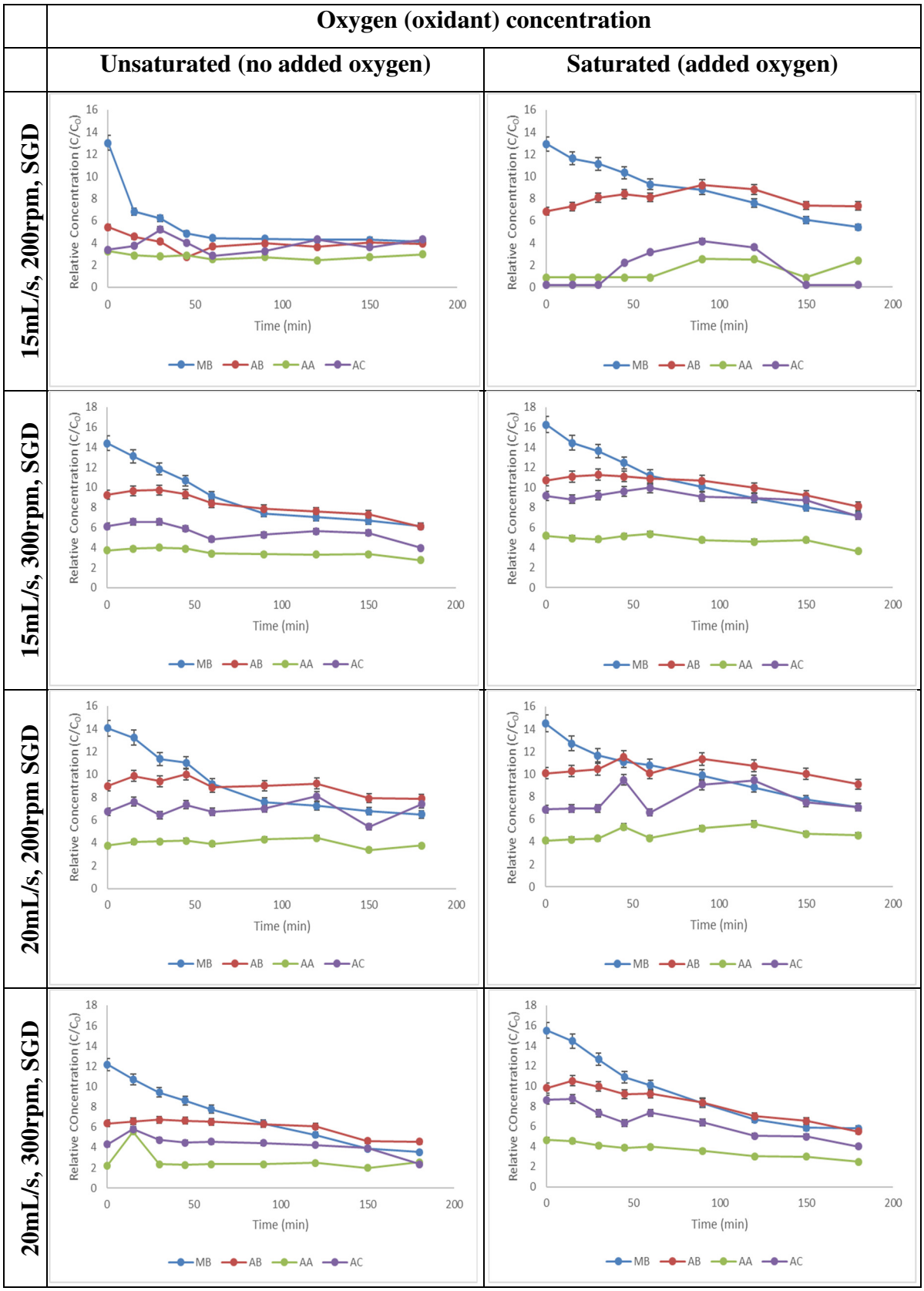

Figure 7.10: Reaction profile comparison of the reaction intermediates for methylene blue photocatalysed on the square grooved disc – SGD (initial concentration = 15 mg/l) (MB = methylene blue; AB = azure B; AA = azure A; AC = azure C).

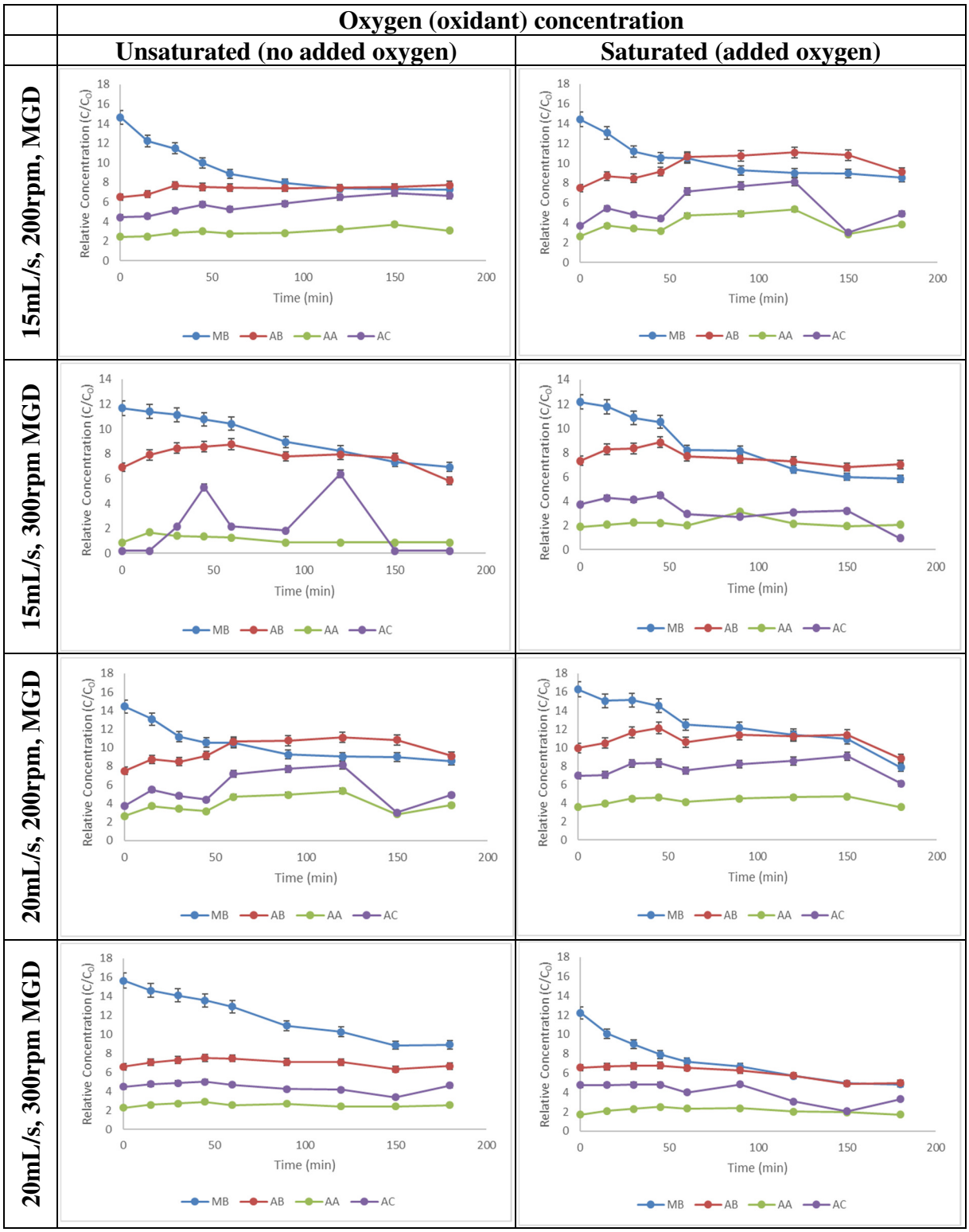

Figure 7.11: Reaction profile comparison of the reaction intermediates for methylene blue photocatalysed on the mesh grooved disc – MGD (initial concentration = 15 mg/L) (MB = methylene blue; AB = azure B; AA = azure A; AC = azure C).

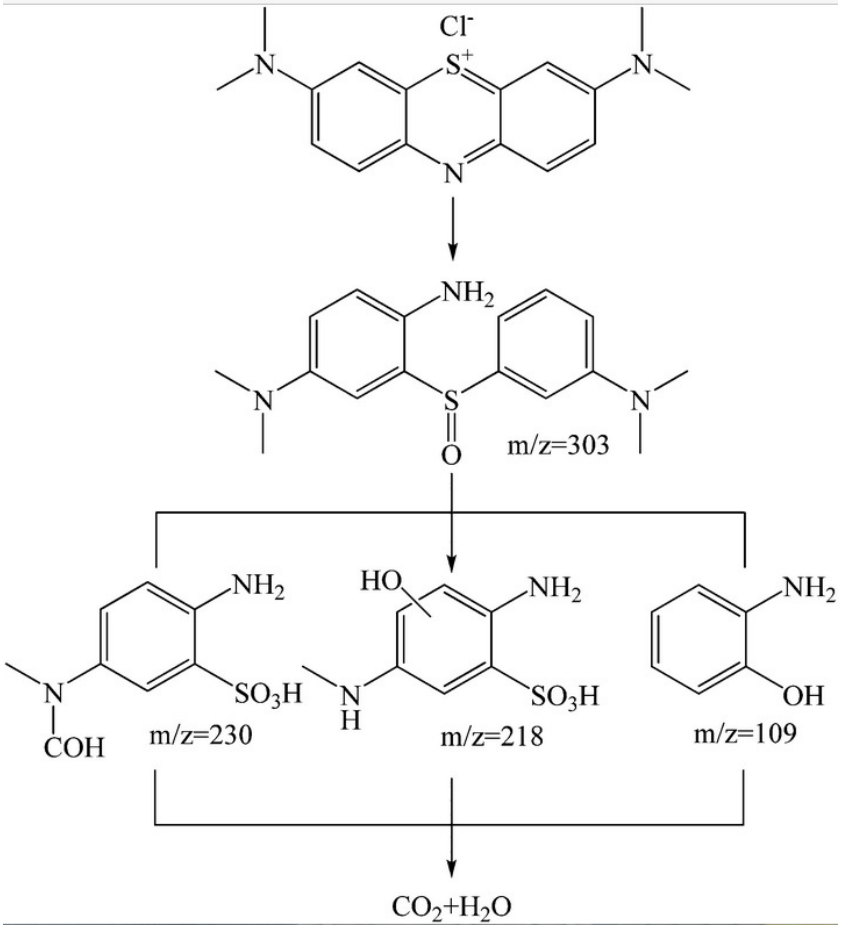

Figure 7.12: Possible degradation pathway of dyes MB (Xia *et al.*, 2015)

MB degradation pathways are given in Figure 7.12. MB was degraded to single ring structure products and three main single ring structure by-products were observed in the sample.

Finally, investigating the effect of the two main pSDR control parameters (spinning speed and inlet flowrate), it was found that the optimal (highest reaction rate) (Fig. 7.13) was at 300 rpm and 20 mL/s for the square grooved disc and smooth disc without added oxygen, while for mesh grooved disc the optimal was at 300 rpm and 15 mL/s with added oxygen. These results indicate that the optimal parameter for all discs depending on rotational speed which is 300 rpm. These results also again indicate that the square grooved disc produces the greatest process intensification of all of the reactors, with the highest degradation of MB and azo dye reaction intermediates.

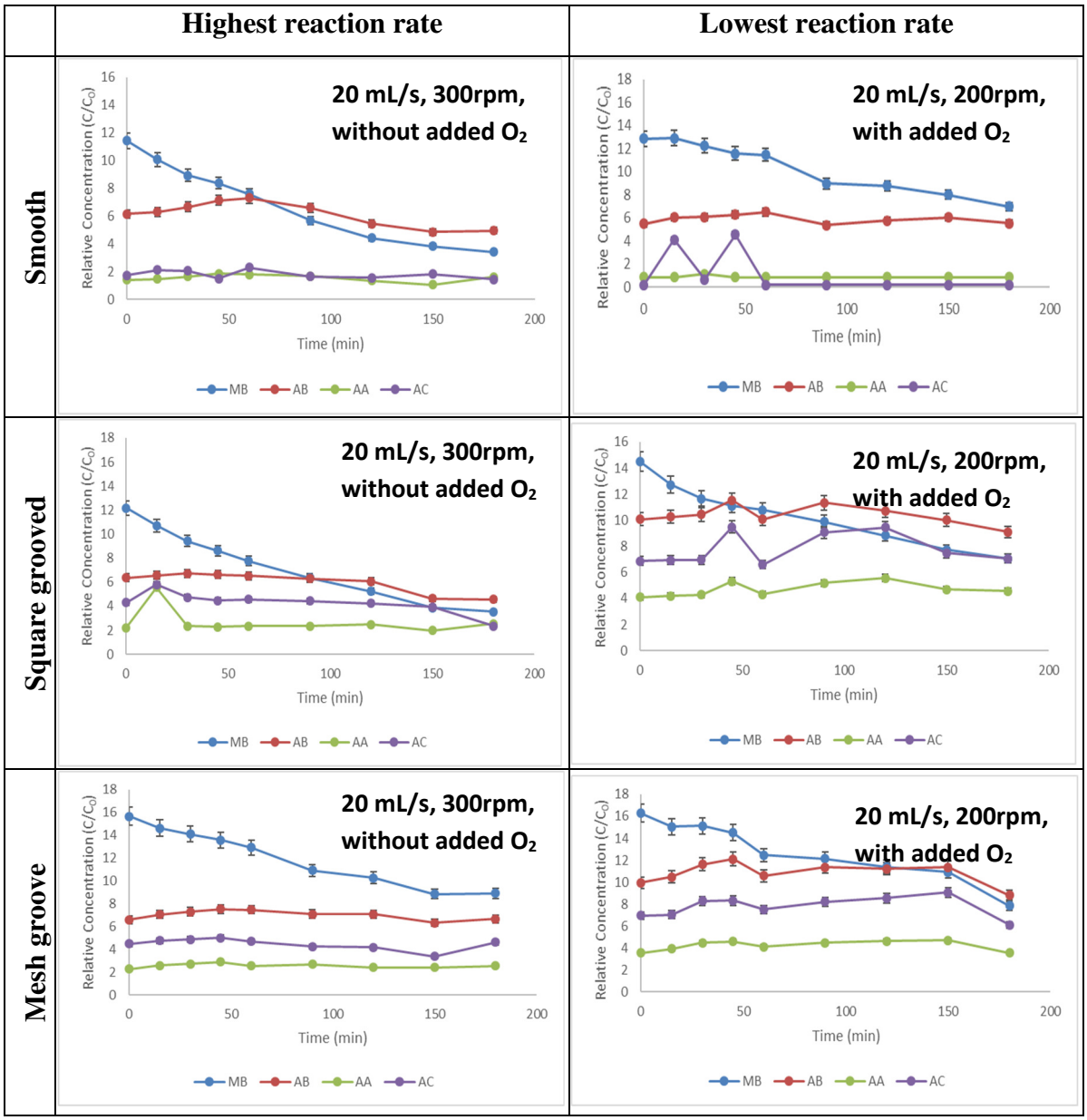

Figure 7.13: Reaction profile comparison of the highest and lowest reaction rate intermediates for methylene blue photocatalysed (MB = methylene blue; AB = azure B; AA = azure A; AC = azure C).

This result proven by studies in Chapter 5. From hydrodynamic studies, using a textured disc appears to even out the flow across the surface of the disc, which would increase the local UV penetration onto the disc surface (less scattering) and provide more uniform volumetric utilisation of the catalyst (Section 5.2). While, the RTD investigation (Section 5.3) provides a valuable insight into the operating conditions of the SDR which generate flow profiles approaching plug flow behaviour. The textured discs in particular made the flow more plug flow – as quantified by a higher number

of tanks in series. This indicates, as with the visual analysis/hydrodynamic studies that higher spinning speeds, higher inlet flowrates and a textured disc should result in conditions more favourable for higher reaction rates. The Villermaux-Dushman experiment (Section 5.4) performed in the spinning disc reactor clearly show that the best micromixing conditions were generally achieved at high disc rotational speeds, high feed flow rates and using textured discs.

7.3 Characterisation of the pSGDR for Ibuprofen

The aim of this work was to compare the degradation rate (Figure 7.14) and reaction rate (Figure 7.15) of SD and SGD at different spinning speeds and flowrates. SGD was chosen for the textures disc as a comparison to SD. This is supported by studies from Chapter 5 (hydrodynamic studies, RTD studies and Villermaux-Dushman experiment) and MB benchmark experiments for 3 different disc texture.

Several experiments were performed to evaluate removal efficiencies and photocatalytic reaction rates IBU using the SD and SGD. Photocatalytic degradation of IBU was investigated at an influent concentration of 25mg/L (121 µmol/L).

Fig. 7.14 shows the relative degradation of IBU vs. time for concentration 25mg/L during pSDR and PSGDR treatment with Fig 7.15 showing this converted into rate versus concentration data.

7.3.1 Effect of Spinning Speed

Figure 7.14 show that IBU degradation is higher at flowrates of 15 and 20mL/s. There is a negligible effect of spinning speed at each flow rate for the higher inlet flowrates (also shown in reaction rate, Figure 7.15). The scatter at the lowest flowrate of 10 mL/s is likely due to poor mixing and uneven flow (including dry patches) at these conditions (as shown in Chapter 5). This reason is that with increasing rotational speed of the disc will decreased the film thickness. The increase formation of waves due to grooves induces instabilities in the liquid film, supposed to resulting in an improved mass transfer (Figure 5.3, Section 5.2). These are slightly different results compare to MB, where IBU as the parent compound was completely degraded after 180min. This maybe influence by the colourless IBU compare to MB. This indicates that although

the optimal film thickness and waves formation achieved for MB degradation as like IBU degradation, it still cannot overcome the negative effects of a darker reactant feed in a photocatalytic reactor.

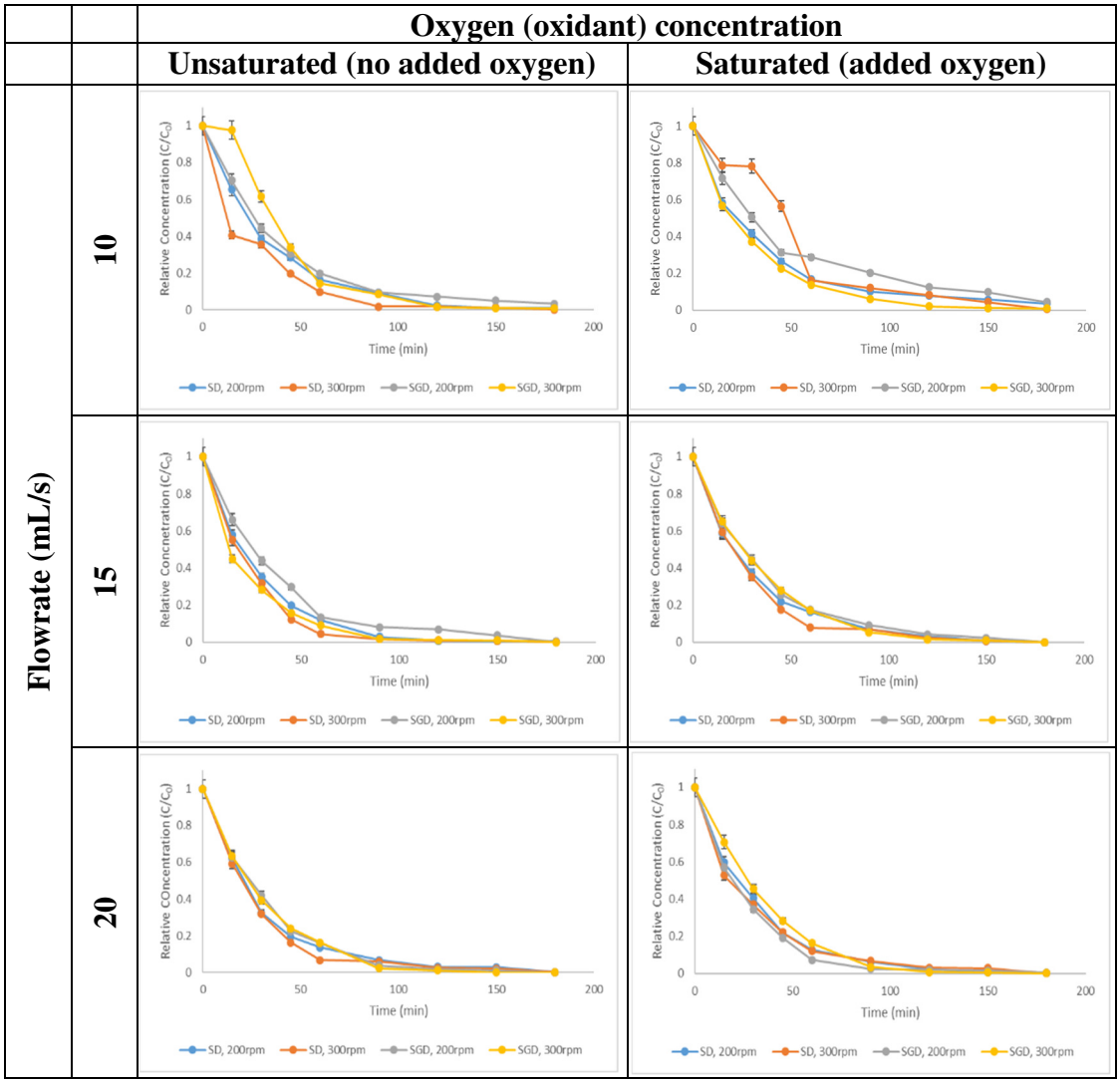

Figure 7.14: Relative concentration of ibuprofen degradation at different flowrates, rotational speed and disc surface configuration.

7.3.2 Effect of Inlet Flowrate

Figures 7.14 and 7.15 show gives a more consistent reaction profile for higher inlet flowrate, which again is consistent with the more even flow produced at the higher flowrates in Chapter 5 – however this also produces a thicker film and therefore can decrease reaction rate (this not really apply for IBU because it is colourless). At lower

inlet flowrate (10 mL/s) the discs are not wetted well compare to inlet flowrate 20mL/s (Figure 5.2 and 5.4) this also can affect the mixing of the IBU and liquid-catalyst contact. Again, these more optimal conditions can be attributed to increased micromixing (Section 5.4) and a smoothing of the liquid thin film on the disc surface as discussed in Section 5.2.

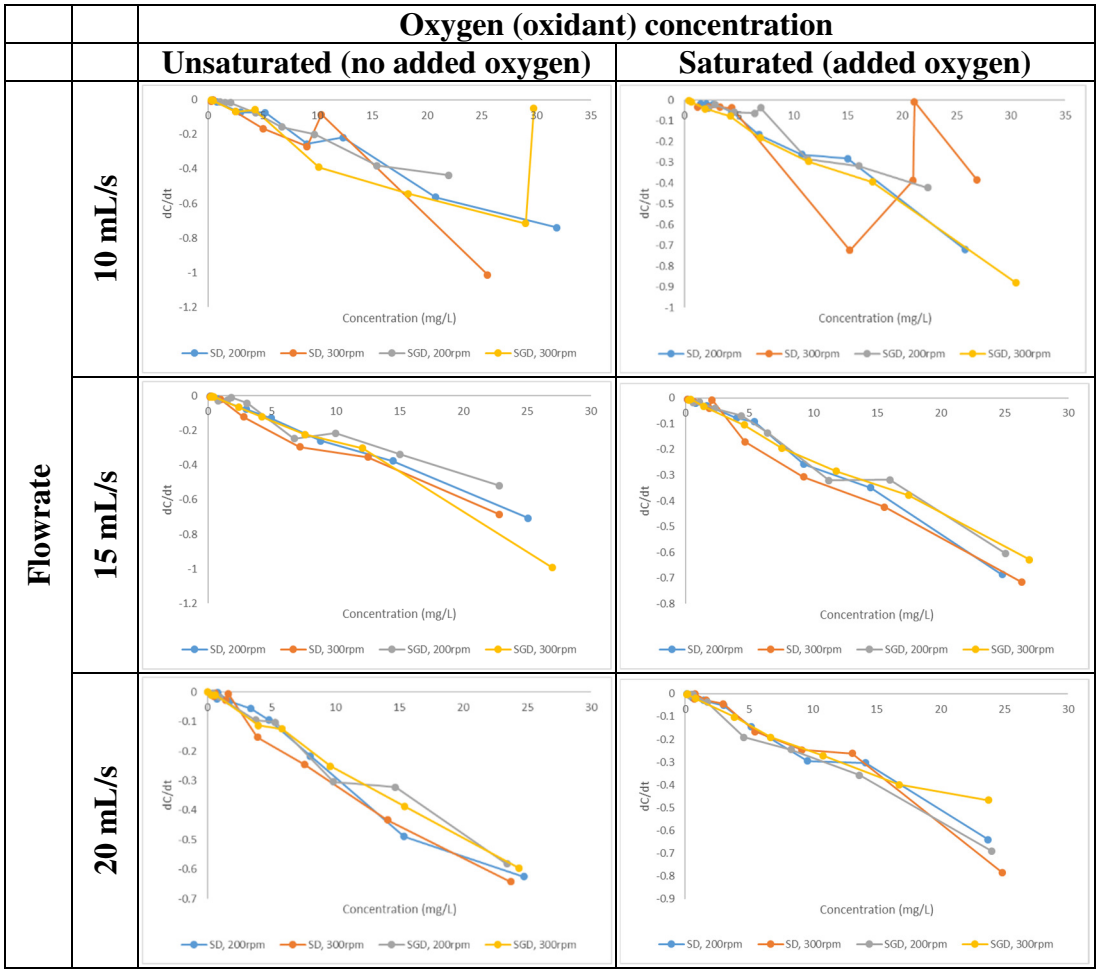

Figure 7.15: Reaction rate of ibuprofen degradation at different flowrates, rotational speed and disc surface configuration.

7.3.4 Effect of Disc Surface

Figure 7.14 and 7.15 indicate that the smooth disc is more optimal for ibuprofen degradation compared to the square grooved disc. Increasing spinning speed and inlet flow rate have the largest effect in increasing extent of oxidation – this can be attributed

to increased micromixing (Section 5.4) and a smoothing of the surface of the disc increasing UV penetration to the photocatalyst surface as discussed in Section 5.2.

7.3.5 Effect of Added Oxygen

Generally, the supply of additional oxygen is expected to enhance the photocatalytic degradation due to the greater availability of the oxidant for the photocatalytic degradation, as previously outlined. However, again additional saturated oxygen did not improve the conversion of IBU (Fig. 7.16). This again shows that the pSDR can self-oxygenate sufficiently to maintain the photocatalytic oxidation process at low substrate concentration and that the combination of this self-oxygenation and saturated oxygen supply has a detrimental effect on the photocatalytic reaction through either active site blockage or reduction of light intensity to the photocatalyst.

7.3.6 Overall comparison of reaction rates

Quantifying reaction rates confirms these results:

- A higher disc rotational speed (spinning speed) increases the reaction rate
- A lower flowrate increases reaction rate for this system – this is the opposite to the MB case
- The smooth glass disc is optimal – this is also different to the MB case, where the GSD was optimal.

The differences are likely due to the differences in mechanism of the photocatalytic degradation. Methylene blue adsorbs onto the surface of the photocatalyst (Al-Shamali, 2013), whilst ibuprofen does not adsorb and instead is preferentially degraded in solution. Literature confirms this: hydroxyl radicals, strongly active and degrading, react very rapidly together with aromatic ring compounds (Sakthivel *et al.*, 2003). However, in the case of IBU photocatalytic process, the hydroxyl radicals showed to have only moderate contribution to the initial molecule transformation upon UV irradiation. IBU having a more open chemical structure with only one aromatic ring and carboxyl in its structure, can also be oxidised preferentially via the photogenerated holes, often involved in the decarboxylation reaction, rather than by

the non-selective HO• radicals. Méndez-Arriaga, Esplugas and Giménez, (2008) state in their work that high oxidation levels can be assured by direct decarboxylation avoiding the hydroxylation step. In the same work though, it is suggested that in the presence of excess hydroxyl radicals, such as in aerated conditions, IBU acts more efficiently as a scavenger of those hydroxyl radicals and diminishes almost totally its concentration by the hydroxylation process.

Therefore, a lower flowrate gives a longer residence time for the ibuprofen on the disc surface, the surface area for adsorption is less important and micromixing of the ibuprofen within the thin film, which is higher and higher spinning speeds would increase reaction rate.

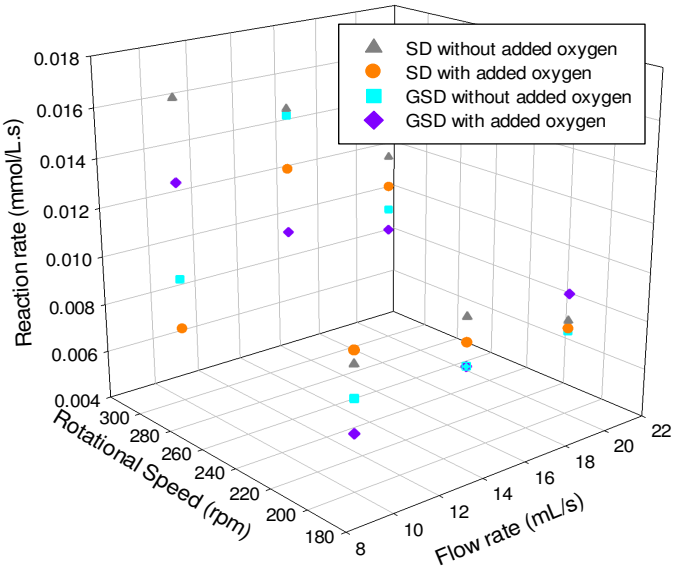

Figure 7.16: Reaction rate of ibuprofen mineralisation in the spinning grooved disc reactor.

Although IBU nearly degrade completely (Figure 7.15 and 7.16), this was not necessarily indicative of total mineralization (Madhavan, Grieser and Ashokkumar, 2010). Therefore, TOC analyses were performed to determine the extent of IBU mineralization. From Figure 7.17, the TOC data revealed that IBU was not mineralized to a similar extent, even after a treatment time as long as 180 min. For instance, the highest mineralization rate was only 85% for a smooth disc and 80% for grooved disc

achieved upon the application of the pSDR. Moreover, the mineralization rates derived from direct photolysis were negligible. These findings point out that while most of the original IBU was not mineralized, recalcitrant by-products have been generated under these conditions. The removal percentages of IBU and TOC after 60 min were 90 and 30%, respectively. The findings indicated the generation of intermediates products during IBU degradation. Total IBU removal was observed after a longer period of treatment (180 min). However, total mineralization was not achieved, with 60 to 70 % TOC removal after 180 min of treatment, respectively.

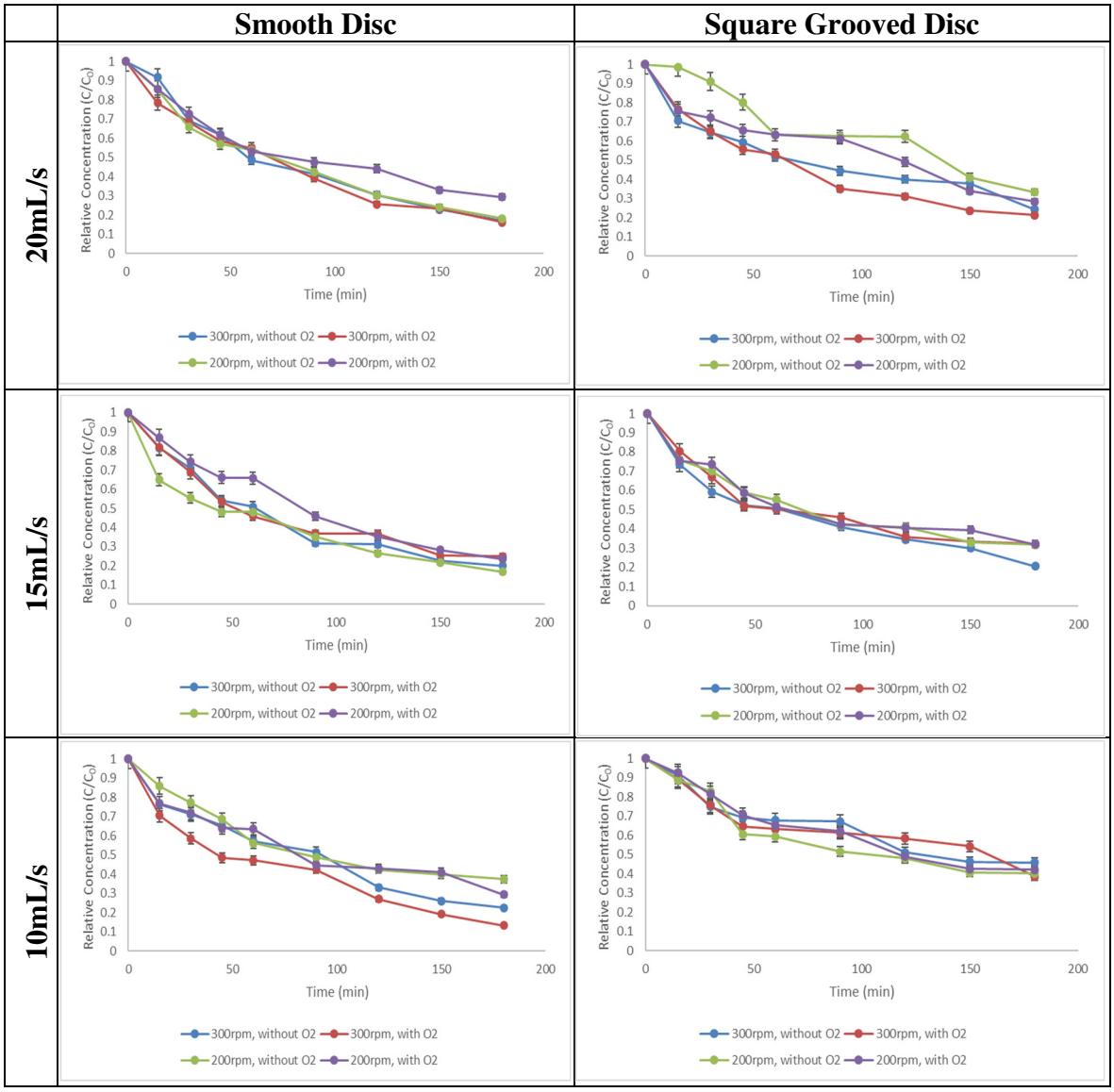

Figure 7.17. Relative concentration of TOC mineralisation degradation in the spinning grooved disc reactor.

Looking at the TOC degradation rate (Figure 7.18), the following conclusions can be made:

- The smooth disc surface used in this work provides an improved in reaction rate compared to the grooved disc.
- Investigating the effect of the two main pSDR control parameters (spinning speed and inlet flowrate), it was found that the optimal (highest reaction rate) was at 300 rpm and 15 mL/s for the smooth disc without added oxygen, indicating that the self-aeration of oxygen by the pSDR spinning liquid film contacting air produces sufficient and more optimal oxidant input.

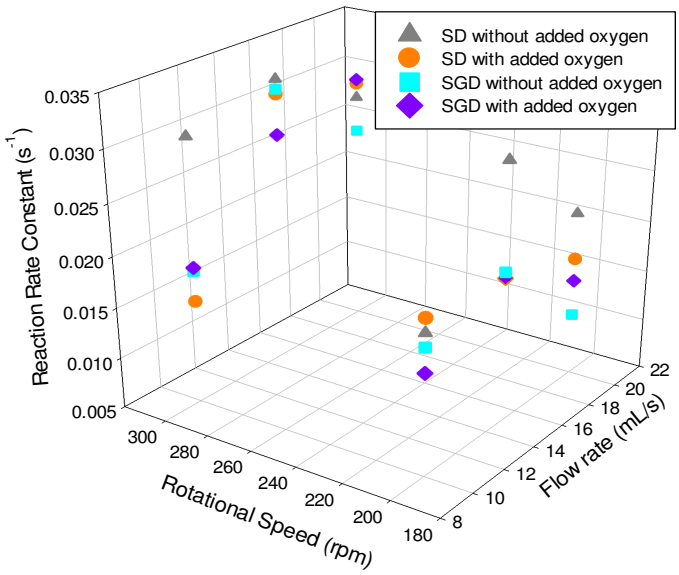

Figure 7.18: Reaction rate constant of TOC mineralisation of ibuprofen in the SGDR.

7.3.7 Intermediate Analysis

Figure 7.19 shows the by-products detected by LC–MS from the photocatalytic treatment (in marked circle) and possible transformation pathways followed by ibuprofen. The most plausible route of degradation (or transformation) of ibuprofen is due to a dominant photochemical scavenger of the OH• mediated process by the inclusion of the radical in the methylpropyl phenyl positions I (1-hydroxyIBU) and II (2-hydroxyIBU)), and in the arylcarboxylic moiety (III and IV). Direct demethylation or decarboxylation was not observed.

During the photocatalytic reaction, the generation of by-products increases until a maximum concentration is reached. Moreover, Packer *et al* (2003) assured that the half-life time of IBU in the environment can be function of the OH• concentration. Ibuprofen degradation by OH• scavenger reaction is a slow process in a normal environment. In contrast, the application of a photocatalytic treatment on the degradation of ibuprofen increases the concentration rate of the hydroxyl radical, thus promoting the generation of faster hydroxyl metabolites. The metabolites generated during the photocatalysis process are also reported as a product of the biochemical pathway (Zweiner *et al*, 2002) but no more than 10% of the original amount of ibuprofen. By photocatalytic means, it is possible to increase the percentage up to 100% conversion of the initial ibuprofen concentration.

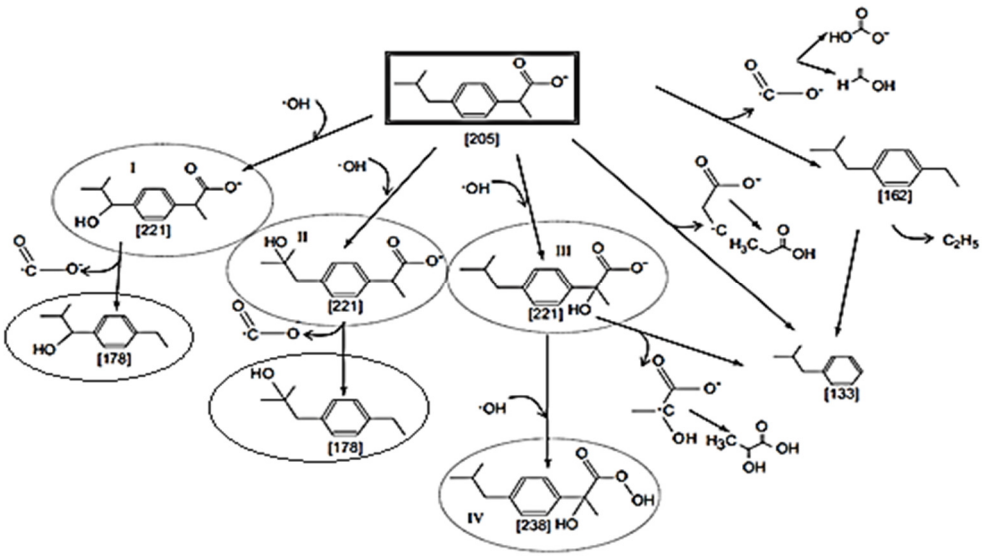

Fig. 7.19: Intermediates observed at the end of photocatalytic treatment of IBU.

Figure 7.20 and 7.21 shows the formation and degradation of the intermediates at different flow rate, rotational speed and surface structure. During photocatalytic process of ibuprofen, many intermediates were produced and destructed in the solution simultaneously. Three aromatic intermediates were tentatively identified in the solution by LC-MS. The three major identified reaction species were m/z =178.14, m/z = 221.12, and m/z = 238.12. Fig. 7.20 and 7.21 show that for all reactions, parent molecule IBU was fully oxidised in the reaction time studied.

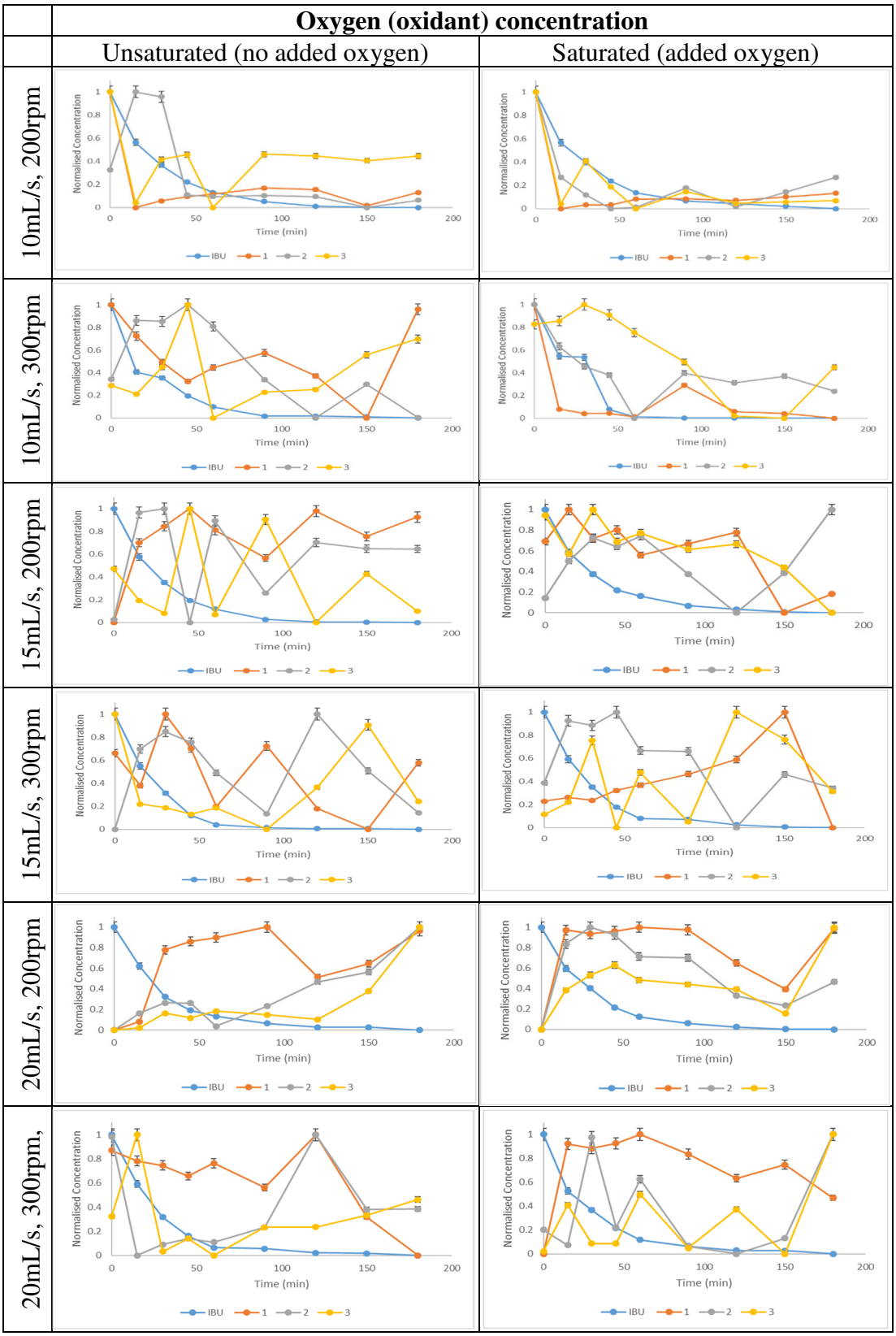

Figure 7.20: Reaction profile comparison of the reaction intermediates for ibuprofen photocatalysed (smooth disc – SD) [**1**: m/z = 178.14; **2**: m/z = 221.12; **3**: m/z = 238.12].

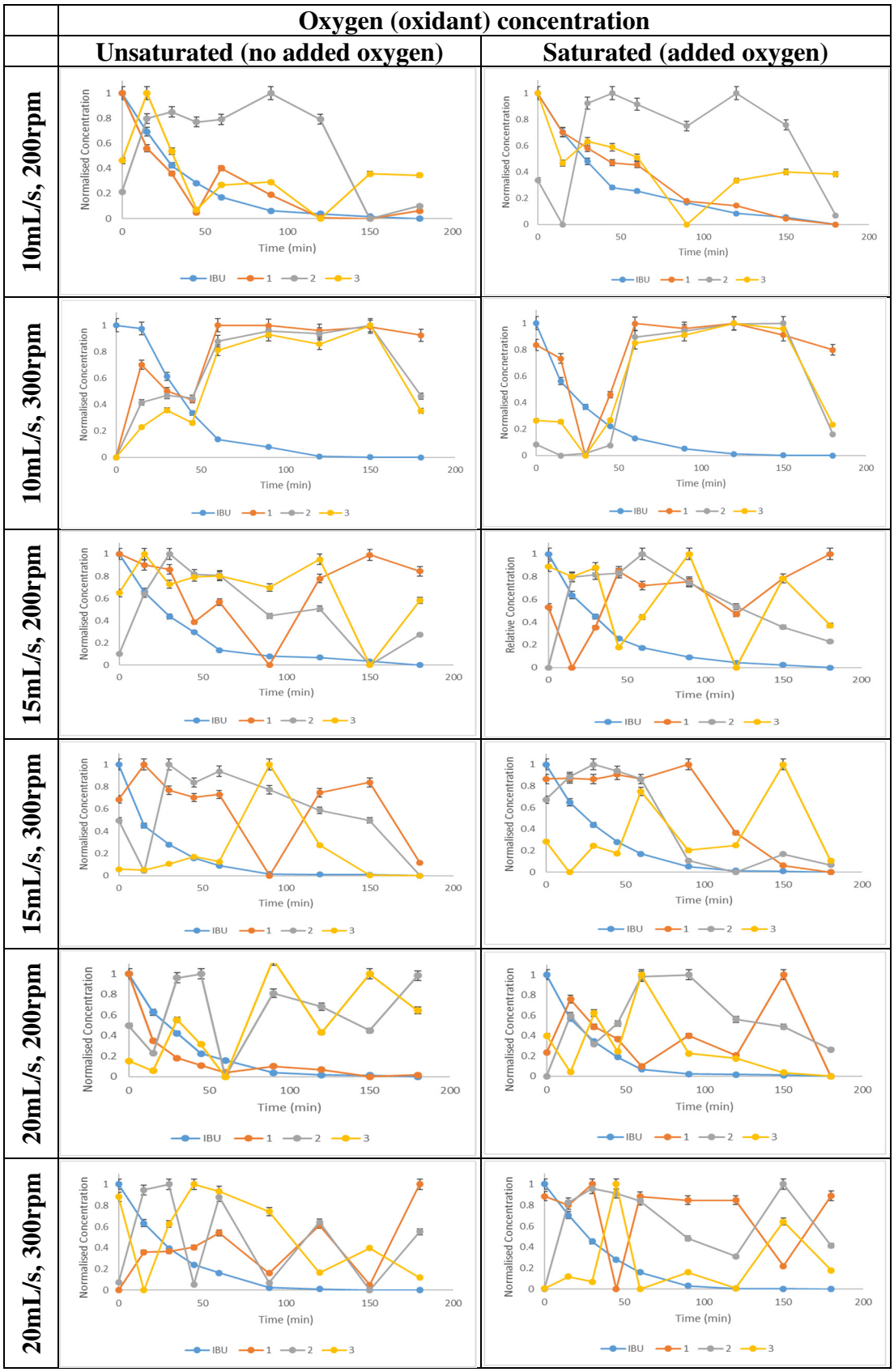

Figure 7.21: Reaction profile comparison of the reaction intermediates for ibuprofen photocatalysed (square grooved – SGD) [**1**: m/z = 178.14; **2**: m/z = 221.12; **3**: m/z = 238.12].

In addition (Figure 7.20 and 7.21), a variety of aliphatic carboxylic acid intermediates were identified by comparing their retention time of HPLC and LC-MS. Most of these intermediates produced have been reported by Mendez-Arriaga, Gimenez and Esplugas (2010) induced by ·OH in advanced oxidative degradation process of ibuprofen. This similarity suggests that ·OH plays an important role in ibuprofen mineralization throughout the photocatalytic degradation.

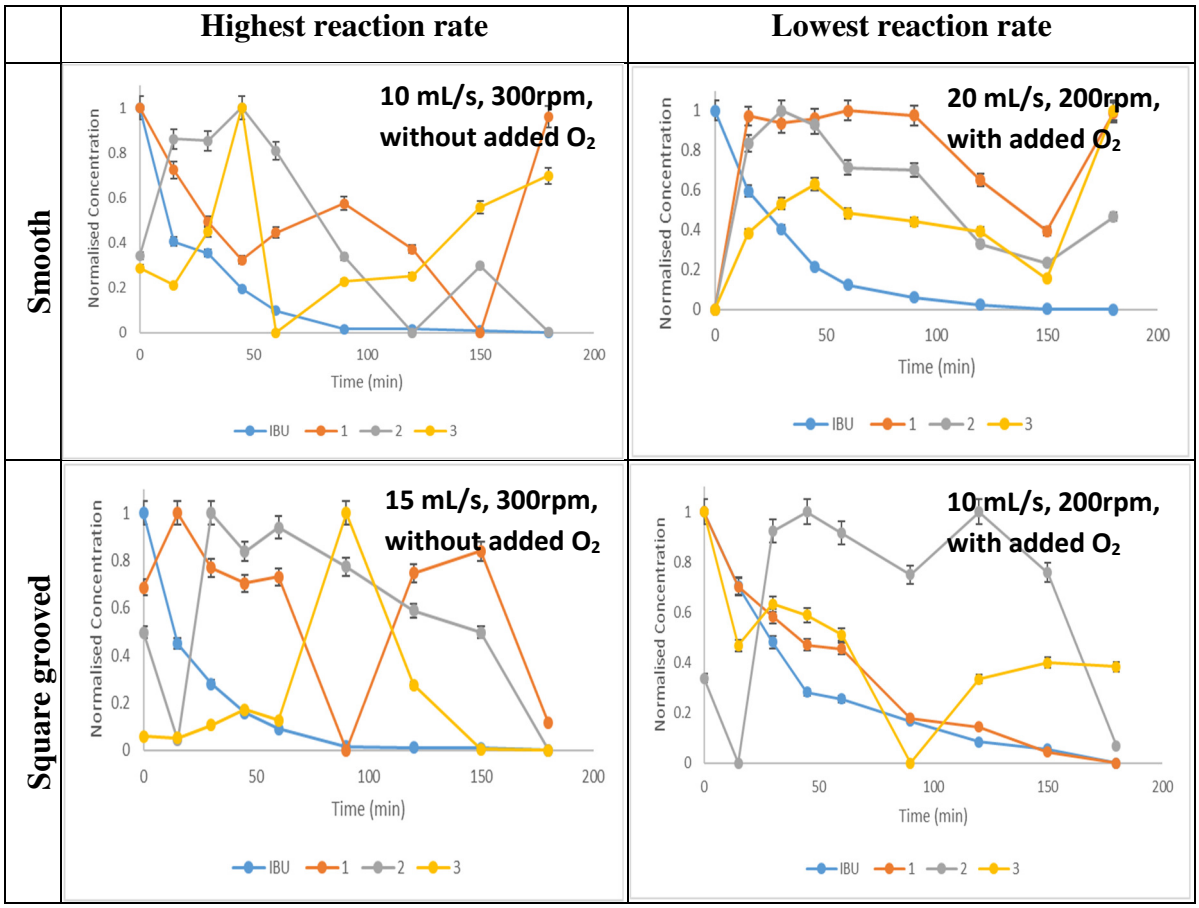

Figure 7.22: Reaction profile comparison of the highest and lowest reaction rate intermediates for ibuprofen photocatalysed [**1**: m/z = 178.14; **2**: m/z = 221.12; **3**: m/z = 238.12].

This prove that the removal of the initial compound does not indicate that the total mineralization was achieved. Therefore, a study of the total organic carbon (TOC) quantification was also studied (Section 7.3.6).

The LC-MS results show that the aromatic intermediates including hydroxylated ibuprofens and their decarboxylated and demethylated derivatives were rapidly formed and then destructed during photocatalytic process. The initial reaction step in ibuprofen degradation mainly attributed by ·OH attack on ibuprofen. In this study, three isomers of monohydroxylated ibuprofen (MW= 221.12) were detected in the solution. In addition, derivative of multihydroxylated ibuprofen with MW=238.12 was also detected. This result is consistent with the previous reports (Li *et al.*, 2014) that ·OH attack can occur on ibuprofen to yield a variety of hydroxylated ibuprofen. Furthermore, ·OH attack on the hydroxylated species of ibuprofen result in decarboxylation and demethylation at the ibuprofen side chains which yields smaller aromatic intermediates such as 1-[4-(2-Methylpropyl)phenyl]ethanone (MW = 178.14).

Finally, investigating the effect of the two main pSDR control parameters (spinning speed and inlet flowrate), it was found that the optimal (highest reaction rate) (Fig. 7.22) was at 300 rpm and 10 mL/s for the smooth disc without added oxygen, while for square grooved disc the optimal was at 300 rpm and 15 mL/s without added oxygen. These results indicate that the optimal parameter for all discs depending on rotational speed which is 300 rpm. These results indicate that the smooth disc produces better process intensification, with the highest degradation of IBU and reaction intermediates.

7.4 Conclusion

Two model compounds were investigated for the photocatalytic degradation in a SDR with different disc texture (smooth disc, mesh disc and grooved disc). Methylene blue (MB) and ibuprofen (IBU) are the study compound, and the following conclusions were made regarding the performance of the SDR:

- There were no significant differences in MB degradation between different mesh sizes. Compared to the smooth disc, with a lower photocatalytic surface area, it can be seen that the meshes did not produce any process intensification. It is hypothesised that this is due to two factors: firstly, there is a shadowing on glass disc by the meshes, reducing the light exposed surface area and therefore reducing the effective surface area of the photocatalyst. The mesh also disrupts

the liquid film to a greater extent than expected, producing dry patches across the mesh surface, further reducing the effective surface area of the photocatalyst.

- In MB degradation, the square grooved disc surface used in this work provides an improved in reaction rate compared to the smooth disc and mesh grooved disc. From hydrodynamic studies, using a textured disc appears to even out the flow across the surface of the disc, which would increase the local UV penetration onto the disc surface (less scattering) and provide more uniform volumetric utilisation of the catalyst. While, the RTD investigation provides a valuable insight into the operating conditions of the SDR which generate flow profiles approaching plug flow behaviour. The Villermaux-Dushman experiment (Section 5.4) performed in the spinning disc reactor clearly show that the best micromixing conditions were generally achieved at high disc rotational speeds, high feed flow rates and using textured discs.

- Although IBU nearly degrade completely in all experiments, this was not necessarily indicative of total mineralization (Madhavan, Grieser and Ashokkumar, 2010). From TOC result revealed that IBU was not mineralized to a similar extent. The findings indicated the generation of intermediates products during IBU degradation.

- Finally, results have shown that degradation rate can be optimised through identification of the optimal rotating speed, disc surface structure (meshes/grooves/smooth), oxidant input and volumetric flowrate. The optimal was found to be at 300 rpm rotational speed. Overall this work shows that the reactor and photocatalyst surface macrostructure and design plays an important role in increasing photocatalytic treatment efficiency especially for coloured solution. Moreover, the process intensification (higher reaction rates and photonic efficiency) and self-aeration demonstrated here and in previous work (Boiarkina, Pedron and Patterson, 2011; Boiarkina, Norris and Patterson, 2013a, 2013b), further demonstrates the significant advantages of the pSDR over other photocatalytic reactors.

CHAPTER 8: CONCLUSIONS AND RECOMMENDATIONS FOR FUTURE WORK

8.1 Conclusions

This thesis investigates the use of a spinning disc reactor as a process intensification technology for the photocatalytic degradation of two model wastewaters; methylene blue and ibuprofen. The pSDR was designed specifically with the application of photocatalysis in mind, which resulted in a novel bottom inlet feed in order to avoid light obstruction above the immobilised catalyst on the disc. The performance of the reactor was assessed through experiments: hydrodynamics study, residence time distribution study and micromixing study; photocatalytic spinning disc reactor experiments and finally photocatalytic spinning mesh/grooved disc reactor experiments and the following were found:

- From hydrodynamic studies, using a textured disc appears to even out the flow across the surface of the disc, which would increase the local UV penetration onto the disc surface (less scattering) and provide more uniform volumetric utilisation of the catalyst. This is an atypical need for most SDRs, where the typical characteristics of increasing disc rotational speed and feed flowrate show more complete film formation. However, since a more uniform film surface is needed for a photocatalytic SDR, the optimal film structures for enhanced reaction rates in other SDRs (that do not rely on high intensity of UV on the surface of the disc) may be different.
- The RTD investigation provides a valuable insight into the operating conditions of the SDR which generate flow profiles approaching plug flow behaviour. RTD analysis showed that the flow pattern on the spinning disc became close to plug flow with the increase of spinning speed and flow rate. The textured discs in particular made the flow more plug flow – as quantified by a higher number of tanks in series. This indicates, as with the visual analysis/hydrodynamic studies that higher spinning speeds, higher inlet flowrates and a textured disc should result in conditions more favourable for higher reaction rates.

- The Villermaux-Dushman experiment performed in the spinning disc reactor clearly show that the SDR is a device suitable for obtaining a high degree of micromixing efficiency. The mixing quality can be influenced by several process parameters such as the disc rotational speed, feed flowrate, and surface structure all proved to be important hydrodynamic parameters in determining the micromixing characteristics in SDR. The effect of the process parameters on the mixing efficiency has clearly been demonstrated by use of the iodide–iodate reaction. The best micromixing conditions were generally achieved at high disc rotational speeds, high feed flow rates and using textured discs.

- A higher overall degradation for model wastewaters with a lower starting concentration 5 mg/L, will be degraded faster. In particular, at higher dye concentrations above 10 mg/L, more light was scattered by the dye solution and fewer photons are able to reach the TiO_2 surface. Thus, the generation of electron-hole pairs was greatly reduced, and in turn, the dye degradation was reduced due to absence of the oxidizing species. In contrast, at lower concentration, the lower degradation efficiency may be attributed to the mass transfer resistance notwithstanding the mass-transfer intensified by disc rotation.

- For the smooth discs and for the degradation of methylene blue, a supply of oxidant increases reaction rate – indicating that at the conditions that these reactions were run at, there is insufficient mass transfer area and mixing (including micromixing) on the disc to supply the reaction with oxygen and this is likely the rate limiting factor in the reactions where oxygen is not supplied.

- At 300rpm, the reaction without oxygen being fed at saturation has the highest reaction rate. This is not expected and indicates that perhaps excess oxygen is detrimental to this reaction. When oxygen is supplied, there is no significant difference between the degradations at the different flow rates. This indicates that the differences in residence times do not make a difference in the overall degradation at these conditions.

- There is no significant difference seen at the lower flowrate (10 mL/s) between adding oxygen or not which indicates that the rate of oxygen mass transfer into the surface of the liquid film on the disc is sufficient to keep the reaction going – it does not become limiting. However, at the higher flowrate (15 mL/s), adding oxygen increases the reaction rate. This indicates that the rate of mass transfer through the liquid film surface is limiting at the higher flowrate.

- There were no significant differences in MB degradation between different mesh sizes. Compared to the smooth disc, with a lower photocatalytic surface area, it can be seen that the meshes did not produce any process intensification. It is hypothesised that this is due to two factors: firstly, there is a shadowing on glass disc by the meshes, reducing the light exposed surface area and therefore reducing the effective surface area of the photocatalyst. The mesh also disrupts the liquid film to a greater extent than expected, producing dry patches across the mesh surface, further reducing the effective surface area of the photocatalyst.

- In MB degradation, the square grooved disc surface used in this work provides an improved in reaction rate compared to the smooth disc and mesh grooved disc. From hydrodynamic studies, using a textured disc appears to even out the flow across the surface of the disc, which would increase the local UV penetration onto the disc surface (less scattering) and provide more uniform volumetric utilisation of the catalyst. While, the RTD investigation provides a valuable insight into the operating conditions of the SDR which generate flow profiles approaching plug flow behaviour. The Villermaux-Dushman experiment (Section 5.4) performed in the spinning disc reactor clearly show that the best micromixing conditions were generally achieved at high disc rotational speeds, high feed flow rates and using textured discs.

- Although IBU nearly degrade completely in all experiments, this was not necessarily indicative of total. From TOC result revealed that IBU was not mineralized to a similar extent. The findings indicated the generation of intermediates products during IBU degradation.

- Finally, results have shown that degradation rate can be optimised through identification of the optimal rotating speed, disc surface structure

(meshes/grooves/smooth), oxidant input and volumetric flowrate. The optimal was found to be at 300 rpm rotational speed. Overall this work shows that the reactor and photocatalyst surface macrostructure and design plays an important role in increasing photocatalytic treatment efficiency especially for coloured solution. Moreover, the process intensification (higher reaction rates and photonic efficiency) and self-aeration demonstrated here and in previous work (Boiarkina, Pedron and Patterson, 2011; Boiarkina, Norris and Patterson, 2013a, 2013b), further demonstrates the significant advantages of the pSDR over other photocatalytic reactors.

8.2 Recommendations for Future Work

Several further questions have arisen regarding the applications of SDRs that require further research although the pSDR has been shown to be an effective process intensification technology for photocatalysis.

The durability, long term catalytic activity, mass transfer effects, reaction mechanisms and reaction kinetics of these immobilized catalysts should be quantified and understand to determine under what conditions stable reactor operation and process intensification is achieved and compare this to other types of spinning disc reactors.

The experimental reactor characterisations and computational analysis, involving systematic kinetic analysis (including quantifying mass transfer), residence time distribution (RTD) quantification and high speed camera analysis of the flows in the meshes/grooved should be combined to reconcile the mechanisms underpinning the above results and determine the key parameters for scale-up (before numbering-up) of the reactors.

The range of different mesh materials produced, mesh sizes, mesh thicknesses and how this affects shadowing in the reactor, catalyst coating, reaction rates, mixing in the reactor etc. should be looked into. An also different type of grooved disc can be produced, groove pattern, groove size, groove depth and how this affects catalyst coating, reaction rates, mixing in the reactor etc. Mass transfer coefficients will be determined using the appropriate dimensionless relationships. Research needs to be conducted into further investigating and characterising the methods of producing

stable catalysts on meshes/groove. Mesh/groove discs are not a common immobilisation support for nanostructured photocatalysts, so a range of techniques need to be assessed. This will allow a range of nanostructures to be formed on the meshes/groove.

Different type of contaminant compound commonly found in wastewaters can be used. Even real wastewater also can be applied. For all reactors, the feed and product streams will be sampled and analysed by UV-Vis, HPLC, LC-MS and/or GC-MS to identify the reaction intermediates and products and determine the extent of oxidation. Based on the identified intermediates and products, reaction mechanisms and pathways both in the liquid and solid phases will be inferred. To determine catalyst degradation, fouling and/or deactivation, the surface structure and deposits on unused and used catalysts will be imaged/analysed using SEM, TEM, XRD and ATR-FTIR. Atomic absorption (AA) spectroscopy will be used to determine the concentration of any leached catalyst into the wastewater.

REFERENCES

Ajona, J. I. and Vidal, A. (2000) 'The use of CPC collectors for detoxification of contaminated water: design, construction and preliminary results.', *Solar Energy*, 68, pp. 109–120.

Akyol, A. and Bayramoglu, M. (2010) 'Preparation and characterization of supported ZnO photocatalyst by zincate method', *Journal of Hazardous Materials*, 175(1–3), pp. 484–491. doi: 10.1016/j.jhazmat.2009.10.031.

Al-Shamali, S. S. (2013) 'Photocatalytic Degradation of Methylene Blue in the Presence of TiO2 Catalyst Assisted Solar Radiation', *Australian Journal of Basic and Applied Sciences*, 7(4), pp. 172–176.

Ali, A. M., Emanuelsson, E. A. C. and Patterson, D. A. (2011) 'Conventional versus lattice photocatalysed reactions: Implications of the lattice oxygen participation in the liquid phase photocatalytic oxidation with nanostructured ZnO thin films on reaction products and mechanism at both 254nm and 340nm', *Applied Catalysis B: Environmental*. Elsevier B.V., 106(3–4), pp. 323–336. doi: 10.1016/j.apcatb.2011.05.033.

Aoune, A. and Ramshaw, C. (1999) 'Process intensification: heat and mass transfer characteristics of liquid films on rotating discs', *International Journal of Heat and Mass Transfer*, 42(14), pp. 2543–2556. doi: 10.1016/S0017-9310(98)00336-6.

Atmaca, E. (2009) 'Treatment of landfill leachate by using electro-Fenton method', *Journal of Hazardous Materials*, 163, pp. 109–114.

Boiarkina, I. (2012) *Investigation of a Spinning Disc as a Thin Film Photocatalytic Reactor for the Degradation of Recalcitrant Wastewaters*.

Boiarkina, I., Norris, S. and Patterson, D. A. (2013a) 'Investigation into the effect of flow structure on the photocatalytic degradation of methylene blue and dehydroabietic acid in a spinning disc reactor', *Chemical Engineering Journal*. Elsevier B.V., 222, pp. 159–171. doi: 10.1016/j.cej.2013.02.025.

Boiarkina, I., Norris, S. and Patterson, D. A. (2013b) 'The case for the photocatalytic spinning disc reactor as a process intensification technology: Comparison to an

annular reactor for the degradation of methylene blue', *Chemical Engineering Journal*. Elsevier B.V., 225, pp. 752–765. doi: 10.1016/j.cej.2013.03.125.

Boiarkina, I., Pedron, S. and Patterson, D. A. (2011) 'An experimental and modelling investigation of the effect of the flow regime on the photocatalytic degradation of methylene blue on a thin film coated ultraviolet irradiated spinning disc reactor', *Applied Catalysis B: Environmental*. Elsevier B.V., 110, pp. 14–24. doi: 10.1016/j.apcatb.2011.08.008.

Boodhoo, K. V. K. and Al-Hengari, S. R. (2012) 'Micromixing Characteristics in a Small-Scale Spinning Disk Reactor', *Chemical Engineering & Technology*, 35(7), pp. 1229–1237.

Boodhoo, K. V. K. and Jachuk, R. (2000) 'Process intensification: spinning disk reactor for styrene polymerisation.', *Applied Thermal Engineering*, 20(12), pp. 1127–1146.

Brechtelsbauer, C., Lewis, N., Oxley, P., Ricard, F. and Ramshaw, C. (2001) 'Evaluation of a spinning disc reactor for continuous processing', *Organic Process Research and Development*, 5(1), pp. 65–68. doi: 10.1021/op0000834.

Burns, J. R. and Jachuck, R. J. J. (2005) 'Determination of liquid-solid mass transfer coefficients for a spinning disc reactor using a limiting current technique', *International Journal of Heat and Mass Transfer*, 48(12), pp. 2540–2547. doi: 10.1016/j.ijheatmasstransfer.2004.11.029.

Burns, J. R., Jamil, J. N. and Ramshaw, C. (2000) 'Process intensification: operating characteristics of rotating packed beds — determination of liquid hold-up for a high-voidage structured packing', *Chemical Engineering Science*, 55(13), pp. 2401–2415. doi: 10.1016/S0009-2509(99)00520-5.

Burns, J. R., Ramshaw, C. and Jachuk, R. (2003) 'Measurement of liquid film thickness and the determination of spin-up radius on a rotating disc using an electrical resistance technique.', *Chemical Engineering Science*, 58(11), pp. 2245–2253.

Buser, H. R., Poiger, T. and Muller, M. D. (1999) 'Occurrence and environmental behavior of the chiral pharmaceutical drug ibuprofen in surface waters and in

wastewater', *Environmental Science and Technology*, 33(15), pp. 2529–2535. doi: 10.1021/es981014w.

Carp, O., Huisman, C. L. and Reller, A. (2004) 'Photoinduced reactivity of titanium dioxide', *Progress in Solid State Chemistry*, 32(1–2), pp. 33–177. doi: 10.1016/j.progsolidstchem.2004.08.001.

Černigoj, U., Štangar, U. L. and Trebše, P. (2007) 'Evaluation of a novel Carberry type photoreactor for the degradation of organic pollutants in water', *Journal of Photochemistry and Photobiology A: Chemistry*, 188(2–3), pp. 169–176. doi: 10.1016/j.jphotochem.2006.12.009.

Chang, H. T., Wu, N. and Zhu, F. (2000) 'A Kinetic Model for Photocatalytic Degradation of Organic Contaminants in a Thin-Film TiO2 Catalys', *Water Research*, 34(2), pp. 407–416.

Cheng, Z., Quan, X., Xiang, J., Huang, Y. and Xu, Y. (2012) 'Photocatalytic degradation of bisphenol A using an integrated system of a new gas-liquid-solid circulating fluidized bed reactor and micrometer Gd-doped TiO2 particles', *Journal of Environmental Sciences (China)*. The Research Centre for Eco-Environmental Sciences, Chinese Academy of Sciences, 24(7), pp. 1317–1326. doi: 10.1016/S1001-0742(11)60897-8.

Choina, J., Kosslick, H., Fischer, C., Flechsig, G. U., Frunza, L. and Schulz, A. (2013) 'Photocatalytic decomposition of pharmaceutical ibuprofen pollutions in water over titania catalyst', *Applied Catalysis B: Environmental*. Elsevier B.V., 129, pp. 589–598. doi: 10.1016/j.apcatb.2012.09.053.

Dimitrakopoulou, D., Rethemiotaki, I., Frontistis, Z., Xekoukoulotakis, N. P., Venieri, D. and Mantzavinos, D. (2012) 'Degradation, mineralization and antibiotic inactivation of amoxicillin by UV-A/TiO 2 photocatalysis', *Journal of Environmental Management*. Elsevier Ltd, 98(1), pp. 168–174. doi: 10.1016/j.jenvman.2012.01.010.

Dionysiou, D. D., Burbano, A. A., Suidan, M. T., Baudin, I. and Laîné, J. M. (2002) 'Effect of oxygen in a thin-film rotating disk photocatalytic reactor', *Environmental Science and Technology*, 36(17), pp. 3834–3843. doi: 10.1021/es0113605.

Donaldson, A. A. and Zhang, Z. (2011) 'Coupled transport phenomena in corrugated photocatalytic reactors', *Chinese Journal of Chemical Engineering*. Chemical Industry and Engineering Society of China (CIESC) and Chemical Industry Press (CIP), 19(5), pp. 763–772. doi: 10.1016/S1004-9541(11)60054-2.

Ehrampoosh, M. (2011) 'Removal of methylene blue dye from textile simulated sample using tubular reactor and tio2/uv-c photocatalytic process', *Iranian Journal of …*, 8(1), pp. 35–40. Available at: http://journals.tums.ac.ir/abs/18090.

Emslie, A. G., Bonner, F. T. and Peck, L. G. (1958) 'Flow of a viscous liquid on a rotating disk', *Journal of Applied Physics*, 29(5), pp. 858–862. doi: 10.1063/1.1723300.

Esplugas, S., Bila, D. M., Krause, L. G. T. and Dezotti, M. (2007) 'Ozonation and advanced oxidation technologies to remove endocrine disrupting chemicals (EDCs) and pharmaceuticals and personal care products (PPCPs) in water effluents', *Journal of Hazardous Materials*, 149(3), pp. 631–642. doi: 10.1016/j.jhazmat.2007.07.073.

Expósito, A. J., Patterson, D. A., Mansor, W. S. W., Monteagudo, J. M., Emanuelsson, E., Sanmartín, I. and Durán, A. (2016) 'Antipyrine removal by TiO2 photocatalysis based on spinning disc reactor technology', *Journal of Environmental Management*, 187, pp. 504–512. doi: 10.1016/j.jenvman.2016.11.012.

Falk, L. and Commenge, J.-M. (2010) 'Performance comparison of micromixers', *Chemical Engineering Science*, 65(1), pp. 405–411. doi: 10.1016/j.ces.2009.05.045.

Feitz, A. J., Boyden, B. H. and Waite, T. D. (2000) 'Evaluation of two solar pilot scale fixed bed photocatalytic reactors.', *Water Research*, 34, pp. 3927–3932.

Feng, X., Patterson, D. A., Balaban, M. and Emanuelsson, E. A. C. (2014) 'Characterization of liquid flow in the spinning cloth disc reactor: Residence time distribution, visual study and modeling', *Chemical Engineering Journal*. Elsevier B.V., 235, pp. 356–367. doi: 10.1016/j.cej.2013.09.025.

Fogler, H. (2016) *Elements of Chemical Reaction Engineering*. 5th edn. Edited by P.-H. International.

Fournier, M.-C., Falk, L. and Villermaux, J. (1996) 'A new parallel competing

reaction system for assessing micromixing efficiency—Experimental approach', *Chemical Engineering Science*, 51(22), pp. 5053–5064. doi: 10.1016/0009-2509(96)00270-9.

Frank, S. and Bard, A. (1977) 'Heterogeneous photocatalytic oxidation of cyanide ion in aqueous solutions at titanium dioxide powder', *Journal of the American Chemical Society*, 99(1), pp. 303–304.

Fujishima, A. and Honda, K. (1972) 'Electrochemical Photolysis of Water at a Semiconductor Electrode', *Nature*, 238(5358), pp. 37–38. doi: 10.1038/238037a0.

Geng, Q. and Cui, W. (2010) 'Adsorption and photocatalytic degradation of reactive brilliant red K-2BP by TiO2/AC in bubbling fluidized bed photocatalytic reactor', *Industrial and Engineering Chemistry Research*, 49(22), pp. 11321–11330. doi: 10.1021/ie101533x.

Van Gerven, T., Mul, G., Moulijn, J. and Stankiewicz, A. (2007) 'A review of intensification of photocatalytic processes', *Chemical Engineering and Processing: Process Intensification*, 46(9 SPEC. ISS.), pp. 781–789. doi: 10.1016/j.cep.2007.05.012.

Geyer, K. and Seeberger, P. H. (2009) 'Microreactors as the Key to the Chemistry Laboratory of the Future', in *Systems Chemistry*, pp. 87–108.

Gonzalez, M. and Braun, A. M. (1995) 'VUV photolysis of aqueous solutions of nitrate and nitrite.', *Research on Chemical Intermediates*, 21(8/9), pp. 837–859.

Gonzalez, M., Oliveros, E., Worner, M. and Braun, A. M. (2004) 'Vacuum-ultraviolet photolysis of aqueous reaction systems', *Journal of Photochemistry and Photobiology C: Photochemistry Reviews*, 5, pp. 225–246.

Górak, A. and Stankiewicz, A. (2011) 'Intensified Reaction and Separation Systems', *Annual Review of Chemical and Biomolecular Engineering*, 2(1), pp. 431–451. doi: 10.1146/annurev-chembioeng-061010-114159.

Guettaï, N. and Ait Amar, H. (2005) 'Photocatalytic oxidation of methyl orange in presence of titanium dioxide in aqueous suspension. Part I: Parametric study', *Desalination*, 185(1–3), pp. 427–437. doi: 10.1016/j.desal.2005.04.048.

Han, W., Zhang, P., Zhu, W., Yin, J. and Li, L. (2004) 'Photocatalysis of p-chlorobenzoic acid in aqueous solution under irradiation of 254 nm and 185 nm UV light', *Water Research*, 38, pp. 4197–4203.

Haseidl, F., Pottbacker, J. and Hinrichsen, O. (2016) 'Gas-Liquid mass transfer in a rotor-stator spinning disc reactor: Experimental study and correlation', *Chemical Engineering and Processing: Process Intensification*. Elsevier B.V., 104, pp. 181–189. doi: 10.1016/j.cep.2016.03.003.

Hernández, J. M. P., Huitle, C. A. M., Mar, J. L. G. and Ramírez, A. H. (2009) 'Recent advances in the application of electrofenton and photoelectro-fenton process for removal of synthetic dyes in wastewater treatment', *Journal of Environmental Engineering Management*, 19(5), pp. 257–265.

Hoffmann, M. R., Martin, S., Choi, W. and Bahnemann, D. W. (1995) 'Environmental Applications of Semiconductor Photocatalysis', *Chemical Reviews*, 95(1), pp. 69–96. doi: 10.1021/cr00033a004.

Houas, A., Lachheb, H., Ksibi, M., Elaloui, E., Guillard, C. and Herrmann, J.-M. (2001) 'Photocatalytic degradation pathway of methylene blue in water', *Applied Catalysis B: Environmental*, 31(2), pp. 145–157. doi: 10.1016/S0926-3373(00)00276-9.

Idaka, E., Ogawa, T. and Horitsu, H. (1987) 'Reductive Metabolism of Aminoazobenzenes by Pseudomonas cepacia', *Bulletin Environmental Contamination Toxcology*, pp. 100–107.

Jachuck, R. J. J. and Ramshaw, C. (1994) 'Process intensification: Heat transfer characteristics of tailored rotating surfaces', *Heat Recovery Systems and CHP*, 14(5), pp. 475–491. doi: 10.1016/0890-4332(94)90051-5.

Jacobsen, N. C. and Hinrichsen, O. (2012) 'Micromixing efficiency of a spinning disk reactor', *Industrial and Engineering Chemistry Research*, 51(36), pp. 11643–11652. doi: 10.1021/ie300411b.

Jiang, H., Zhang, G., Huang, T., Chen, J., Wang, Q. and Meng, Q. (2010) 'Photocatalytic membrane reactor for degradation of acid red B wastewater', *Chemical Engineering Journal*, 156(3), pp. 571–577. doi: 10.1016/j.cej.2009.04.011.

Jović, F., Kosar, V., Tomašić, V. and Gomzi, Z. (2012) 'Non-ideal flow in an annular photocatalytic reactor', *Chemical Engineering Research and Design*, 90(9), pp. 1297–1306. doi: 10.1016/j.cherd.2011.12.014.

Kapteijn, F., Heiszwolf, J. J., Nijhuis, T. van and Moulijn, J. A. (1999) 'Monoliths in multiphase catalytic processes: aspects and prospects', *Cattech*, 3(1), pp. 24–41.

Khuzwayo, Z. and Chirwa, E. M. N. (2015) 'Modelling and simulation of photocatalytic oxidation mechanism of chlorohalogenated substituted phenols in batch systems: Langmuir-Hinshelwood approach', *Journal of Hazardous Materials*. Elsevier B.V., 300, pp. 459–466. doi: 10.1016/j.jhazmat.2015.07.034.

Kim, M.-J., Choo, K.-H. and Park, H.-S. (2010) 'Photocatalytic degradation of seawater organic matter using a submerged membrane reactor', *Journal of Photochemistry and Photobiology A: Chemistry*. Elsevier B.V., 216(2–3), pp. 215–220. doi: 10.1016/j.jphotochem.2010.08.011.

Kolpin, D. W., Furlong, E. T., Meyer, M. T., Thurman, E. M., Zaugg, S. D., Barber, L. B. and Buxton, H. T. (2002) 'Pharmaceuticals, hormones, and other organic wastewater contaminants in U.S. streams, 1999-2000: A national reconnaissance', *Environmental Science and Technology*, 36(6), pp. 1202–1211. doi: 10.1021/es011055j.

Kumazawa, H., Inoue, M. and Kasuya, T. (2003) 'Photocatalytic Degradation of Volatile and Nonvolatile Organic Compounds on Titanium Dioxide Particles Using Fluidized Beds', *Industrial and Engineering Chemistry Research*, 42, pp. 3237–3244.

Kümmerer, K. (2001) 'Drugs in the environment: emission of drugs, diagnostic aids and disinfectants into wastewater by hospitals in relation to other sources – a review', *Chemosphere*, 45(6), pp. 957–969. doi: 10.1016/S0045-6535(01)00144-8.

Legrini, O., Oliveros, E. and Braun, A. M. (1993) 'Photochemical processes for water treatment', *Chemical Reviews*, 93(2), pp. 671–698. doi: 10.1021/cr00018a003.

Levenspiel, O. (1999) *Chemical Reaction Engineering*. 3rd edn. John Wiley and Sons, Inc.

Li, X., Wang, Y., Yuan, S., Li, Z., Wang, B., Huang, J., Deng, S. and Yu, G. (2014) 'Degradation of the anti-inflammatory drug ibuprofen by electro-peroxone process', *Water Research*, 63, p. 8193.

Li Puma, G. and Yue, P. L. (2001) 'A novel fountain photocatalytic reactor: model development and experimental validation', *Chemical Engineering Science*, 56(8), pp. 2733–2744. doi: 10.1016/S0009-2509(00)00528-5.

Lim, T. H. and Kim, S. D. (2004) 'Trichloroethylene degradation by photocatalysis in annular flow and annulus fluidized bed photoreactors', *Chemosphere*, 54(3), pp. 305–312. doi: 10.1016/S0045-6535(03)00753-7.

Ling, C. M., Mohamed, A. R. and Bhatia, S. (2004) 'Performance of photocatalytic reactors using immobilized TiO 2 film for the degradation of phenol and methylene blue dye present in water stream', *Chemosphere*, 57(7), pp. 547–554. doi: 10.1016/j.chemosphere.2004.07.011.

Lopez, J., Einschlag, F., Gonzalez, M., Capparelli, A., Oliveros, E., Hashem, T. and Braun, A. M. (2000) 'Hydroxyl radical initiated photodegradation of 4-chloro-3,5 dinitrobenzoic acid in aqueous solution', *Journal of Photochemistry and Photobiology A: Chemistry*, 137, pp. 177–184.

Madhavan, J., Grieser, F. and Ashokkumar, M. (2010) 'Combined advanced oxidation processes for the synergistic degradation of ibuprofen in aqueous environments', *Journal of Hazardous Materials*. Elsevier B.V., 178(1–3), pp. 202–208. doi: 10.1016/j.jhazmat.2010.01.064.

Malato, S., Blanco, J., Richter, C., Milow, B. and Maldonado, M. I. (1999) 'Pre-industrial experience in solar photocatalytic mineralization of real wastewaters. Application to pesticide container recycling.', *Water Science Technology*, 40, pp. 123–130.

McCullagh, C., Robertson, P. K. J., Adams, M., Pollard, P. M. and Mohammed, A. (2010) 'Development of a slurry continuous flow reactor for photocatalytic treatment of industrial waste water', *Journal of Photochemistry and Photobiology A: Chemistry*. Elsevier B.V., 211(1), pp. 42–46. doi: 10.1016/j.jphotochem.2010.01.020.

Meeuwse, M., Hamming, E., van der Schaaf, J. and Schouten, J. C. (2011) 'Effect of rotor-stator distance and rotor radius on the rate of gas-liquid mass transfer in a rotor-stator spinning disc reactor', *Chemical Engineering and Processing: Process Intensification*. Elsevier B.V., 50(10), pp. 1095–1107. doi: 10.1016/j.cep.2011.05.022.

Meeuwse, M., Lempers, S., Schaaf, J. and Schouten, J. C. (2007) 'Liquid-Solid Mass Transfer and Reaction in a Rotor-Stator Spinning Disc Reactor', *Macromolecules*, 40(1), pp. 1366–1368.

Meeuwse, M., Schaaf, J. van der, Kuster, B. F. M. and Schouten, J. C. (2010) 'Gas-liquid mass transfer in a rotor-stator spinning disc reactor', *Chemical Engineering Science*, 65, pp. 466–471.

Meeuwse, M., Schaaf, J. Van Der and Schouten, J. C. (2010) 'Mass Transfer in a Rotor−Stator Spinning Disk Reactor with Cofeeding of Gas and Liquid', *Industrial & Engineering Chemistry Research*, 49(4), pp. 1605–1610.

Méndez-Arriaga, F., Esplugas, S. and Giménez, J. (2008) 'Photocatalytic degradation of non-steroidal anti-inflammatory drugs with TiO2 and simulated solar irradiation', *Water Research*, 42(3), pp. 585–594. doi: 10.1016/j.watres.2007.08.002.

Mendez-Arriaga, F., Gimenez, J. and Esplugas, S. (2010) 'Degradation of the emerging contaminant ibuprofen in water by photo-Fenton', *Water Research*, 44(2), pp. 589–595.

Mills, A. and Le Hunte, S. (1997) 'An overview of semiconductor photocatalysis', *Journal of Photochemistry and Photobiology A: Chemistry*, 108(1), pp. 1–35. doi: 10.1016/S1010-6030(97)00118-4.

Mohammadi, S. and Boodhoo, K. V. K. (2012) 'Online conductivity measurement of residence time distribution of thin film flow in the spinning disc reactor', *Chemical Engineering Journal*. Elsevier B.V., 207–208, pp. 885–894. doi: 10.1016/j.cej.2012.07.120.

Oppenländer, T. (2003) *Photochemical purification of water and air*. Wiley-VCH.

Oxley, P., Brechtelsbauer, C., Ricard, F., Lewis, N. and Ramshaw, C. (2000)

‘Evaluation of Spinning Disk Reactor Technology for the Manufacture of Pharmaceuticals’, *Industrial & Engineering Chemistry Research*, 39(7), pp. 2175–2182. doi: 10.1021/ie990869u.

Özcan, A., Şahin, Y., Koparal, A. S. and Oturan, M. A. (2009) ‘Proposed transformation p’, *Journal of Environmental Engineering Management*, 19(5), pp. 267–275.

Pask, S. D., Nuyken, O. and Cai, Z. (2012) ‘The spinning disk reactor: an example of a process intensification technology for polymers and particles’, *Polymer Chemistry*, 3(10), p. 2698. doi: 10.1039/c2py20237a.

Petrovic, M. and Barceló, D. (2007) ‘LC-MS for identifying photodegradation products of pharmaceuticals in the environment’, *Trends in Analytical Chemistry*, 26(6), pp. 486–493.

Pozzo, R. L., Brandi, R. J., Cassano, A. E. and Baltanás, M. A. (2010) ‘Photocatalytic oxidation of oxalic acid in dilute aqueous solution, in a fully illuminated fluidized bed reactor’, *Chemical Engineering Science*, 65(4), pp. 1345–1353. doi: 10.1016/j.ces.2009.10.002.

Ramshaw, C. (1985) ‘Process Intensification - a Game for N Players’, *The Chemical Engineering*, 416, pp. 30–33.

Rao, N. N., Chaturvedi, V. and Li Puma, G. (2012) ‘Novel pebble bed photocatalytic reactor for solar treatment of textile wastewater’, *Chemical Engineering Journal*. Elsevier B.V., 184, pp. 90–97. doi: 10.1016/j.cej.2012.01.004.

Ray, A. K. (1998) ‘A new photocatalytic reactor for destruction of toxic water pollutants by advanced oxidation process’, *Catalysis Today*, 44, pp. 357–368. doi: 10.1016/S0920-5861(98)00210-7.

Richardson, M. L. and Bowron, J. M. (1985) ‘The fate of pharmaceutical chemicals in the aquatic environment’, *Journal of Pharmacy and Pharmacology*, 37(1), pp. 1–12. doi: 10.1111/j.2042-7158.1985.tb04922.x.

Robert, D. and Malato, S. (2002) ‘Solar photocatalysis: A clean process for water detoxification’, *Science of the Total Environment*, 291(1–3), pp. 85–97. doi:

10.1016/S0048-9697(01)01094-4.

Sakthivel, S., Neppolian, B., Shankar, M. V, Arabindoo, B., Palanichamy, M. and Murugesan, V. (2003) 'Solar photocatalytic degradation of azo dye: comparison of photocatalytic efficiency of ZnO and TiO_2', *Solar Energy Materials and Solar Cells*, 77(1), pp. 65–82. doi: 10.1016/S0927-0248(02)00255-6.

Sarathy, S. R. and Mohseni, M. (2006) 'An Overview of UV-based Advanced Oxidation Processes for Drinking Water Treatment', *IUVA News*, 8(June), p. 16.

Schneider, M. A., Maeder, T., Ryser, P. and Stoessel, F. (2004) 'A microreactor-based system for the study of fast exothermic reactions in liquid phase: Characterization of the system', *Chemical Engineering Journal*, 101(1–3), pp. 241–250. doi: 10.1016/j.cej.2003.11.005.

Sclafani, a, Palmisano, L. and Schiavello, M. (1990) 'Influence of the Preparation Methods of TiO2 on the Photocatalytic Degradation of Phenol in Aqueous Dispersion', *Journal of Physical Chemistry*, 94, pp. 829–832. doi: 10.1021/j100365a058.

Selli, E., Bianchi, C. L., Pirola, C., Cappelletti, G. and Ragaini, V. (2008) 'Efficiency of 1,4-dichlorobenzene degradation in water under photolysis, photocatalysis on TiO2 and sonolysis', *Journal of Hazardous Materials*, 153(3), pp. 1136–1141. doi: 10.1016/j.jhazmat.2007.09.071.

Serpone, N. and Emeline, A. V. (2002) 'Suggested terms and definitions in photocatalysis and radiocatalysis', *International Journal of Photoenergy*, 4(3), pp. 91–131.

Serpone, N., Terzian, R., Lawless, D., Kennepohl, P. and Sauvé, G. (1993) 'On the usage of turnover numbers and quantum yields in heterogeneous photocatalysis', *Journal of Photochemistry and Photobiology, A: Chemistry*, 73(1), pp. 11–16. doi: 10.1016/1010-6030(93)80027-7.

Stankiewicz, A. (2001) 'Process intensification in in-line monolithic reactor', *Chemical Engineering Science*, 56, pp. 359–364.

Stankiewicz, A. and Moulijn, J. A. (2000) 'Process Intensification: Transforming

Chemical Engineering', *Chemical Engineering Progress*, 96(1), pp. 22–34.

Stankiewicz, A. and Moulijn, J. A. (2004) *Re-engineering the Chemical Processing Plant*. Marcel Dekker Inc., New York.

Stasinakis, A. S. (2008) 'Use of selected advanced oxidation processes (AOPs) for wastewater treatment a mini review', *Global NEST Journal*, 10(3), pp. 376–385.

Stephan, B., Ludovic, L. and Dominique, W. (2011) 'Modelling of a falling thin film deposited photocatalytic step reactor for water purification: Pesticide treatment', *Chemical Engineering Journal*. Elsevier B.V., 169(1–3), pp. 216–225. doi: 10.1016/j.cej.2011.03.016.

Sweeney, E. A., Chipman, J. K. and Forsythe, S. J. (1994) 'Evidence for direct-acting oxidative genotoxicity by reduction products of azo dyes', *Environmental Health Perspectives*, 102(SUPPL. 6), pp. 119–122. doi: 10.1289/ehp.94102s6119.

Tennakone, K. and Wijayantha, K. (2005) 'Photocatalysis of CFC degradation by titanium dioxide', *Applied Catalysis A: General*, 57(1), pp. 9–12.

Tsibranska, I., Peshev, D., Peev, G. and Nikolova, A. (2009) 'Modelling of mass transfer in film flow of shear thinning liquid on a horizontal rotating disk.', *Chemical Engineering and Processing: Process Intensification*, 48(3), pp. 823–827.

Turchi, C. S. and Ollis, D. F. (1990) 'Photocatalytic degradation of organic water contaminants: Mechanisms involving hydroxyl radical attack', *Journal of Catalysis*, 122(1), pp. 178–192. doi: 10.1016/0021-9517(90)90269-P.

Vatanpour, V., Daneshvar, N. and Rasoulifard, H. (2009) 'Electro-fenton degradation of synthetic dye mixture: influence of intermediate', *Journal of Environmental Engineering Management*, 19(5), pp. 277–282.

Vicevic, M., Boodhoo, K. V. K. and Scott, K. (2007) 'Catalytic isomerisation of α-pinene oxide to campholenic aldehyde using silica-supported zinc triflate catalysts: I. Kinetic and thermodynamic studies', *Chemical Engineering Journal*, 133(1), pp. 31–41. doi: 10.1016/j.cej.2006.11.014.

Vicevic, M., Novakovic, K., Boodhoo, K. V. K. and Morris, J. (2008) 'Kinetics of styrene free radical polymerisation in the spinning disc reactor.', *Chemical*

Engineering Journal, 135(1–2), pp. 78–82.

Visscher, F., van der Schaaf, J., de Croon, M. H. J. M. and Schouten, J. C. (2012) 'Liquid-liquid mass transfer in a rotor-stator spinning disc reactor', *Chemical Engineering Journal*. Elsevier B.V., 185–186, pp. 267–273. doi: 10.1016/j.cej.2012.01.002.

Wang, R., Ren, D., Xia, S., Zhang, Y. and Zhao, J. (2009) 'Photocatalytic degradation of Bisphenol A (BPA) using immobilized TiO2 and UV illumination in a horizontal circulating bed photocatalytic reactor (HCBPR)', *Journal of Hazardous Materials*, 169(1–3), pp. 926–932. doi: 10.1016/j.jhazmat.2009.04.036.

Wang, X.-P., Yu, Y., Hu, X.-F. and Gao, L. (2000) 'Hydrophilicity of TiO2 films prepared by liquid phase deposition', *Thin Solid Films*, 371(1–2), pp. 148–152. doi: 10.1016/S0040-6090(00)00995-0.

Wang, Y. (2000) 'Solar photocatalytic degradation of eight commercial dyes in TiO2 suspensions.', *Water Research*, 34, pp. 990–994.

Wilhelm, P. and Stephan, D. (2007) 'Photodegradation of rhodamine B in aqueous solution via SiO2@TiO2 nano-spheres', *Journal of Photochemistry and Photobiology A: Chemistry*, 185(1), pp. 19–25.

Winkler, J. (2013) *Titanium Dioxide Production, Properties and Effective Usage*.

Wong, P. K. and Yuen, P. Y. (1996) 'Decolorization and biodegradation of methyl red by Klebsiella pneumoniae RS-13', *Water Research*, 30(7), pp. 1736–1744. doi: 10.1016/0043-1354(96)00067-X.

Xia, S., Zhang, L., Pan, G., Qian, P. and Ni, Z. (2015) 'Photocatalytic degradation of methylene blue with a nanocomposite system: synthesis, photocatalysis and degradation pathways', *Phys. Chem. Chem. Phys.* Royal Society of Chemistry, 17(7), pp. 5345–5351. doi: 10.1039/C4CP03877K.

Yang, H.-G., Li, C.-Z., Gu, H.-C. and Fang, T.-N. (2001) 'Rheological Behavior of Titanium Dioxide Suspensions.', *Journal of colloid and interface science*, 236(1), pp. 96–103. doi: 10.1006/jcis.2000.7373.

Yatmaz, H. C., Wallis, C. and Howarth, C. R. (2001) 'The spinning disc reactor -

Studies on a novel TiO2 photocatalytic reactor', *Chemosphere*, 42(4), pp. 397–403. doi: 10.1016/S0045-6535(00)00088-6.

Yurdakal, S., Loddo, V., Palmisano, G., Augugliaro, V., Berber, H. and Palmisano, L. (2010) 'Kinetics of 4-methoxybenzyl alcohol oxidation in aqueous solution in a fixed bed photocatalytic reactor', *Industrial and Engineering Chemistry Research*, 49(15), pp. 6699–6708. doi: 10.1021/ie9008056.

Zhang, Z., Wu, H., Yuan, Y., Fang, Y. and Jin, L. (2012) 'Development of a novel capillary array photocatalytic reactor and application for degradation of azo dye', *Chemical Engineering Journal*. Elsevier B.V., 184, pp. 9–15. doi: 10.1016/j.cej.2011.02.057.

Zhu, S., Yang, X., Yang, W., Zhang, L., Wang, J. and Huo, M. (2012) 'Application of porous nickel-coated TiO 2 for the photocatalytic degradation of aqueous quinoline in an internal airlift loop reactor', *International Journal of Environmental Research and Public Health*, 9(2), pp. 548–563. doi: 10.3390/ijerph9020548.

APPENDICES

Appendix A: Safety Operation Procedures and Hazard Analysis

Appendix A1: Preparation of Sol-Gel Solution

1. The following procedure is for the preparation of sol-gel solution.
2. Clean the following equipment thoroughly:
   - 500mL volumetric flask
   - Magnetic stirrer flea
   - Three small 60mL beakers
   - Two 250mL measuring cylinders
3. The following equipment is necessary:
   - Magnetic stirrer
   - Wax tape
   - Fume hood

Neoprene gloves have been determined to be best suitable for handling the chemicals.

4. All of the following steps are to be carried out in fume hood as all the chemicals are highly volatile.
5. Prepare 340mL of synthesized TiO_2 mixture via sol–gel route.
6. Mix 0.34 mol of titanium isopropoxide (Aldrich, 97%), and 2.72 mol isopropanol (Sigma-Aldrich, 99.5%), under constant stirring at room temperature.
7. Stir this mixture for 2h to undergo a hydrolysis process for the formation of homogeneous solution.
8. Mix 0.374 mol distilled water and 0.017 mol acetic acid (Sigma-Aldrich, ≥99.7%) and add drop wise to the above-hydrolysed mixture under constant stirring.
9. Once the stirred mixture has become cloudy add 1.02 mol (116.50 mL) acetylacetone (Sigma-Aldrich, 99%) and stir for a further 30 min. This increases the stability of the mixture, which can last for several months.
10. Seal the mixture and allow to age for a minimum of one day.

HAZOP analysis of Sol-Gel Method			
Potential Hazards	**Causes**	**Consequences**	**Recommendations**
Fumes (inhalation)	Chemical containers left open, inhalation of fumes during preparation of sol.	Systemic health effects, lung irritation.	All work to be carried out in fume cabinet, including decanting of chemicals. Storage of solution should be in appropriate area and paraffin wax should be used to ensure tight seal.
Flammable Liquid	Fire caused by ignition of liquid.	Injury and property damage.	Keep away from ignition sources, solvents to be stored in designated cabinets. Carbon dioxide is suitable extinguishing media.
Flammable Vapour	Fire caused by ignition of vapour.	Injury and property damage.	Keep away from ignition sources, solvents to be stored in designated cabinets, close containers promptly after use. Carbon dioxide is suitable extinguishing media.
Chemical Spill	Accident (e.g. knocking over bottle).	Harmful vapours released, slippery floor.	Store chemicals in designated areas, don't place containers in the way of significant

			laboratory movement. Know where the absorbent material s for chemical spill are in the lab for immediate clean up (vermiculite is suitable). If the spill is outside of the fumehood, drop on absorbent material and then leave to let room ventilate. Avoid breathing vapours.
Skin burns (eye burns)	Glacial acetic acid contact with skin (accidental spill).	Chemical burns, lesions.	Wear suitable protective gloves (at least neoprene disposable, although PVC is recommended), wear protective goggles. Wash immediately with water.
Violent chemical reaction with incompatible chemicals.	Unsuitable storage of material or incorrect handling (e.g. adding water to acid).	Violent reaction producing heat, resulting in contact with skin and eyes causing chemical burns.	Be aware of incompatible chemicals from MSDS (e.g. strong basis, oxidising and reducing agents, metals). Store away from incompatible materials.

Appendix A2: Spinning Disc Reactor Operating Procedure

The SDR operating procedure is as follows:

1. A fresh disc is cleaned with de-ionised water to remove any loose catalyst. Then it will be fitted and secured to the spinning shaft to replace the one used for the previous reaction. If a disc is reused for a repeat reaction, the disc shall be cleaned with a solution of hydrogen peroxide in water and irradiated for one hour to ensure complete removal of any adsorbates.
2. The buffer will be filled with 150mL of the reacting solution, sealed and secured.
3. The balance of the solution will be poured into the reactant reservoir.

4. The pipes coming in and out of the reactant reservoir, the magnetic stirrer bar and the oxygen sparger will be arranged such that they did not interfere with each other (e.g. the sparged oxygen did not get sucked up as bubbles into the reactor inlet pipework, and the stirrer did not hit the sparger).
5. The pipework will be secured to a retort stand as it exhibited strong vibrations from the peristaltic pump.
6. All transparent parts of the reactor will be covered with aluminium foil. This is done to remove the possibility of photolysis or photocatalysis (if any catalyst is lost to the solution) from ambient light outside the reactor.
7. The magnetic stirrers under the buffer and reactant reservoir will be switched on to 500rpm to maintain constant agitation and mixing of solutions.
8. The spinning disc is switched on, and then the pump will be switched on to a high flow rate ($30mL.s^{-1}$) to blow out any bubbles in the pipework and nozzle. Then, the flow rate and rotational speed will be adjusted to that required for the reaction.
9. The reactor lid will be closed and run for 20 to 30 min in the dark to allow absorption to take place and for the concentration of the reactant to reach equilibrium. A 0.5mL will be taken at the end of the adsorption phase.
10. The UV light and oxygen will be switched on and the oxygen flow rate adjusted to that desired and run for the time specified. 0.5mL samples will be taken using a syringe from the reactant reservoir, and immediately refrigerated to prevent degradation. Samples will be taken 15, 30, 45, 60, 90, 120, 150 and 180 minutes into the reaction. Samples will be analysed by HPLC.
11. The temperature of the reactant will be kept constant with the Liebig condenser (acting as a heat exchanger).
12. To shut down the reactor; the oxygen, magnetic stirrers and UV light will be switched of first to prevent unnecessary oxygen and power consumption during the rest of the shutdown procedure.
13. The pump will be switched off and then reversed for a few seconds to suck any flow back into the reservoir from the nozzle.
14. The disc rotational speed will be increased to maximum to remove any remaining liquid on the surface of the disc, and then stopped.
15. The reactor and buffer will be cleaned with acetone and thoroughly rinsed with de-ionised water before the next reaction. The reactor reservoir will be cleaned

with detergent, followed by acetone and de-ionised water. The pipework will be rinsed using tap water followed by rinsing with de-ionised water.

Keywords:

- No – negation of the design intent
- Less – quantitative decrease
- More – quantitative increase
- Part of – qualitative decrease
- As well as – qualitative increase
- Reverse – opposite to intent
- Other than – complete substitution

SPINNING DISC REATOR – DESIGN HAZOP				
PARTICIPANTS: Wan Salida Wan Mansor, Darrell Patterson				
NODE: Spinning Shaft, Stationary Bearing Housing and Glass Disc				
ELEMENT	**KEYWORD**	**CAUSE**	**CONSEQUENCE**	**ACTIONS**
Glass Disk	Sharp edges	Manufacturing process	Inflicting wounds during disk replacement operation	Manufacturer has blunted sharp edges
	Breakage	Human error/Centrifugal forces generated during spinning	Inflicting wounds	Operational (clean up) procedure has been written, when operating with lid open wear face shield so that glass does not spin out and spray onto face (especially during testing phase, as we cannot be sure what will happen here)
Rotating Mechanism	More (rotation)	Human error	Water splashing onto motor, glass disc breakage	Wear face shield during testing phase; splash guard installed in front of motor; start disc with lowest possible rotational speed, gradually speeding it up; at the testing phase, where the spray level of liquid from the edge of the disc is unknown, the edges of the trough are to be sealed to the housing using paraffin wax tape;
	Less/None	Human error/motor fault/broken connection	Accidental electric shock/electrocution whilst trying to check for fault	Faults that look electrical in nature to be checked by qualified personnel only; don't fiddle with what looks like an electrical problem while the equipment is live;
	Fingers/hair/objects in the way of spinning parts	Human error	Inflicting wounds – loss of appendages	Require operational procedure (taking care, tie back hair, wear safety glasses etc.)
NODE: Housing, Catching Dish and Motor				

ELEMENT	KEYWORD	CAUSE	CONSEQUENCE	ACTIONS
Motor Power Supply Electricity	More	Faulty wiring, liquid spillage	Electric shock	Operational procedure; splash guard incorporated into design to stop water reaching motor; motor mounted from housing box – water cannot accumulate on or around it; reactor is grounded; at the testing phase, where the spray level of liquid from the edge of the disc is unknown, the edges of the trough are to be sealed to the housing using paraffin wax tape;
Catching Dish (flow)	More	Human error, incorrect pump selection	Overflow of catching dish, shorting of motor	Catching dish to have an overflow line that is to go to drain; flow can accumulate in bottom of box as motor is suspended from wall; at the testing phase, where the spray level of liquid from the edge of the disc is unknown, the edges of the trough are to be sealed to the housing using paraffin wax tape;
	Less	Pump setting	N/A	
Inlet Flow Pressure	High	Incorrect pump selection	Waste water hitting lamp; waste water sprayed into eyes	Lamp to have protective sleeve on it which is to fit into handles with O-rings; proper pump selection and verification with tap water without lid – face helmet to be worn when lid open
NODE: Overview				
ELEMENT	**KEYWORD**	**CAUSE**	**CONSEQUENCE**	**ACTIONS**
Maintenance	Incorrect, none	Human error	Malfunctioning equipment	Require operational procedure (maintenance schedule etc.); maintenance to be done by qualified personnel only; design build for disassembly; inspection record booklet
Effluent	Any	Experimental procedure	Hazardous waste produced	Require operational procedure and waste minimisation/disposal strategy

Appendix B: Calibration Curves

1. UV-Vis

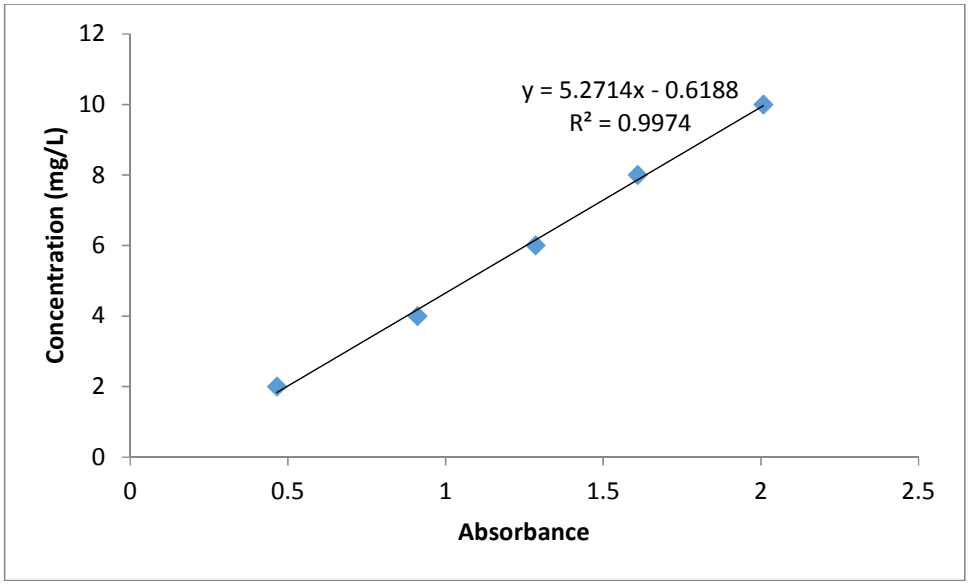

2. HPLC

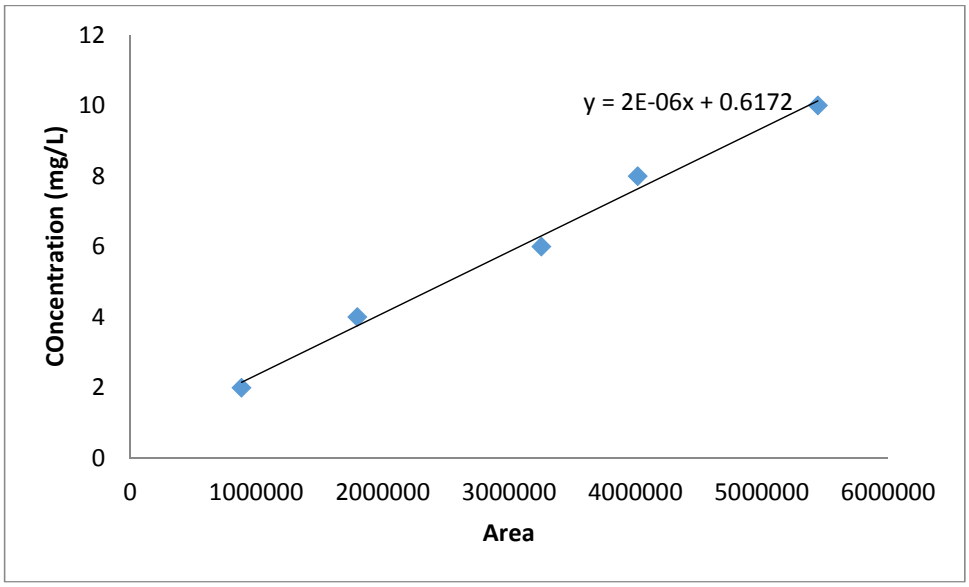

APPENDIX C: Calculation of average flux over surface of disc.

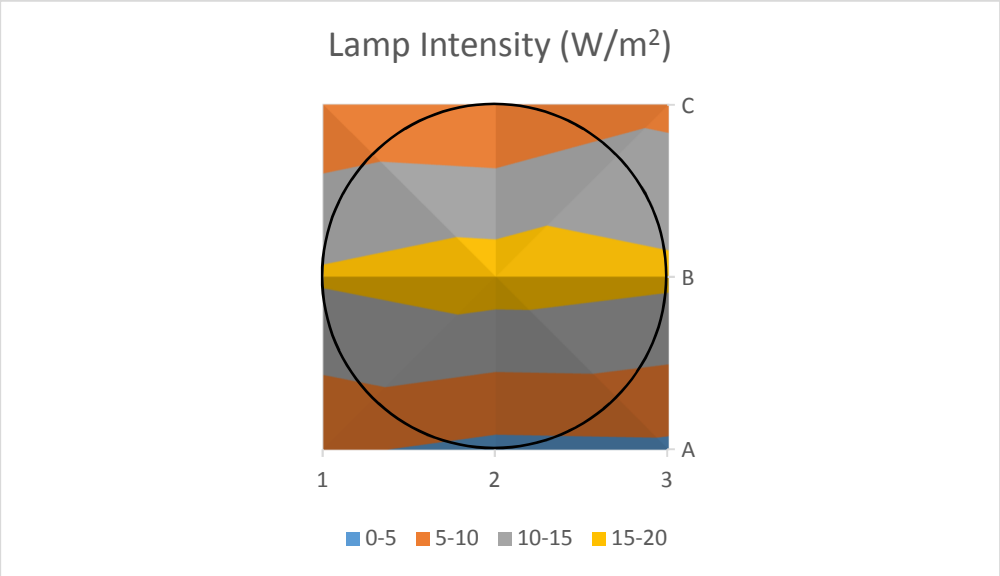

	1	2	3
A	5.7	3.8	4.06
B	15.66	17.62	16.12
C	6.2	5.5	8.78

SA (m^2)	Quadrant	Irradiance (W/m^2)	SA x Irradiance
1A	0.002531	5.7	0.0144267
1B	0.004212	15.66	0.06595992
1C	0.002531	6.2	0.0156922
2A	0.004212	3.8	0.0160056
2B	0.003059	17.62	0.05389958
2C	0.004212	5.5	0.023166
3A	0.002531	4.06	0.01027586
3B	0.004212	16.12	0.06789744
3C	0.002531	8.78	0.02222218
		Total SA x Irradiance =	0.28954548W
		Total SA =	$0.030031m^2$
		Average Irradiance =	**$9.641553062W/m^2$**